OIL IN THE ARCTIC

David P. Hoult, et al

Massachusetts Institute of Technology
Cambridge, Massachusetts

March 1975

Report No. CG-D-96-75
Task No. 4108.2.3

OIL IN THE ARCTIC

DAVID P. HOULT
STEPHEN WOLFE
STEPHEN O'DEA
JEAN P. PATUREAU

MARCH 1975

FINAL REPORT

Prepared for

DEPARTMENT OF TRANSPORTATION
UNITED STATES COAST GUARD
Office of Research and Development
Washington, D.C. 20590

This document is disseminated under the sponsorship of the Department of Transportation in the interest of information exchange. The United States Government assumes no liability for its content or use thereof.

The contents of this report do not necessarily reflect the official view or policy of the Coast Guard, and they do not constitute a standard, specification or regulation.

This report, or portions thereof, may not be used for advertising publication, or promotional purposes. Citation of trade names and manufacturers does not constitute endorsements or approval of such products.

W. L. KING
Captain, U. S. Coast Guard
Chief, Environmental and
Transportation Technology Division
Office of Research and Development
U. S. Coast Guard Headquarters
Washington, D. C. 20590

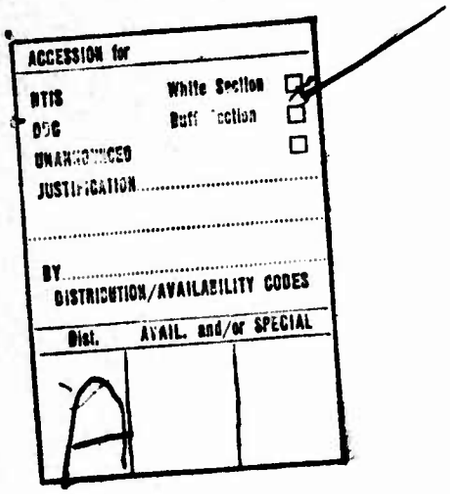

Technical Report Documentation Page

1. Report No.	2. Government Accession No.	3. Recipient's Catalog No.
CG-D-96-75		

4. Title and Subtitle	5. Report Date
OIL IN THE ARCTIC	March 1975
	6. Performing Organization Code
	8. Performing Organization Report No.

7. Author(s)	
David P. Hoult, Stephen Wolfe, Stephen O'Dea, Jean P. Patureau	

9. Performing Organization Name and Address	10. Work Unit No. (TRAIS)
Massachusetts Institute of Technology 77 Massachusetts Avenue Cambridge, Massachusetts 02139	4108.2.3
	11. Contract or Grant No. DOT-CG-12438-A
	13. Type of Report and Period Covered FINAL REPORT
12. Sponsoring Agency Name and Address Department of Transportation United States Coast Guard Office of Research and Development Washington, D. C. 20590	14. Sponsoring Agency Code

15. Supplementary Notes

16. Abstract

This report describes the results of several researches on the behavior of oil spilled in the arctic. Included are studies on evaporation, spreading and maximum extent of oil spilled on ice, and the behavior of oil spilled under ice. Physically sound theories are developed which correlate well with laboratory and field data.

17. Key Words	18. Distribution Statement
Oil pollution, Arctic oil pollution, Oil on ice, Oil under ice	Document is available to the public through the National Technical Information Service, Springfield, Virginia 22151

19. Security Classif. (of this report)	20. Security Classif. (of this page)	21. No. of Pages	22. Price
Unclassified	Unclassified	218	

Form DOT F 1700.7 (8-72) Reproduction of completed page authorized

PREFACE

The work reported below includes the theses research of Stephen Wolfe, Stephen O'Dea and Jean P. Patureau. These students performed a significant amount of the work reported herein. Their research resulted in Masters theses completed in The Department of Mechanical Engineering, M.I.T., and available from the M.I.T. libraries.

TABLE OF CONTENTS

LIST OF SYMBOLS

h	=	height of ice surface
x	=	distance along ice surface
τ	=	an increment of distance
$\langle ( ) \rangle$	=	$\lim_{L \to \infty} \frac{1}{L} \int_{n_0}^{\infty} ( ) \, dx$
$\delta(h)dh$	=	probability that h lies between h and h + dh
σ_h	=	mean square roughness height
k	=	a parameter
T	=	the wavelength of the surface
H	=	thickness of oil layer
Δ	=	difference in specific gravity of oil and water or air
ρ	=	density of oil
Q	=	rate of release of oil
r	=	radius of oil pool
Smp	=	surface area of average pocket
Vmp	=	volume of average pocket
$Smax$	=	average area covered by oil
u^*	=	air friction velocity
z	=	air roughness height
λ	=	a parameter
c_i	=	density of ith component of oil vapor
ρH_2O	=	density of water

S_i	=	solubility of the component
u^*_w	=	water friction velocity
n_i	=	moles of ith fraction
M_i	=	molecule weight of ith fraction
N	=	total number of moles
V_i	=	volume of ith fraction
ρ_i	=	density of ith fraction
m_i	=	mass of ith fraction
x_i	=	ith mole fraction
P^o_i	=	saturated vapor pressure of ith fraction
P_i	=	vapor pressure of ith fraction
T_{B_i}	=	Boiling temperature at atmospheric pressure
P_B	=	atmospheric pressure
R	=	gas constant
T	=	absolute temperature
A	=	exposed area
$\tau(T_B)$	=	characteristic time to evaporate ith species

OIL SPILLS IN THE ARCTIC

1. INTRODUCTION

With the discovery of large oil reserves in the Arctic, there naturally arises questions about the behavior of oil spilled, as it may change the fragile Arctic environment. To date, there have been few oil spills in the Arctic. Nevertheless, one expects that tankers, pipelines and drilling will all contribute to the oil spillage, much as happens in warmer waters. However, as there is little in the way of a historical record of oil spilled in the Arctic, it is not presently possible to determine which of these sources is the most significant.

The environmental concerns aroused by potential oil spillage are founded broadly on two ideas. First, the characteristic time for biological degradation in the high Arctic is believed to be quite long, on the order of ten years. This means that if spillage in an area is more frequent than once a decade, we might expect permanent changes in the environment. Second, crude oil is generally a dark color. If spilled on ice or tundra, it will change the solar albedo of the area covered. Such a change in solar heating is known to drastically change tundra. Of course, there is also the toxic effect of oil on flora and fauna - but a discussion of such biological effects is beyond the scope of this report.

There are a number of new features which arise in Arctic oil spills. First is the role of ice. Sea ice has a variable density, ranging from perhaps 0.70 (gm/cc) to 0.91 (gm/cc), the latter value being associated with old ice containing very little brine. The actual ice density depends on how the ice formed, and its subsequent history.

In contrast, the density of North Slope crude oil is 0.89. After aging two weeks in the Arctic summer, this density rises to about 0.95[1]. Hence the oil can be either heavier or lighter than the sea ice.

Suppose now that a large volume of oil is spilled in a lead. Subsequent to the spill, the lead closes. On a hydrostatic argument, one can say that if the oil is heavier than the ice, it will be forced under the ice pack. The important idea here is that we must consider both situations - oil under and over the ice.

A second new feature is that of surface roughness. It is well known[2] that sea ice is rough, and that the roughness elements have a more or less random character, with "hills" and "valleys". These statistical properties of the Arctic surface are extremely variable - the rms roughness height can be as small as several inches or as large as several feet. Similar statements can be made for tundra[2].

Roughness is important, because, if oil is spilled on a rough surface, it will run down into the "valleys" and remain in these "pockets". See Figs. 1 and 2. After oil spilled has stopped spreading, its area is determined by the extent of these pockets or puddles. Of course, the rough surface also modifies the way in which oil spreads over the surface.

These effects may also be present if oil spreads under the ice. In that case, puddles form at the high points of the ice-water interface.

A third feature is the fact that crude oils are sticky, and they stick to ice. This feature means that ice traps oil, preventing its free release and spread in the environment. Of course, in the Arctic summer, the ice adjacent to oil can melt, and the oil released. Hence one would expect that oil spilled in the

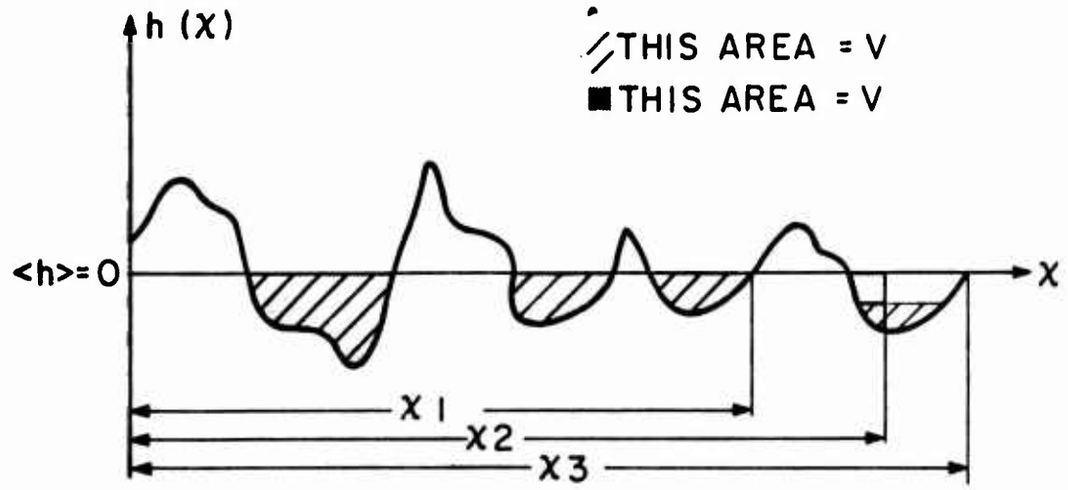

FIG. 1 GENERAL ASPECT OF ONE REALIZATION OF THE PROFILE

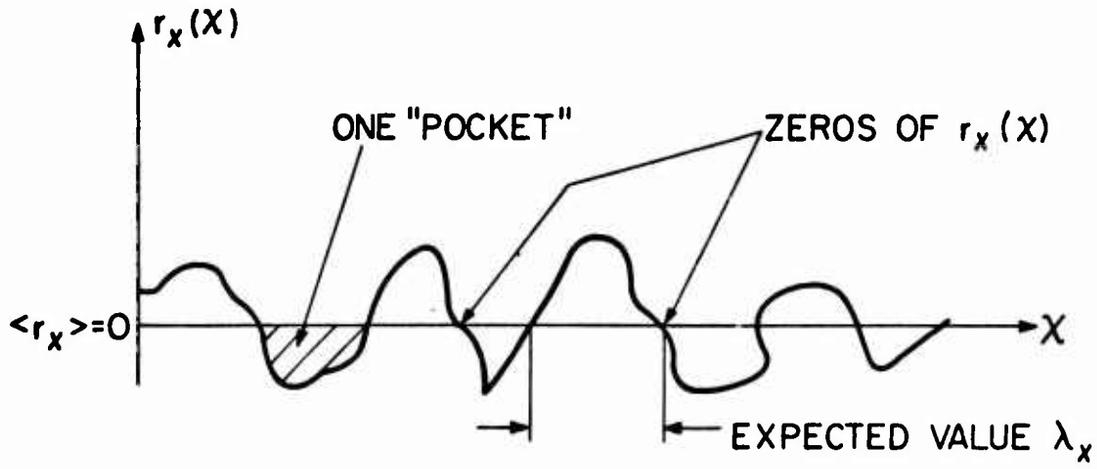

FIG. 2 AVERAGE LONGITUDINAL DIMENSION OF A POCKET

Arctic would be cyclically trapped and released.

A fourth new feature has to do with how oil spreads on water. This is a topic which is fairly well understood[3]. The new feature in the Arctic situation is that the surface tension spreading regime[1] is apparently absent. Thus, Arctic oil spills do not spread to a thin film (driven by surface tension) as do their warm water counterparts.

The purposes of this report are twofold. First, we shall give a description of the short term history of an oil spill - including the rate of spread, the area covered by the oil, and the effects of leads. In each of these areas, our knowledge is based upon a physically sound theory which successfully correlates carefully controlled laboratory data, and what field data is available.

Second, we discuss the evolution of oil, from a non-biological point of view. A model of oil aging is developed, and its predictions compared with field observation. The stickiness of oil on sea ice has been measured, and the results correlated with a theory which predicts how thick a layer of oil can stick to the ice in Arctic conditions.

From these studies we show that the evolution of an oil spill in the Arctic is a much slower phenomena than in temperate waters. The area covered, even from a supertanker spill, is quite small, on the order of some few square kilometers. Thus the technological problem of combatting Arctic oil spills is much different than that in temperate water: it is not likely that barriers will be useful or needed. A system with rapid response time is not required. On the other hand, there seems to be no presently known way to locate easily, much less remove, oil trapped under oil in ice.

2. DESCRIPTION OF SPILL

In this section we give an analysis of the events immediately following the release of oil in the Arctic. To do this we must develop a description of the rough ice surface. We shall consider the ice to have an average height $\langle h \rangle$, above sea level. The actual height of the ice is then equal to

$$h(x) = \langle h \rangle + h'(x) \tag{1}$$

$h'(x)$ denotes the variable roughness of the ice surface. Where h' is negative, oil spilled will tend to accumulate.

The data on h' are typically gotten[3] from a laser profilometer mounted on an aircraft flying over ice. The signal which results from such a measurement appears essentially random. There seem to be no features which distinguish one area of rough ice from another (nor should there be, on physical grounds). If no statistical distinction can be made between different areas of rough ice, then mathematically speaking the random variable, $h'(x)$ may be considered a stationary stochastic function.

To study the pocketing of oil on the rough ice surface, one is lead to ask over what extent h' is negative, so as to determine how large the pocket is.

But, the standard analysis of ice roughness amounts to computing the power spectrum of h'. The power spectrum P is the Fourier transform of the auto correlation function, (f is a dummy variable)

$$\langle h'(x)\, h'(x + \tau) \rangle = \int_{-\infty}^{\infty} P(f) \cos 2 f \, df \tag{2}$$

We can make such a statement because, as no region of the surface is statistically distinct from other regions, the average, $\langle h'(x)\ h'(x+\tau)\rangle$ only depends on τ. Then P only depends on f.

Up to now, we have been discussing how one region of the surface is correlated with another, located at an arbitrary distance τ away. However, the actual data are now more restrictive, as the aircraft flies straight while the profilometer records surface roughness. For our application τ is a distance along the surface parallel to the flight path.

$$\langle \underline{h}'(x)\ \underline{h}'(x+\tau)\rangle \quad \text{where} \quad \underline{h}'(x) = \begin{cases} h'(x), & h < 0 \\ 0 \text{ elsewhere} \end{cases} \tag{3}$$

This is a major theoretical problem. In this report, we shall only summarize the mathematical theory we have developed[4]. A detailed physical description of the results will be given.

It turns out that to relate (3) to (2), additional information, beyond P(f) is required. Basically, we use the fact that h is normally distributed, i.e. if $\delta(h)dh$ gives the fraction of the time h will be between h and h + dh, then $\delta(h)$ has the form

$$\delta(h) = \frac{1}{\sqrt{2\pi}\sigma_h} \exp\left[\frac{-(h - \langle h\rangle)^2}{2\sigma_h}\right] \tag{4}$$

Here, $\sigma_h = \langle (h')^2\rangle$, the mean square roughness height. Figure (3) compares $\int_{-\infty}^{h} \delta(\tau)d\tau$ against h for a suitable value of σ_h. The solid line is the theory, and the points are field data from reference (3).

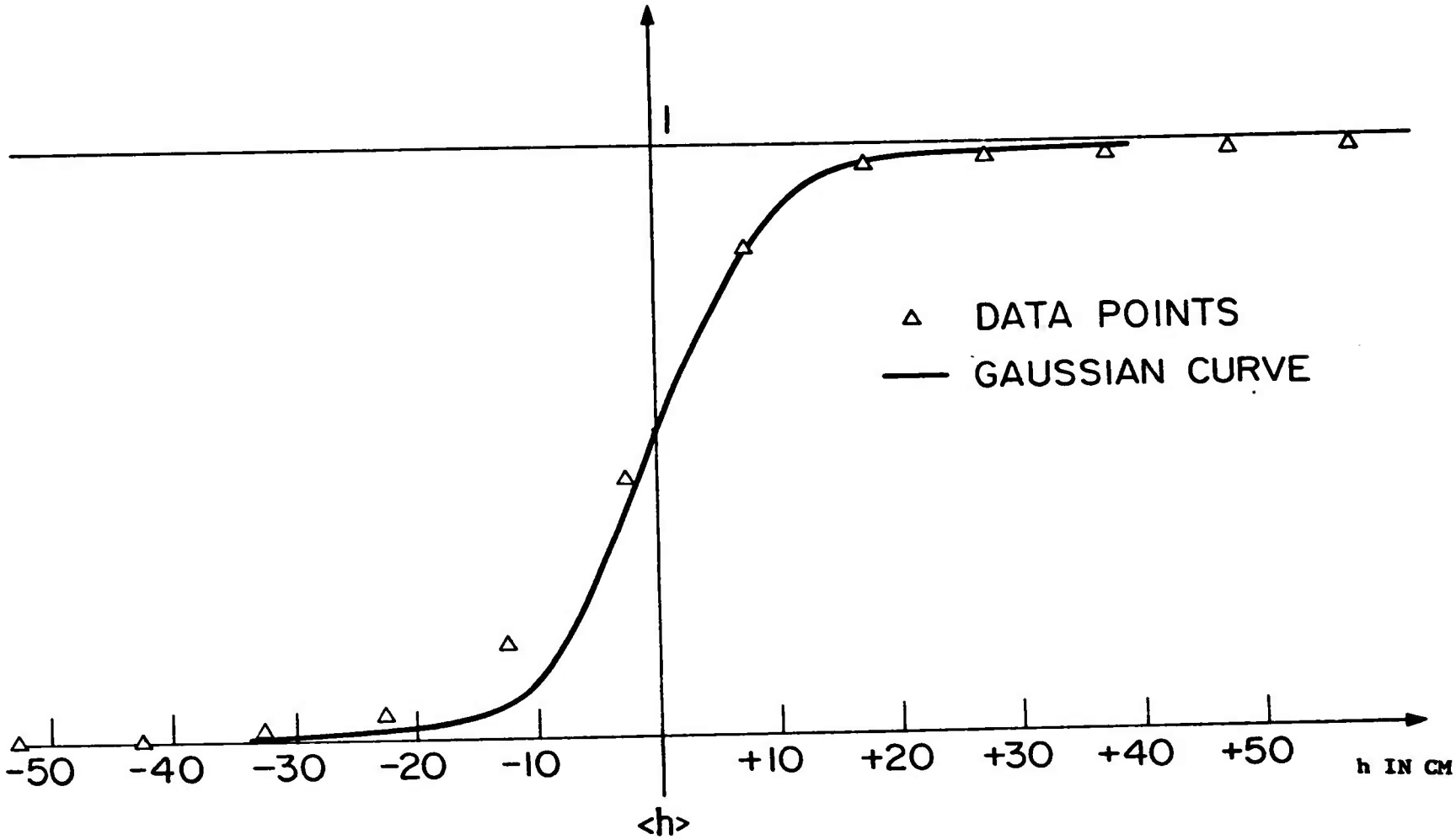

FIG. 3 VERIFICATION FOR h NORMALLY DISTRIBUTED

The remaining parameters which characterize the surface are measures of the horizontal scales of the surface. We have found that the field data[3] fit a power spectrum calculated by assuming

$$\langle h'(x)\, h'(x+\tau)\rangle = \frac{\sigma_h}{1+k\tau^2} \cos\frac{2\pi\tau}{T} \qquad (5)$$

provided suitable choices of k, T and σ_h are used. Figures (4, 5 and 6) show the comparison between field data and Eq. (5).

Physically, $\sqrt{\sigma_h}$ is the roughness height. T is the horizontal length of a given pocket. $k^{-1/2}$ is the distance in which the correlation between h'(x) and $h'(x+\tau \approx x + k^{-1/2})$ becomes negligible.

Suppose now that a surface, characterized by σ_h, k and T is specified. Let oil be released on this surface. The oil spreads, and we next proceed to estimate how fast the oil spreads.

There is little doubt that the oil spreads due to gravity. Let capital H be the thickness of the oil layer, and Δ the difference in specific gravity between oil and water. Then the driving force is

$$2\pi(\rho\Delta g H)Hr \quad \text{where } \Delta = \begin{cases} 1 \text{ over ice} \\ \Delta \text{ under ice} \end{cases} \qquad (6)$$

as r is the radius of the oil pool at a time t.

After careful study of all available data, we have found that the retarding force is a frictional one, as the oil reaches new pockets. This frictional drag is concentrated at the leading

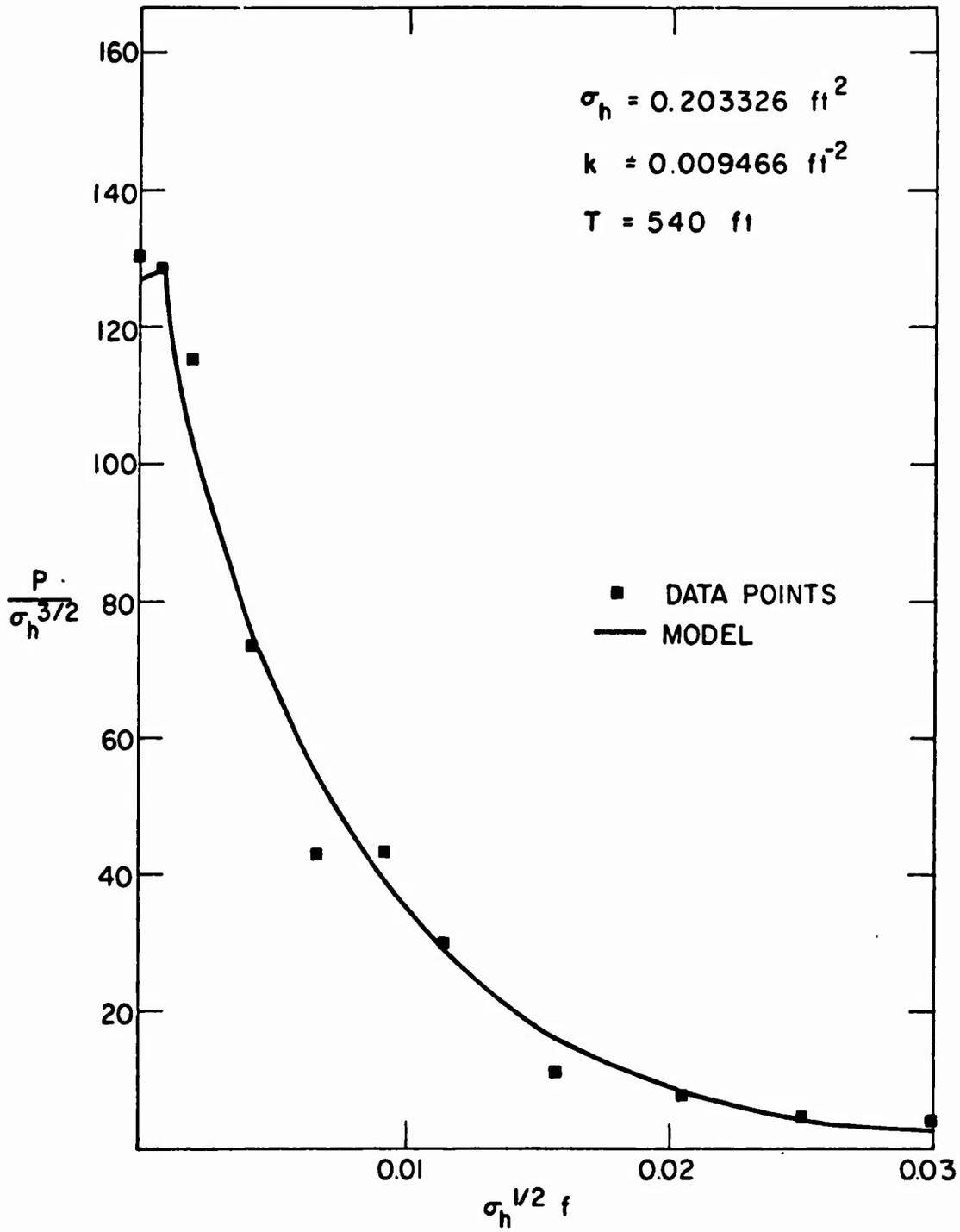

FIG. 4 EXAMPLE OF ONE-DIMENSIONAL POWER SPECTRUM

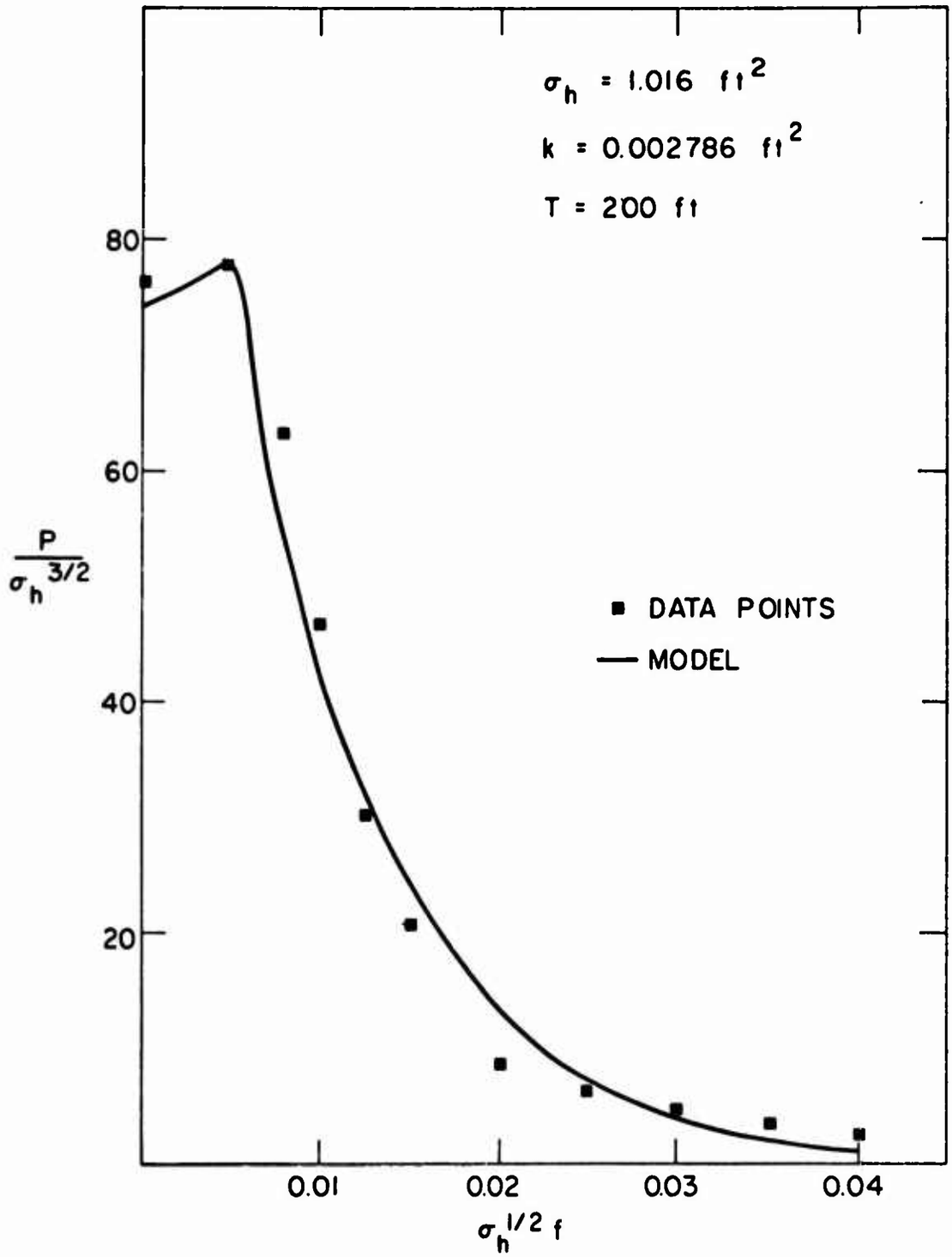

FIG. 5 EXAMPLE OF ONE-DIMENSIONAL POWER SPECTRUM

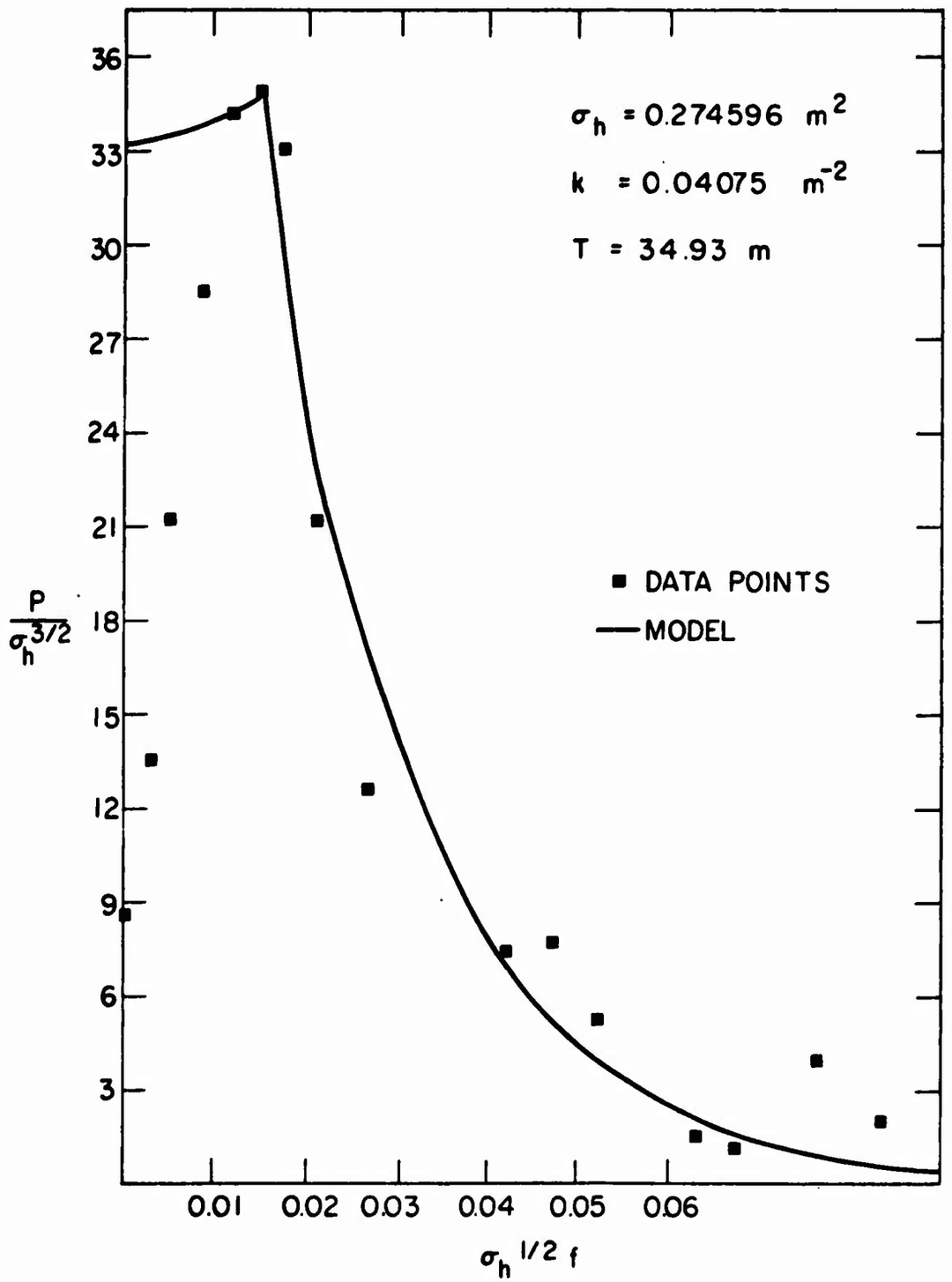

FIG. 6 EXAMPLE OF ONE-DIMENSIONAL POWER SPECTRUM

edge of the oil slick. For radii less than r, the oil flows over filled pockets of oil with essentially no friction.

Because this pocket filling process is controlling the rate at which the oil spreads, it turns out that the oil spreading rate is controlled by rate of release of the oil. For simplicity, we shall assume an average rate of volume released, Q. Continuity then requires that

$$\pi r^2 H = Qt \tag{7}$$

The frictional retarding force is proportional to the "area" of the roughness seen by the approaching oil, ($\langle \underline{h}' \rangle = \frac{1}{2}\sqrt{\sigma_h}$)

$$2\pi r \langle \underline{h}' \rangle$$

The pressure drop experienced as the oil flows into new pockets is proportional to, and is caused by the drag exerted by the rough surface on the oil.

$$\rho \left(\frac{dr}{dt} \right)^2$$

where $\frac{dr}{dt}$ is the velocity of the oil at the leading edge of the slick. Balancing the driving and retarding force gives

$$2\pi(\rho \Delta g H) H r \sim 2\pi r \langle \underline{h}' \rangle \rho \left(\frac{dr}{dt} \right)^2 \tag{8}$$

By using Eq. (7), we can determine that, as $\frac{dr}{dt} \sim \frac{r}{t}$, (the coefficient, 0.25 is determined empirically)

$$r = 0.25 \left(\frac{\Delta g Q^2}{\langle h' \rangle} \right)^{1/6} t^{2/3} \qquad (9)$$

Fig. (7) shows that this simple equation correlates both the laboratory data[5] and field data[1],[6]. In working out calculations of how fast oil spreads over or under ice, Eq. (9) should be used.

The laboratory data were gotten by building several random rough surfaces whose characteristics could be fitted empirically by Eqs. (4 and 5). Experiments were done both for oil spreading under and over the ice surface[5].

Oil spreading in a lead filled with water is easily treated as are other spills over water[7]. That is, there are several phases of oil spreading - inertia, viscous and finally surface tension. There are standard formulae[8] which give the rates of spread. However, there is one important modification which arises in the Arctic; the surface tension phase of oil spread is absent, because the net spreading coefficient is essentially zero. This means that the motion ceases when the oil reaches a certain thickness, on the order of 1cm[1]. Practically speaking, then, Eq. (9) and those referenced[8] provide a method of working out the spreading rate of oil spilled in the Arctic.

The spreading stops when either (a) the oil thickness on water reaches about 1cm, or (b) if the oil fills all the pockets of the ice field. In the first case, the area of water covered by oil is simply proportional to the volume released:

$$\text{Area} = \text{Volume/thickness} \qquad (10)$$

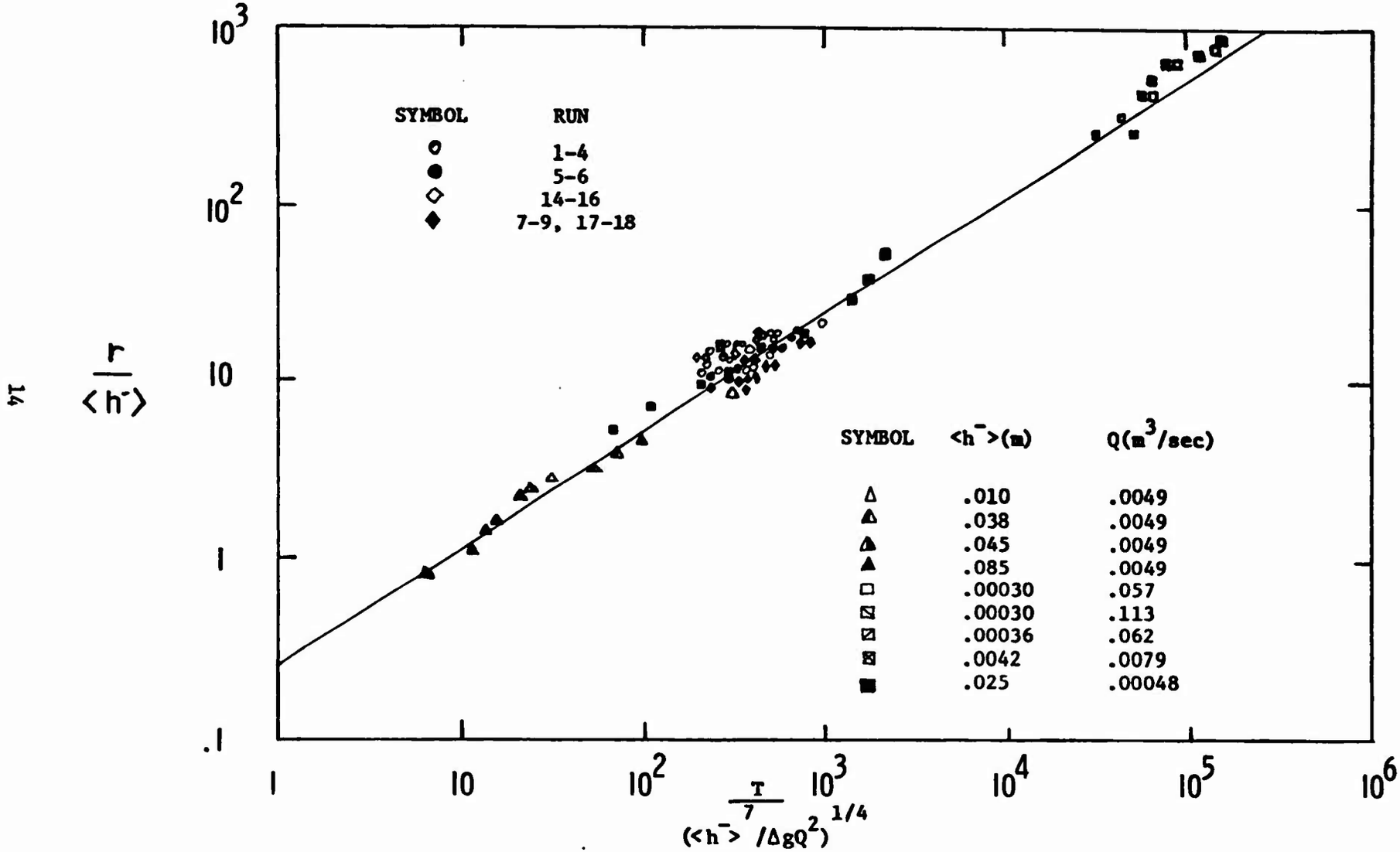

FIG. 7 DIMENSIONLESS RADIUS vs TIME FOR LABORATORY AND FIELD DATA

The situation is more complex in the second case. If the rough ice data is fitted with Eq. (5), then Patureau[4] shows that the surface area of an average pocket, Smp, is

$$Smp = T^2 \tag{11}$$

and the average volume of a pocket is

$$Vmp = \frac{2T^2}{\pi^2} (2\sigma_h)^{1/2} \tag{12}$$

Now the area that an oil slick will occupy depends simply on the average number of pockets which can be filled with oil. Clearly the total area covered must then be proportional to the volume spilled, and inversely proportional to Vmp. The exact result[4] is

$$\langle S_{max} \rangle = Smp \frac{4}{\pi 3/2} \left(\frac{V}{Vmp} \right) \tag{13}$$

$\langle S_{max} \rangle$ is the average area of a spill over or under ice. For a random rough surface, Figs, (8 and 9) compare this result with laboratory data. It is seen that there is fairly good agreement with this result.

Using this result, we can estimate the area covered by an oil spill on ice. Table I shows the results for a spill of $V = 5 \times 10^5$ ft.^{3} (about 15,000 tons) for three sets of T, σ_h gotten from Arctic data[4].

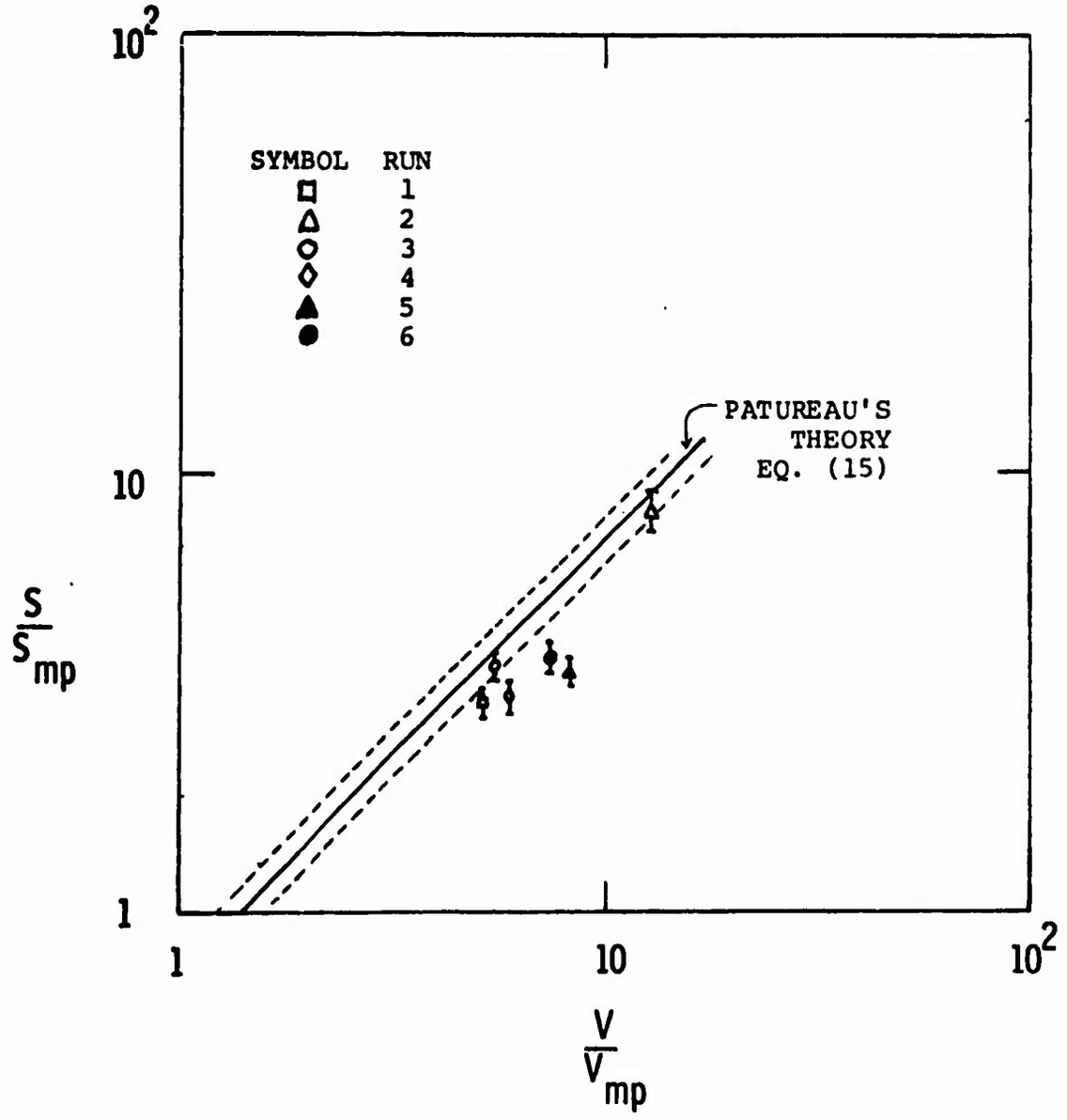

FIG. 8 DIMENSIONLESS VOLUME RELEASED vs SURFACE AREA FOR SURFACE 1

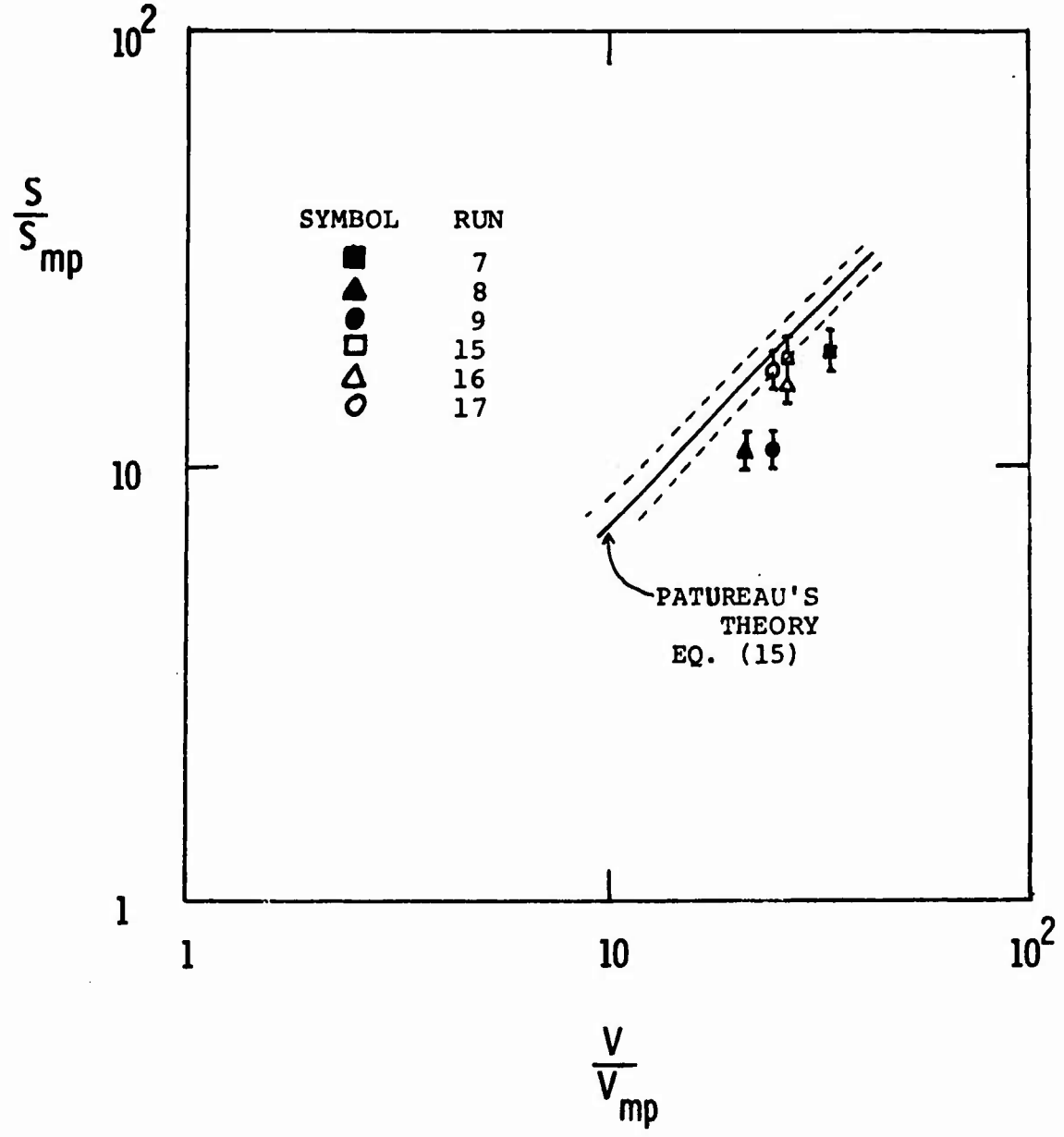

FIG. 9 DIMENSIONLESS VOLUME RELEASED vs SURFACE AREA FOR SURFACE 2

TABLE I

T	σ_h	Smp	$\langle S_{max} \rangle$
115 ft.	2,295 ft.^{2}	1.32×10^4 ft.^{2}	7.29×10^5 ft.^{2}
200 ft.	1.016 ft.^{2}	4×10^4 ft.^{2}	1.24×10^6 ft.^{2}
540 ft.	0.203 ft.^{2}	4×10^4 ft.^{2}	2.78×10^6 ft.^{2}

If a super tanker full of oil, 150,000 tons, were spilled, then for ice described in Table I, one gets areas ranging from 1/4 to 1 square mile as the area covered. Such small areas should be contrasted with the Torrey Canyon experience - in that case, the oil spread to some 300 square miles in area. On Arctic ice, in contrast, the present study predicts a much smaller area.

The calculations of $\langle S_{max} \rangle$ in Table I are based on one dimensional spectra, and the assumption that the statistics are the same in all directions on the ice surface. This is a crude assumption, which was made because no two dimensional spectra of ice field roughness are currently available. However, using a variety of assumptions of the asymmetry of ice roughness elements does not change the result by much more than a factor of three.

Although there is very little field data on the characteristics of the under ice roughness[3], it is approximately true that the ice is in hydrostatic equilibrium. If we assume that this is exactly true, then for the under ice surface, T is the same as that of the over ice roughness, and the roughness height, $\sqrt{\sigma_h}$, is about seven times greater; as 1/7 of the ice is above the mean water level. Thus, the mean pocket volume, Vmp, is seven times greater for the under ice surface. (See ref. 2)

If we consider two cases, one in which a volume V of oil is spilled over the ice, and another where the same volume is spilled under the ice, then the above argument suggests that the area $\langle S_{max} \rangle$ of the oil under the ice is 1/7 that of the area over the ice.

The hydrostatic assumption is too crude to permit the accurate estimate of this area ratio. But it is quite clear that the Vmp, mean pocket volume, under the ice must be much greater than over the ice.

All the results of this section may be summarized as follows: At the end of the spreading phase of an Arctic spill, the oil will be trapped either in a lead or on the ice surface; and the area will be much less than what one would expect in temperate climates. Practically speaking, we expect that a super tanker spill will occupy at most about a square mile in area.

3. EVOLUTION OF OIL IN THE ARCTIC

In this section we consider what happens after the spilled oil has ceased to spread. Then the oil will either be in pockets above or below the ice surface, or in a lead, floating on sea water. From a mechanical point of view, we are interested in whether the oil may migrate, over a long period of time, from the origin of the spill. There are really only two potential causes for such migration. First, there is the slow increase in oil density with time - we refer to this process as aging. In about two weeks, in the Arctic summer,[1] the density of North Slope crude increases to 0.95, which is heavier than virtually all Arctic ice.

In the Arctic summer, the dark oil on the surface of the ice absorbs enough heat to float in a pool of melt water. If

a lead now opens, the oil will flow into it. If the lead then closes, the oil will flow either under or over the ice depending on whether it is lighter or heavier than the surrounding ice. In this sequence of events, the oil density determines whether the oil will flow under or over the ice.

The second major factor in migration of oil is the question of whether oil sticks to ice or not. We have done a separate experiment to determine the stickiness of North Slope crude and diesel oil to sea ice, and find that substantial amounts of oil stick to ice. In particular, this stickiness, discussed below, apparently precludes the dispersion of oil under the ice by the action of currents.

Because of these somewhat unexpected results, the evolution of oil spilled in the Arctic will generally consist of an evaporation of the lighter fractions, causing an increase in density. Second, if the oil is located under the ice, it will stick to the ice. In the winter season, oil located over the ice will stick to the ice also. In summer , the oil located over the ice does not stick, but floats in a pool of melt water.

From this discussion, it is apparent that the evolution of spill oil hinges on an analysis of how the density of the oil changes with time, and how the oil sticks to the ice surface.

A. The Evolution of the Boiling Point Distribution

The purpose of this section is to develop equations which describe the boiling point distribution of crude oil as it ages on ice or water. We assume, firstly, that at all times the oil is well mixed. That is, the concentration of the ith component of oil is always uniform throughout the oil. The argument for this assumption goes as follows:

If the oil spreads to a thin (1 cm) layer on water, intermolecular diffusion will smear out any gradients of concentration in a short time (1 day). On the other hand, if the oil is pocketed in deep pools, the action of wind will be to make waves on the oil surface which will mix the oil. Even in the Arctic winter, when the oil on the ice surface is frozen solid, we believe this will be a good assumption because the time constant for evaporation increases exponentially with decreasing temperature, whereas the mixing time for oil is at most the time for characteristic changes in the ice field, i.e. less than a month. The assumption is that this mixing process will always have a time constant which is less than the time constant for evaporation.

Second, we use a simple turbulent diffusion model, based upon a neutrally stratified air flow over a rough flat plate. There is no question that there will be departures from neutral stability in the air flow over the oil or the Arctic Ocean. However, these departures will be unimportant near the rough surface, as there the roughness elements will dominate the mixing process, provided there is an appreciable wind velocity[9]. Under this assumption, the diffusivity at sea level is

$$ku^*z$$

where z is the roughness height, u^* is the friction velocity and k is Von Karman's constant, having a value of 4/10.

To compute a flux we need to know the gradient of the concentration of the oil vapor in the air. We argue that,

due to the low rate of evaporation, there will be essentially zero vapor concentration for heights greater than z. On the other hand, due to the strong mixing induced by the roughness elements, we must expect finite concentrations for heights less than the roughness height. Hence, the length scale for the concentration gradient is z. The flux is proportional to the concentration times

$$\lambda u^*$$

Third, following Blockker[10], we assume the oil, which is a mixture of a large number of organic components, is considered an ideal thermodynamic mixture. Although this assumption is certainly untrue in detail, we expect that the discrepancies caused by non-ideal behavior will not cause any quantitative changes in the results. This assumption implies Rauolt's law is valid.

In the same vein, the oil vapor of the ith species is considered a perfect gas. The vapor pressure of the ith component over its liquid obeys a Clapeyron equation. These are excellent assumptions because the temperatures of the vapors are all low compared to the critical temperature for the substances involved, and the gases are all dilute.

Finally, let us show that evaporation into the air dominates dissolution of oil into the water. The mass flux per unit area of the ith fraction of oil to the air is

$$c_i \lambda u^*$$

where c_i is the density of the ith component of oil vapor at the oil surface. The flux of the ith component to the water is about

$$\rho_{H_2O} S_i \lambda u_w^*$$

where S_i is the solubility of the ith component in sea water.

Now u_w^* is much smaller than u^*. To see this, consider the case where the oil lies at the water-air interface. At the interface, the turbulent stress is continuous. Hence

$$u_w^* = u^* \sqrt{\frac{\rho_{air}}{\rho_{H_2O}}}$$

Using these results, the ratio of evaporation to air to flux to water is

$$\frac{c_i}{\rho_{H_2O} S_i} \sqrt{\frac{\rho_{H_2O}}{\rho_{air}}}$$

Typical values at 0^oC are $c_i = 10^{-1} \rho_{air}$, $S_i = 10^{-4}$ and $\rho_{H_2O}/\rho_{air} = 10^3$.

Hence the ratio is on the order of 30. We shall ignore dissolution of oil into water.

Consider now a mass of oil, containing i fractions, each with a molecular weight M_i. The mass of each fraction is m. The mole fraction, x_i depends on the number of moles in the ith fraction, n_i, as

$$x_i = \frac{n_i}{N} = \frac{n_i}{\Sigma n_i} \tag{14}$$

The mass of the ith fraction is

$$NM_i x_i = m_i \tag{15}$$

Since the volume occupied by each fraction, V_i is related to the density of each component as

$$m_i = \rho_i V_i$$

it can be seen that the bulk density is

$$\frac{1}{\rho} = \frac{V}{m} = \frac{\Sigma M_i x_i / \rho_i}{\Sigma M_i x_i} \tag{16}$$

Raoult's law[11] states that the partial pressure of the ith component is proportional to its saturated vapor

pressure P_i^o and the mole fraction x_i

$$P_i = x_i P_i^o$$

The saturated vapor pressure is determined by Clapeyron's equation

$$\frac{P_i^o}{P_B} = \exp\left[\frac{qM_i}{R}\left(\frac{1}{T_{B_i}} - \frac{1}{T}\right)\right] \tag{17}$$

This equation relates the ith component to its boiling temperature T_B. At T_B, the ith component has a saturated vapor pressure of P_B = 1 atmosphere. Here q is the latent heat of vaporization and R, the universal gas constant.

Next, we relate the partial pressure P_i to the density of the vapor about the oil, c_i assuming the vapor to be a perfect gas.

$$c_i = \frac{P_i M_i}{RT} \tag{18}$$

Using (14) and (18) in combination we determine the rate of evaporation of the ith component to be, for an exposed area A,

$$\frac{dn_i}{dt} = -\left(\frac{\lambda u^* P_B A}{RT} \exp\left[\frac{qM_i}{RT_B}\left(\frac{T - T_B}{T}\right)\right] \frac{n_i}{N}\right) \tag{19}$$

The solution of (19) gives $n_i(t;T_B)$ and N(t). By equations (14) and (15), this is equivalent to knowing M(t) nd $M_i(t,T_B)$. The evolution of the boiling point distribution is normally represented in graphical form with one axis being the fraction having boiling temperatures higher than T_B^*, that is

$$\frac{1}{m} \sum_{T_B > T_B^*} m_i = \frac{N}{m} \sum_{T_B > T_B^*} M_i x_i \qquad (20)$$

and the other axis being T_B. (T_B^* is a dummy variable)

B. The Evolution of Density in an Oil with a Continuous Distribution of Boiling Points

The purpose of this section is to extend the previous results to an oil of infinitely many components, each with a mole fraction dx. To do this, we must associate with each boiling point a molecular weight, $M(T_B)$. Of course, there is not a one to one relationship between molecular structure of each component of the oil. But it is not realistic to identify each of the large number of components in a typical crude oil. Figure 10 shows the relationship $M(T_B)$ for various classes of hydrocarbons[12]. The solid line shown is simple linear fit for the lower boiling points:

$$M(T_B) = 0.42(T_B - 106°) \qquad (21)$$

(Note that T_B is absolute temperature)

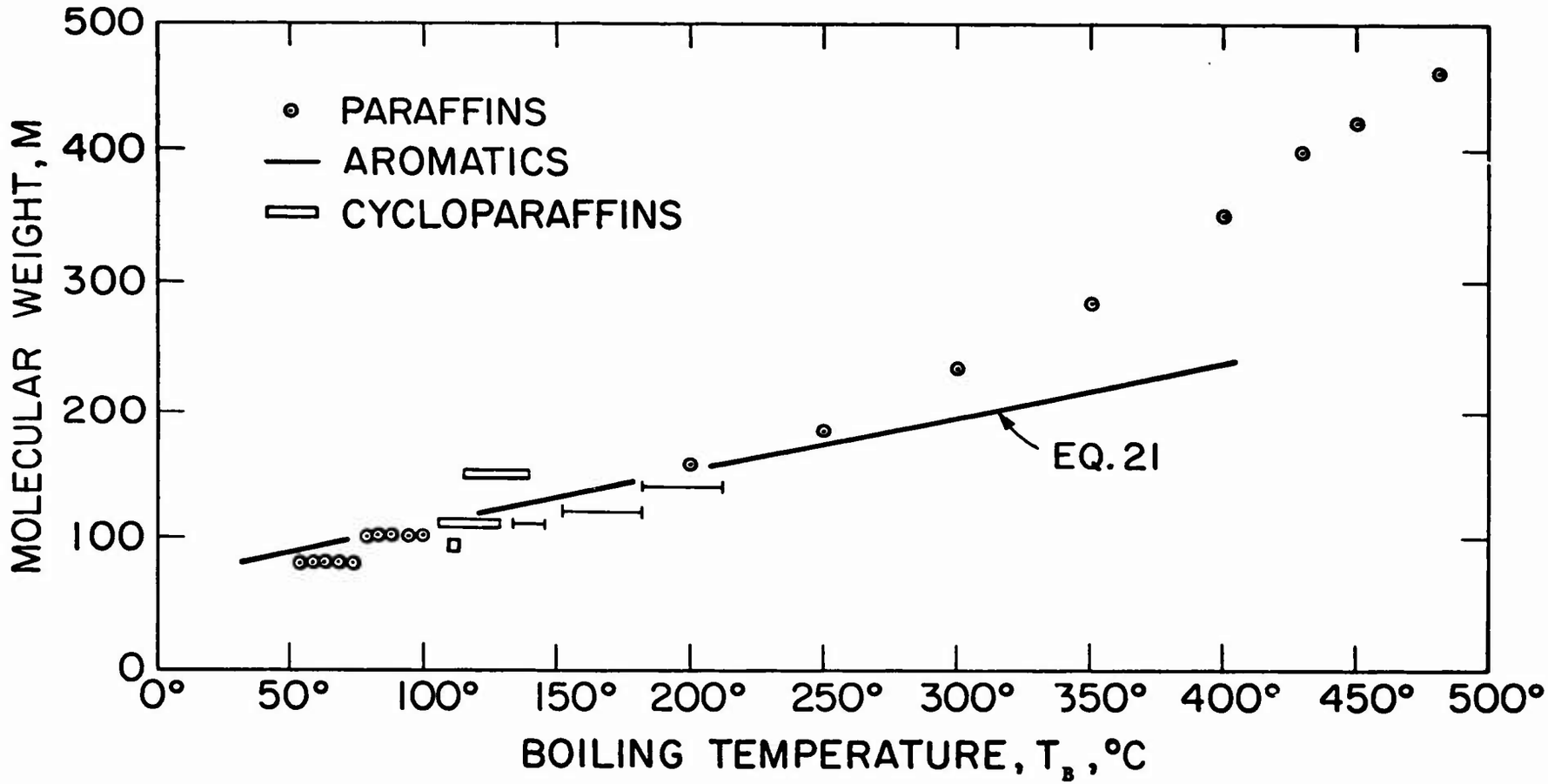
500
400
300
200
100
0
MOLECULAR WEIGHT, M
PARAFFINS
AROMATICS
CYCLOPARAFFINS
EQ. 21
0°
50°
100°
150°
200°
250°
300°
350°
400°
450°
500°
BOILING TEMPERATURE, T_B, °C

FIG. 10

Knowing the molecular weight, we now proceed to consider an oil with incremental mole fractions, $dx(T_B,t)$. The mass of oil is

$$M = N \int_{T_1}^{T_\infty} M dX(T_B) \tag{22}$$

where the integration is carried out over T_B. This convention will apply below.

The boiling point distribution may be defined, using Eqs. (22) and (20) as

$$b(T_B,t) = \frac{\int_{T_B}^{T_\infty} M dx}{\int_{T_1}^{T_\infty} M dx} \tag{23}$$

As the number of moles in each species is $dn = Ndx$, Eq. (19) may be written

$$\frac{d}{dt} N \int_{T_1}^{T_B} dx = - \frac{\lambda u^* P_B}{RT} A \int_{T_1}^{T_B} \exp \left[\frac{qM}{RT_B} \left(\frac{T - T_B}{T} \right) \right] dx \tag{24}$$

To evaluate Eq. (24) we need to know how q depends on T_B. Trouton's rule (see Ref. (10)) is that $\frac{qM}{RT_B}$ is approximately a constant - its value is near 5.0.

Given $b(T_B, t = 0)$ and $N(t = 0)$ Eq. (23) may be used to compute $x(T_B, t = 0)$. Eq. (24) plus the constant,

$$\int_{T_1}^{T_\infty} dx = 1, \; x > 0, \tag{25}$$

then specify how $N(t)$ and (T_B, t) change with time. This determines the evolution of $b(T_B, t)$.

The bulk density is related to x by

$$\frac{1}{\rho} = \frac{\int_{T_1}^{T_\infty} \frac{Mdx}{\rho_i(T_B)}}{\int_{T_1}^{T_\infty} Mdx}$$

If all fractions which have boiling points less than T_B' have been evaporated, then

$$\frac{1}{\rho(T_B')} = \int_{T_B'}^{T_\infty} \frac{Mdx}{\rho_i(T_B)} \Big/ \int_{T_B'}^{T_\infty} Mdx$$

Recognizing that the density changes are always small, to a good approximation, in the range $50^oC < T_B < 500^oC$,

$$\rho(T_B') = \rho(T_B' = 273^o) + \left(\frac{\Delta\rho}{\Delta T_B'}\right)(T_B' - T_1) \tag{26}$$

where $\frac{\Delta\rho}{\Delta T_B'} = 2.8 \times 10^{-4} \frac{gm}{cc\,^oK}$, from Figure 11.

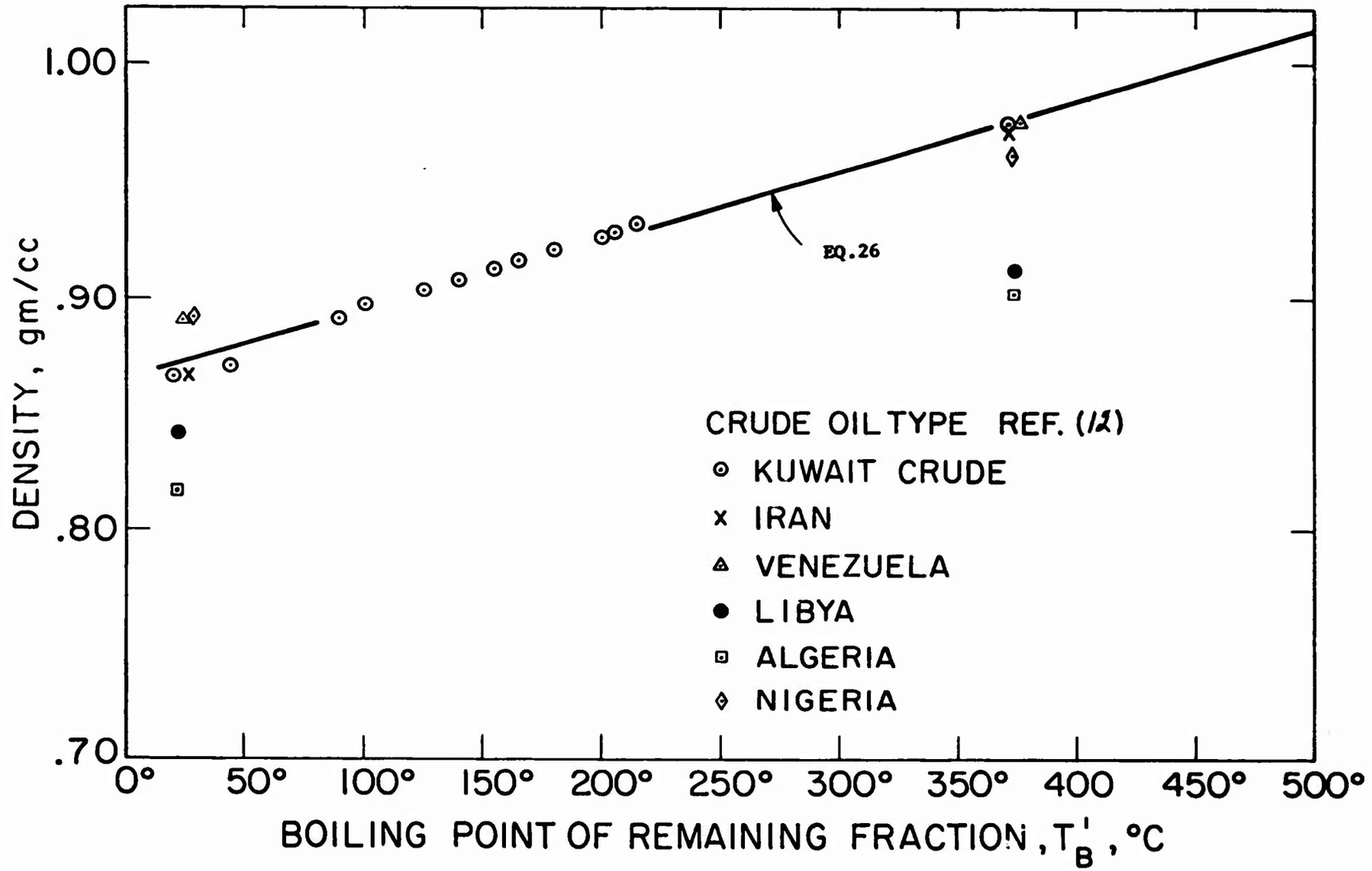
1.00
.90
.80
.70
DENSITY, gm/cc
EQ.26
CRUDE OIL TYPE REF. (12)
KUWAIT CRUDE
IRAN
VENEZUELA
LIBYA
ALGERIA
NIGERIA
0°
50°
100°
150°
200°
250°
300°
350°
400
450°
500°
BOILING POINT OF REMAINING FRACTION, T_B', °C

FIG.//

For Kuwait crude $\rho(T_B' = 273^oK) = 0.869$. In figure 1 of reference (12) we find that, for Kuwait crude $b(T_B)$ is approximately a linear function of T_B; rising from 0 at 50^oC to 1 at 500^oC.

$$b(T_B) = (T_B - 323^oK)/450^oK \tag{27}$$

By differentiating Eq. (23) and using this result, we determine that

$$\frac{dx}{dT_B} = -\frac{A}{M}, \quad A = \text{const} \tag{28}$$

With this result we may invert Eq. (27) to find the density, $\rho_i(T_B)$, of the fraction of oil which boils at T_B. The result, obtained by using Eqs. (24), (25), (26), and keeping only first order changes in $\Delta\rho$ is

$$\rho_i(T_B) = \rho_i(T_1) + (\Delta\rho/\Delta T)\ (T - T_1)\ ;\ \frac{\Delta\rho_i}{\Delta T} = \frac{\Delta\rho(T_B')}{\Delta T} \tag{29}$$

Provided $\rho(T_B')$ and $b(T_B)$ are known for a given crude oil, $\rho_i(T_B)$ may be determined in a manner analogous to the derivation of Eq. (27).

At this point, we see that if $b(T_B, t = 0)$, $N(t = 0)$ and $\rho(T_B', t = 0)$ are given we may perform the following steps to obtain a solution to the problem. First, $\rho_i(T_B)$

is gotten from (T_B', t = 0) and b(T_B, t = 0). Second, Eqs. (24) and (25) are solved to yield N(t) and x(T_B,t). Third, b(T_B,t) is evaluated using Eq. (23). Fourth, ρ(t) is determined using Eq. (29). In this manner, the evolution of the oil is specified.

C. Calculations

For the purpose of calculation, it is simplest to define the characteristic time, τ, as

$$\tau(T_B) = \frac{1}{\frac{\lambda u^* P_B A}{RT} \exp\left[\frac{qM}{RT_B}\left(\frac{T - T_B}{T}\right)\right]} \qquad (30)$$

Figure 12 shows the behavior of the characteristic time for various points and various values of T. In this figure Trouton's rule, $qM/RT_B = 5.0$, was used. This chart shows the significant decrease in aging rate of volatile components as T, the ambient temperature, is decreased.

The first calculation we present is for a two component mixture. The lighter component has a boiling point of 200°C and the heavier, a boiling point of 400°C. For North Slope crude, about 25 percent of the oil has boiling points lower than 200°C and 25 percent has boiling points greater than 400°C. The molecular weights at these boiling points are $M_1(200^\circ C) = 150$, $M_2(400^\circ C) = 350$ from Figure 10. The densities are determined from Eq. (26) and $\rho(T_B' = 273) = .89$ to be $\rho_1 = .94$, $\rho_2 = 1.0$, at T = 273.

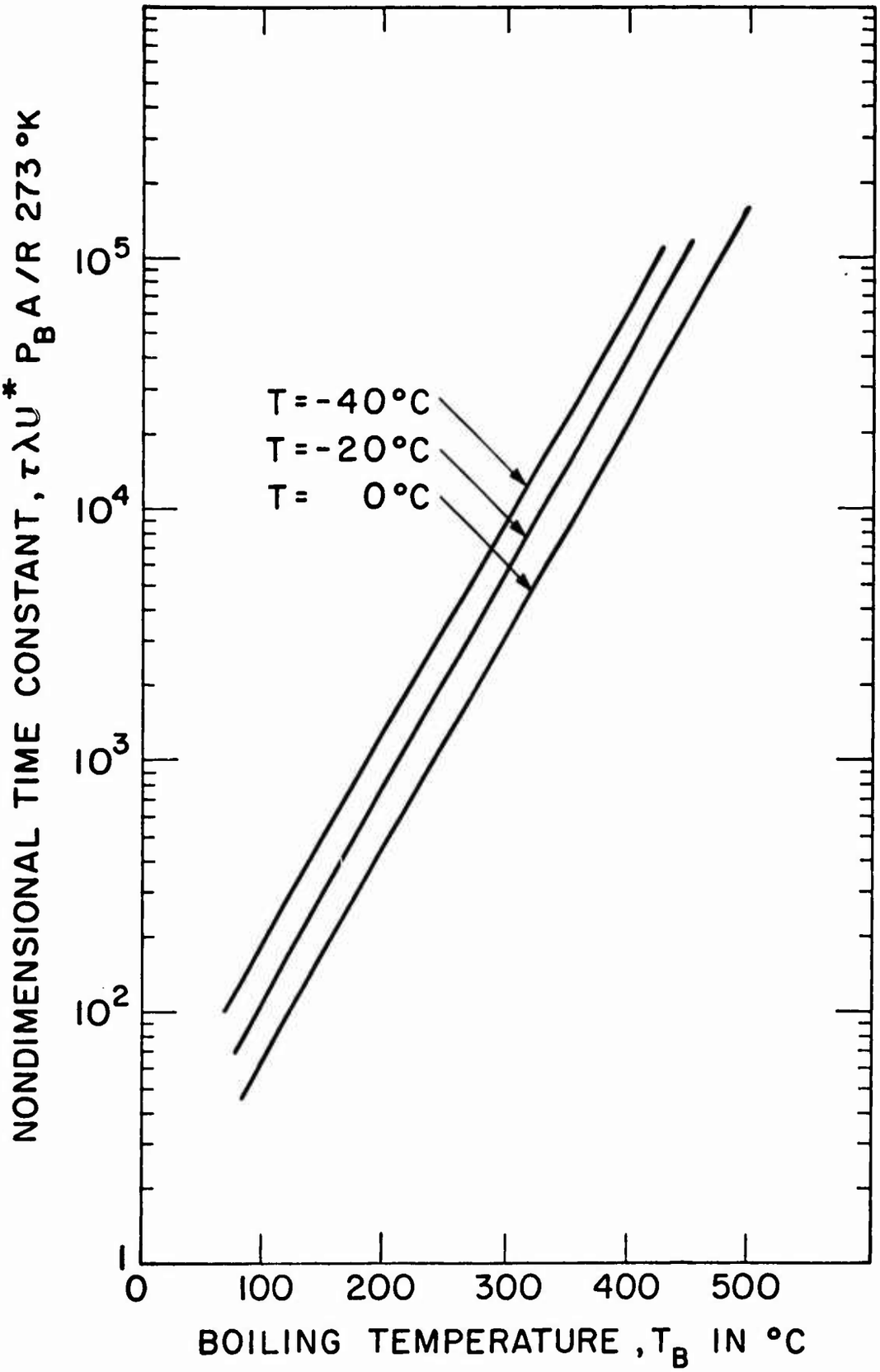
NONDIMENSIONAL TIME CONSTANT, $\tau\lambda U^* P_B A/R\ 273\ °K$
10^5
10^4
10^3
10^2
1
T=-40°C
T=-20°C
T= 0°C
0
100
200
300
400
500
BOILING TEMPERATURE, T_B IN °C

FIG. 12

Under these assumptions the equations of Section 3 take the simple form (from eqs. 14 - 20)

$$n_1 + n_2 = N$$

$$\frac{dn_1}{dt} = -\frac{1}{\tau_1}\frac{n_1}{N}$$

$$\frac{dn_2}{dt} = -\frac{1}{\tau_2}\frac{n_2}{N} \qquad (31)$$

By dividing one equation by the other, we obtain

$$\left(\frac{n_1}{n_1(t=0)}\right)^{\tau_1} = \left(\frac{n_2}{n_2(t=0)}\right)^{\tau_2} \qquad (32)$$

where the initial values, $n_1(t = 0)$ and $n_2(t = 0)$ are determined by the assumption that both fractions have equal mass at $t = 0$:

$$M_1 n_1 = M_2 n_2 ,$$

which gives, for one mole of mixture at time $t = 0$,

$$n_1(t=0) = \frac{M_2}{M_1 + M_2}, \quad n_2(t=0) = \frac{M_1}{M_1 + M_2} \qquad (33)$$

The evolution for $t > 0$ is determined by Eq. (30); hence

$$t/\tau_1 = -\int_{n_1(t=0)}^{n_1(t)} \left[\frac{dn_1}{n_1}\,(n_1 + n_2(0))\left(\frac{n_1}{n_2(0)}\right)^{\tau_1/\tau_2}\right]$$

By carrying out these integrals it can be shown that both fractions completely evaporate in the same time, t_{max} (see Ref. 2)

$$t_{max} = \tau_2\, n_2(t=0) + \tau_1\, n_1(t=0)$$

and

$$t = t_{max} - \tau_1\, n_1(t) - \tau_2\, n_2(t) \qquad (34)$$

Even though the n_1 fraction evaporates much more rapidly initially.

Figure 13 shows the boiling point distribution

$$b(T_{B_1}\,;\,t) = \frac{M_1 n_1}{M_1 n_1 + M_2 n_2}$$

$$b(T_{B_2}\,,\,t) = \frac{M_2 n_2}{M_1 n_1 + M_2 n_2} \qquad (35)$$

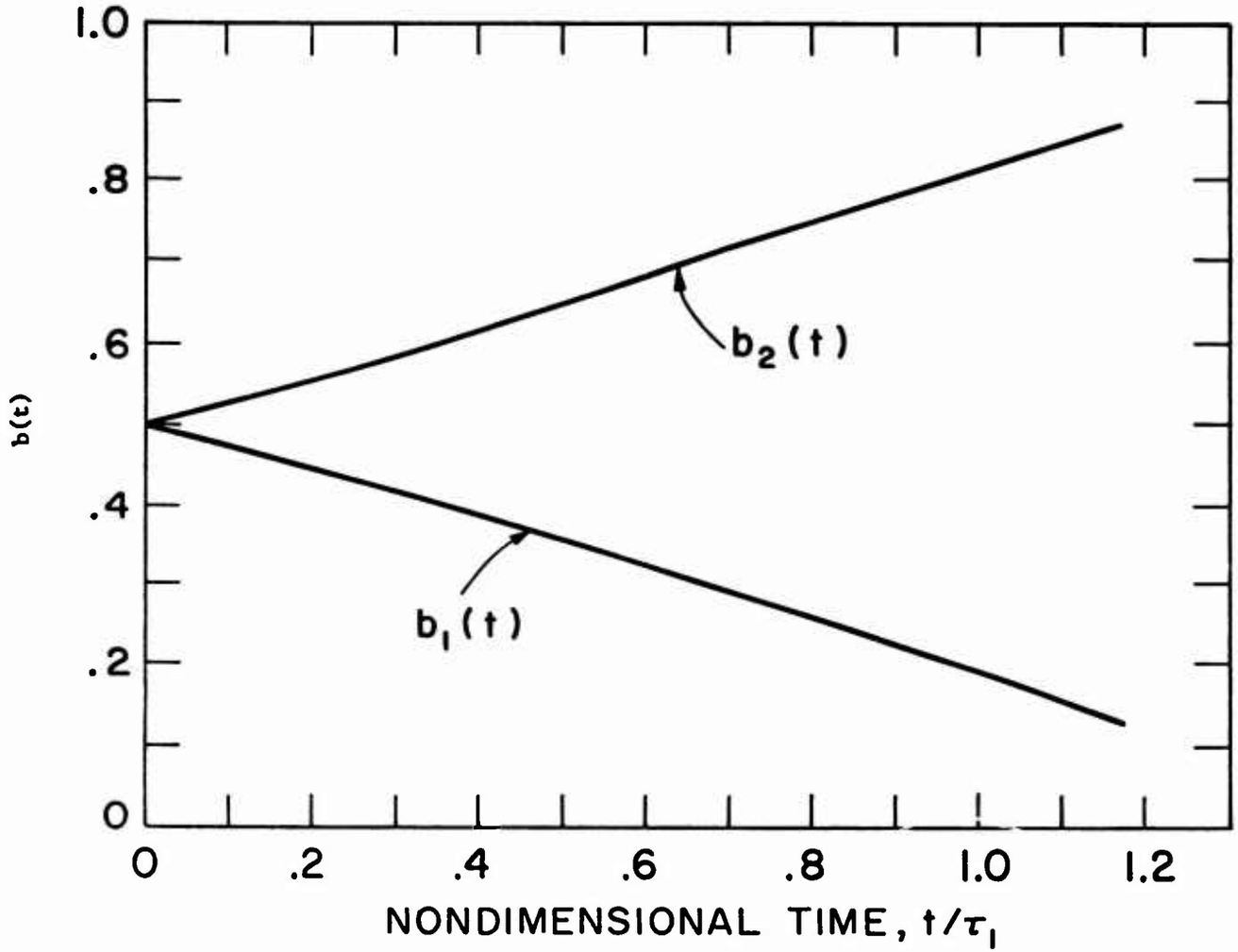

FIG. 13 THE EVOLUTION OF THE BOILING POINT DISTRIBUTION

The evolution of density,

$$\frac{1}{\rho} = \frac{b_1}{\rho_1} + \frac{b_2}{\rho_2} \tag{36}$$

is shown on Figures 15 and 14.

These results bear some discussion. On Figure 13 notice that there is a nearly linear decay in the light fraction, b_1, on a time scale τ_1. This decay produces a nearly linear increase in density as shown in Figures 15 and 14. The two component theory is too crude to predict the exact shape of the density vs. time curve, as observed.

To compare these results with observation[1,6] we estimate the area the oil sample will occupy, and a typical, average value of u^*. Fairly good agreement is obtained between theory and observation if $\lambda = k/10$.

The time scale for the evolution of the density, τ_1, is about 10 days for $T = 273^oK$ (0^oC), and about 14 days for $T = -17^oC$, the temperatures corresponding to summer and winter conditions. Much larger variations in τ_1 are predicted with variations in wind speed. The prediction is that during high winds, the aging process accelerates. This is observed[6]. (See Figure 15). No account is taken of the effect of snow cover, but when the oil was covered with snow, the aging process stopped[6]. (See Figure 15).

To account for the variation of τ_1 with temperature, Figure 12 should be used. Using Figure 13 we then can determine that, for components boiling at 200^oC, the time constant τ_1 is increased from 10 days to 17 days when the

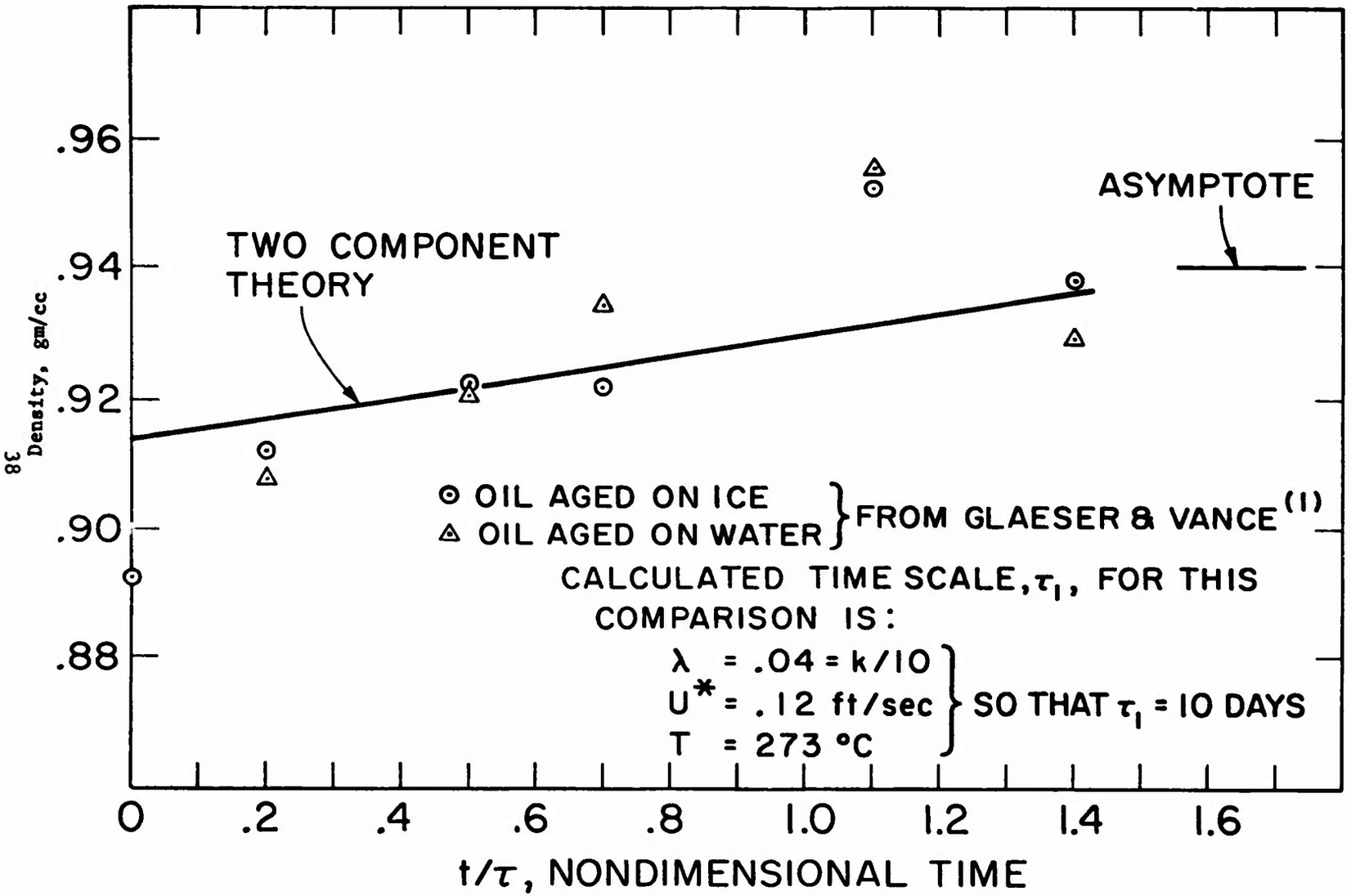
.96
.94
.92
.90
.88
ASYMPTOTE
TWO COMPONENT THEORY
ρ_{38} Density, gm/cc
⊙ OIL AGED ON ICE
△ OIL AGED ON WATER
} FROM GLAESER & VANCE (1)
CALCULATED TIME SCALE, τ_1, FOR THIS COMPARISON IS:
λ = .04 = k/10
U^* = .12 ft/sec
T = 273 °C
} SO THAT τ_1 = 10 DAYS
0
.2
.4
.6
.8
1.0
1.2
1.4
1.6
t/τ, NONDIMENSIONAL TIME

FIG. 14

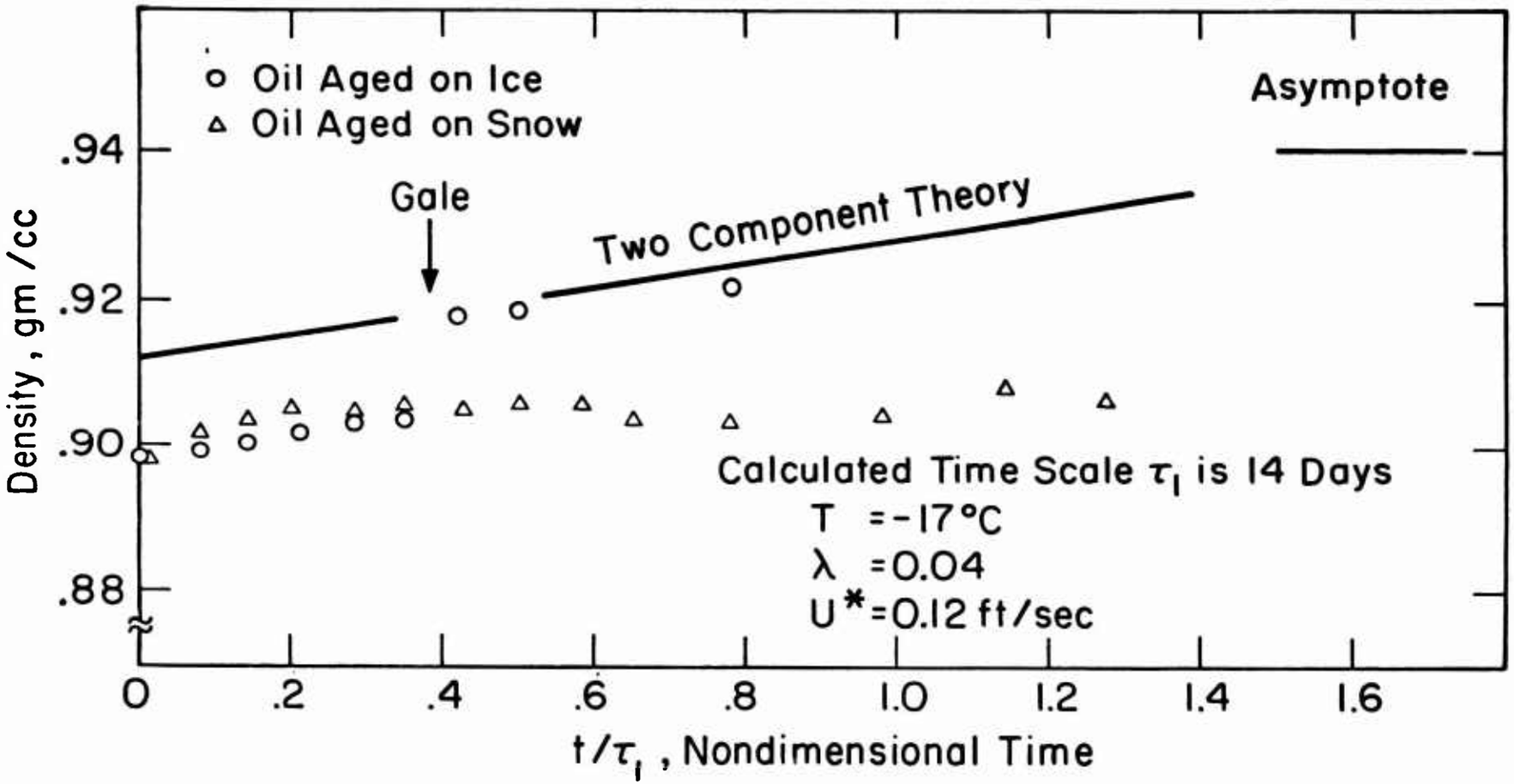
Oil Aged on Ice
Oil Aged on Snow
Asymptote
Gale
Two Component Theory
Density, gm/cc
.94
.92
.90
.88
Calculated Time Scale τ_1 is 14 Days
T = -17°C
λ = 0.04
U* = 0.12 ft/sec
0
.2
.4
.6
.8
1.0
1.2
1.4
1.6
t/τ_1, Nondimensional Time

FIG 15

ambient temperature is decreased to $-20^{o}C$. From Figures 15 and 14, it is clear that τ_1 is the time to evaporate the lighter components of the oil. Thus, we may say that in the Arctic winter, the aging time for oil is approximately doubled. Since it takes about 14 days for most of the lighter fractions to evaporate in the summer, it take about 1 month for the lighter fractions to evaporate in the Arctic winter.

We can show that having a continuous distribution of fractions with various boiling points does not change the picture outlined here. Differentiating Eq. (24) with respect to T_B produces an equation similar to Eq. (31). By analogy with the solution (34) for the two component model, it can be shown that the solution to Eq. (24) is

$$t = N \int_{T_1}^{T_\infty} \tau(T_B) \frac{\partial x}{\partial T_B} \Big|_t dT_B - N \int_{T_1}^{T_\infty} \tau(T_B) \frac{\partial x}{\partial T_B} \Big|_t dT_B$$

Since $N \frac{\partial x}{\partial T_B} dT_B = \frac{\partial n}{\partial T_B} dT_B$ is the moles in the fraction whose boiling point is T_B, this result may be written as

$$t = t_{max} - \int_{T_1}^{T_\infty} \tau(T_B)\, dn(t, T_B)$$

which can be readily recognized as exactly analogous to Eq. (34).

Thus, we may conclude that each fraction of oil decays as described by the simple two component model. Thus, Figure 12 can be used to predict the evaporation time of a

component with an arbitrary boiling point, T_B.

D. The Maximum Size of an Oil Spill

In this section, we summarize the results of Wolfe and Hoult[13]. The detailed report of this portion of the work has been written up as a separate paper, and is included as Appendix A.

If one assumes that, over a long period of time, the oil, due to density changes, migrates under the ice, then the question arises, does the oil stick to the under ice surface? To answer this question, an experiment was performed, in which sea water was frozen by a one-dimensional heat flux, thus simulating the Arctic situation. Oil was injected under the ice, and subsequent events were studied. The heat flux was maintained after the oil was injected.

It was found that, after some time, the ice began to freeze under the oil. If the freezing process continued long enough, an inclusion of oil, in ice, was formed. These results directly imply that if oil is spilled under the Arctic ice in the fall, it will be frozen into sea ice floes as an inclusion during the winter. In this way, a mixture of oil and sea ice is generated. Such mixtures have been observed during the Chetabucktoe Bay spill. Based upon this laboratory verification, we expect that most oil spilled in the Arctic will end up as in a mixture of ice and snow.

Another very interesting observation is that North Slope crude, at the temperature of freezing sea water, is a good insulator compared to the sea ice itself. This was verified by measuring the temperature profile in the ice before and

after the oil was spilled[13]. This result means that the heat will tend to flow around the oil pocket under the ice, rather than through it. Near the edge of the oil pocket, the local heat flux will be higher than the average, and hence the ice will grow more rapidly there. (The heat removed is balanced by the latent heat of freezing of sea water.) Before the oil pocket is completely included in sea ice, there will be a rim of ice around the pocket thicker than the average. It may be that the existence of such a rim might be an aid to locating oil under the ice.

The most important result of Wolfe and Hoult's[13] work is an estimate of how much oil can stick to the under surface of the sea ice. To determine this, after the oil was injected into the freezing apparatus, the ice plug was removed, and the amount of oil remaining measured. A careful study was made of the various mechanisms by which a layer, of thickness, δ, to stick to the under surface of the ice.

It was found that the oil adhered to the ice under surface. If Q/A is the heat flux flowing through the ice and oil, the thickness, δ, is given by the simple formula,

$$\delta = 8 \frac{m^3}{\text{watts}} (Q/A)^{-2}$$

In the Arctic winter, the heat flux through the ice is about 35 watts m^{-2}. This gives a δ of about 6.5mm. If crude oil is spilled from a supertanker, with a total volume of 113,000 m^3, the total area which could be covered by oil is about 17 km^2 (6 square miles).

This is an upper bound, because undoubtedly some of the oil will be trapped in deeper pools.

4. SUMMARY

It is helpful to conclude this report by commenting on the practical application of the results of this work. The most important result, which is substantiated by all the research to date, is that the oil in even a very large Arctic spill will be confined to a very small area due to natural processes. This simple, general, conclusion is supported by both the spreading and pocketing experiments as well as the studies on oil evolution.

As a corollary to this result, it seems clear that, unlike the situation in temperate waters, there is little incentive to promptly clean up large oil spills, as the area of the oil spill will not measurably increase with time, while the oil remains in contact with sea ice.

REFERENCES

1. Glaeser, J.L., and Vance, G.D., "A Study of the Behavior of Oil Spills in the Arctic", Project No. 714108/A/001,002, Commandant (DAT) U.S. Coast Guard Headquarters, Washington, D.C., February, 1971.

2. CRREL - Corps of Engineers, Hanover, New Hampshire, "SEV Arctic Environment Data Package", 1970.

3. Hoult, D.P., "The Spread of Oil on the Sea", Ann. Rev. of Fl. Mech., 4, 1972, pp. 341-368.

4. Patireau, J.P., "Statistical Approach for Determining the Extent of an Oil Spill Over a Rough Surface", M.S. Thesis, Dept. of Mech. Eng., M.I.T., July, 1972.

5. O'Dea, S.R., "Experimental Determination of the Extent of an Oil Spill on Arctic Ice", M.S. Thesis, Dept. of Mech., M.I.T., June, 1973.

6. McMinn, T.J., "Crude Oil Behavior on Arctic Winter Ice", Dept. of Transportation, U.S. Coast Guard, Project 734108, September, 1972.

7. Fay, J.A., "The Spread of Oil on a Calm Sea", in Oil on the Sea, Hoult, D.P., ed., Plenum Press, 1969, pp. 53-63.

8. Fay, J.A., "Physical Processes in the Spread of Oil on a Water Surface", Conference on Prevention and Control of Oil Spills, Washington, D.C., 1971.

9. Lumley, J.L. and Panofsky, H.A., Atmospheric Turbulence, Interscience, New York, 1965.

10. Blokker, P.C., "Spreading and Evaporation of Petroleum Products on Water", 4th International Harbor Conference, Antwerp, June 22-27, 1964.

11. Guggenheim, E.A. "Thermodynamics", p. 239, North Holland, Amsterdam, 1959.

12. Brunnock, J.V., Duckworth, D.F. and Stephene, G.G., "Analysis of Beach Pollutants" in Scientific Aspects of Pollution of the Sea by Oil, The Journal of the Institute of Petroleum, 1968.

13. Wolfe, L.S., and Hoult, D.P., "Effects of Oil Under Sea Ice", Fl. Mech. Lab. Pub. No. 72-10, Dept. of Mech. Eng., M.I.T.

APPENDIX A

EFFECTS OF OIL UNDER SEA ICE

1. INTRODUCTION

The discovery of oil on the Northern Slope of Alaska had raised many questions concerning the effects of oil spills in the Arctic Ocean and other ice filled waters. The handling and transporting of oil in sizable quantities always results in some spillage, the average spillage being on the order of 0.1% of the quantity transported (Blumer, 1969, p. 6). The North Slope borders on the Arctic Ocean which is essentially ice locked for about nine months of the year (SEV Data Package, 1970, p. 11). Even during the summer months the permanent ice cap remains within ten nautical miles of the shore (SEV Data Package, 1970, p. 34). Any sort of waterborn transport of North Slope crude oil will create the possibility of spilling large amounts of crude oil under the ice.

Granted that under ice oil spills are almost certain to occur if Arctic oil operations continue, it is important to know how such spills can be contained and removed if the environmental damage caused by them would be serious enough to warrant such action. In the search for this information the first question to ask is how the oil spill behaves under the ice. Much is known of how oil spreads on temperate waters, both from experimental and theoretical studies and from observations of large scale disasters such as the Torrey Canyon and Santa Barbara Channel incidents. Almost nothing is known of the behavior of an oil spill under sea ice. The speed with which the oil spreads or the ultimate thickness to which it spreads are unknown. The interaction between the oil and the

peculiar microstructure of the lower layer of the sea ice (see Weeks, 1966, pp. 173-178) is also unknown.

There has been a good deal of speculation concerning the way sea ice will interact with trapped oil under it. Three principal modes of behavior have been considered possible.

(1) The sea ice will entrap the oil causing the formation of a matrix of oil and ice.

(2) The ice will entrap the oil in a pool and proceed to form beneath it.

(3) The ice will continue to grow pushing the oil before it.

(See Fig. 1). Such a phenomenon is difficult to observe in field experiments, so laboratory experiments were conducted to determine which of these phenomena occurred and to examine the phenomenon quantitatively, if possible.

2. EXPERIMENTAL APPARATUS AND METHODS

The principal function of the laboratory apparatus was to produce a nearly uniform vertical heat flux in a tank of seawater. The apparatus consisted of a 1.59 cm (5/8 inch) thick plexiglas tank, 30.4 cm (12 inch) square in cross section and 1.06 m (3 1/2 feet) deep topped by a 30.4 cm square stainless steel cold plate. The plate was connected by flexible tubing to a commercial refrigerating unit which circulated freon 12 refrigerant at a set temperature ($\pm$ 1.1 deg) down to -29°C. The tank was tapered 0.034 cm/cm to facilitate removal of the ice and was clad on all sides with 30.4 cm (12 inch) thick urethane foam insulation. The insulation was installed in separate panels which could be removed to make visual observations of the tank. (See Fig. 2). As a reasonable facsimile

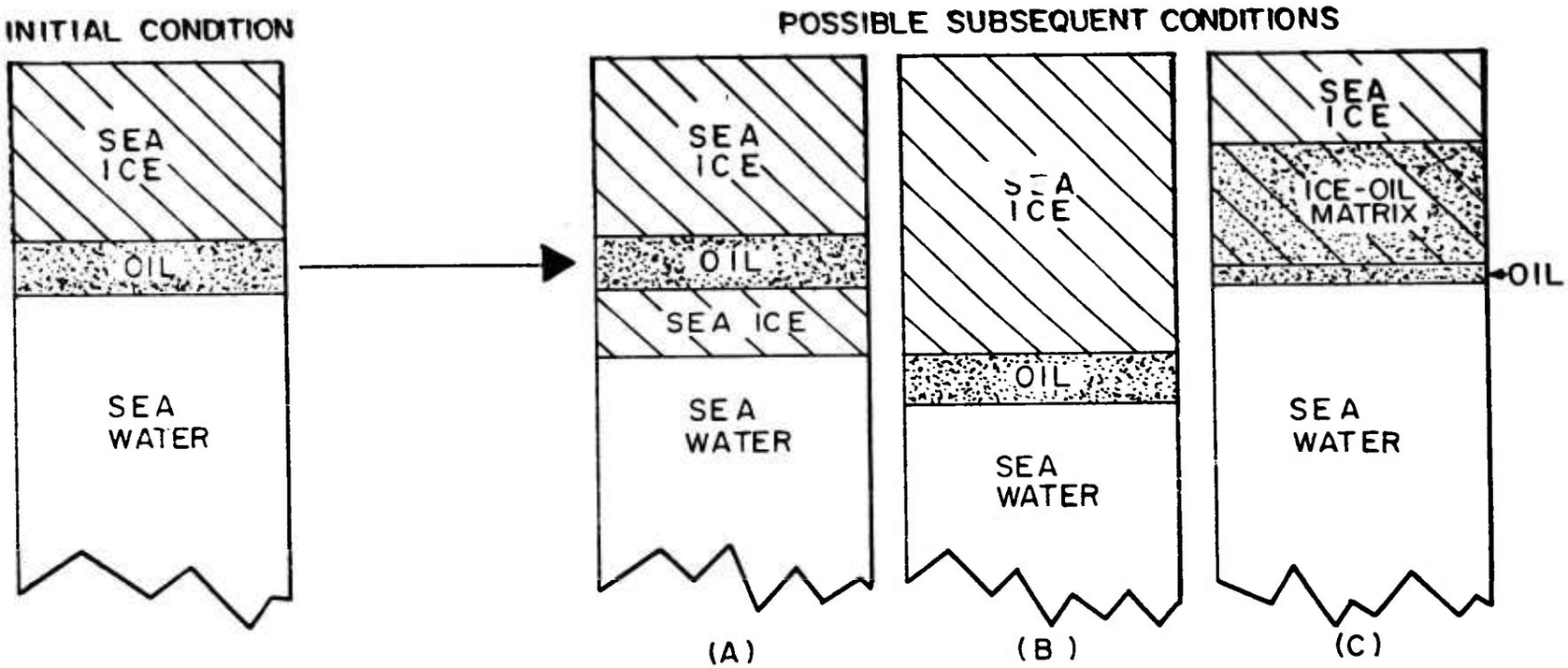

FIGURE 1. POSSIBLE MODES OF OIL ENTRAPMENT.

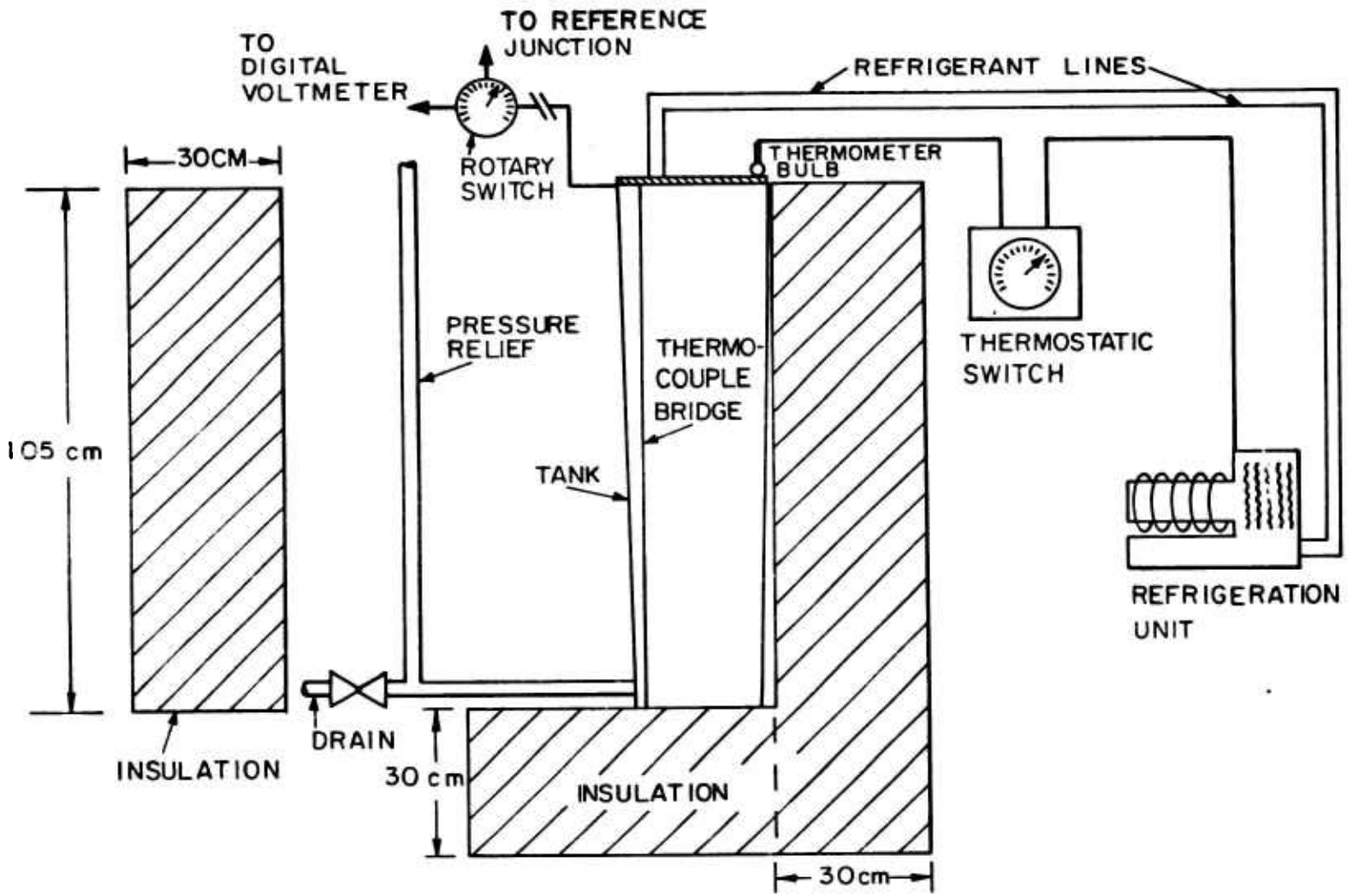

FIGURE 2. SEA ICE TEST CELL SCHEMATIC.

of sea ice has been made in a cylinder of 14 cm diameter, (Lofgren and Weeks, 1969, p. 157) the cross section of the tank was not a limiting consideration. The convection patterns were presumed sufficiently small that proximity of the wall had no effect on circulation in the center of the tank. At first an attempt was made to make the heat flux through the insulating walls very small in comparison with the heat flux through the ice when producing ice at Arctic rates. This was not possible with solid insulating materials commercially available, so to reduce the effects of heat gain, ice was produced at somewhat faster rates than is typical for Arctic conditions in late winter.

The quantities measured during the experiments were the temperature distribution in the ice and water, the salinity of the water beneath the ice, the depth of growth of the ice and the amount of oil injected under the ice. Temperature was measured with a bridge of copper-constantan thermocouples. The salinity of the water beneath the ice was measured by the use of a specially designed, totally submerged hydrometer. The depth of growth of the ice was determined by measuring the depth as seen through the tank with a ruler. The growth velocity of the ice was computed by noting the time that each thickness measurement was made and calculating the arithmetic mean velocity between successive measurements.

As a substitute for seawater solar salt was dissolved in tap water until a salinity of approximately 30 o/oo was achieved. This was used at the start of each experiment, but salt rejection by the ice increased the salinity of the water to between 35 and 40 o/oo by the time oil was placed under it. Two types of oil were used. No. 2 diesel was chosen because it is readily available and because it is a common marine fuel which may be

subject to large scale spills. The other oil used was a North Slope crude oil.

Each experiment was started with an initial plate temperature of -29°C until a few centimeters of ice formed. Then the temperature was set to the temperature at which the experiment was to run. When the ice reached a depth between 12 and 16 cm, oil was injected through the bottom of the tank from a plenum chamber using compressed air to supply the driving pressure. Except in a few trial runs, enough oil was added to completely cover the lower surface of the ice. The average thickness of the oil layer ranged between 1 and 2.6 cm. The oil was allowed to remain until some ice began to form on its lower surface. This took 12 - 24 hours in most cases. The experiment was then terminated and the ice cube removed.

In order to determine the extent to which oil became entrapped in the ice or adhered to its lower surface, the lowermost 2.5 cm of the ice block was sawed off, and the slab of ice was melted. The dimensions of the slab were noted before melting. The oil and water obtained were collected in a graduated cylinder and measured. Because the technique for measurement of the adhering oil is so crude, the limits of uncertainty for this data are rather wide.

Since the porosity of sea ice increases markedly at temperatures near the melting point, an attempt was made to see if there was any marked change in the mode of oil entrapment as the ice melts. The existing apparatus could not actually simulate the melting of sea ice as it occurs in the ocean because the tank had a finite heat gain from the laboratory although there is no similar source of heat in the sea. Nevertheless, the experiment was conducted. After the completion of an experiment performed in the usual manner, the temperature

of the cold plate was raised to -1.4°C, and the ice was allowed to melt. Temperature profiles were recorded every two hours and visual observations of the ice were made.

A more detailed description of the experimental apparatus methods is available in Wolfe, 1972, pp. 14-22.

3. EXPERIMENTAL OBSERVATIONS AND RESULTS

3.1 Sea Ice Growth Rate

A steady state approximation to the flow of heat from the sea water to the cold plate may be used. The rate of formation of ice equal to the rate of heat flux divided by the heat of formation of the ice, as shown below.

$$V = \frac{Q/A}{\rho_{ice} L} \qquad (1)$$

Since the thermal conductivity of the ice is essentially constant over the range of temperatures encountered, and the flow of heat is uniform upwards, the temperature gradient in the ice is constant. Since the cold ice surface is at the top of the sea water, the "sea" is well mixed and of uniform temperature approximately equal to the liquidus temperature of a NaCℓ and water solution of concentration 35 o/oo.

The temperature data can be nondimensionalized and normalized by dividing the temperature difference between the local temperature and the water temperature by the

total temperature difference between the water and the cold plate.

$$T^* = \frac{T - T_w}{T_{plate} - T_w}$$

Distance is normalized by measuring the distance from the lower surface of the ice to the thermocouple and dividing this by the total thickness of the ice.

$$z^* = z/h$$

All of the temperature data obtained before the addition of the oil is shown plotted in this manner in Fig. 3. It demonstrates that within the limited of experimental error, the temperature gradients are uniform and that the resistance of the thermal boundary layer at the ice-water interface is negligible.

The heat flow from the warm laboratory to the test cell retards the rate of formation of ice below that predicted by Eq. (1) above. The rate of heat gain by the ice tank from the lab should be nearly constant for all growth conditions, and thus the rate of formation should approach that given by Eq. (1) for high rates of growth. The available temperature and growth rate data may be nondimensionalized and normalized by dividing the product of the heat of formation of ice and the measured growth rate, ρLV, by the heat

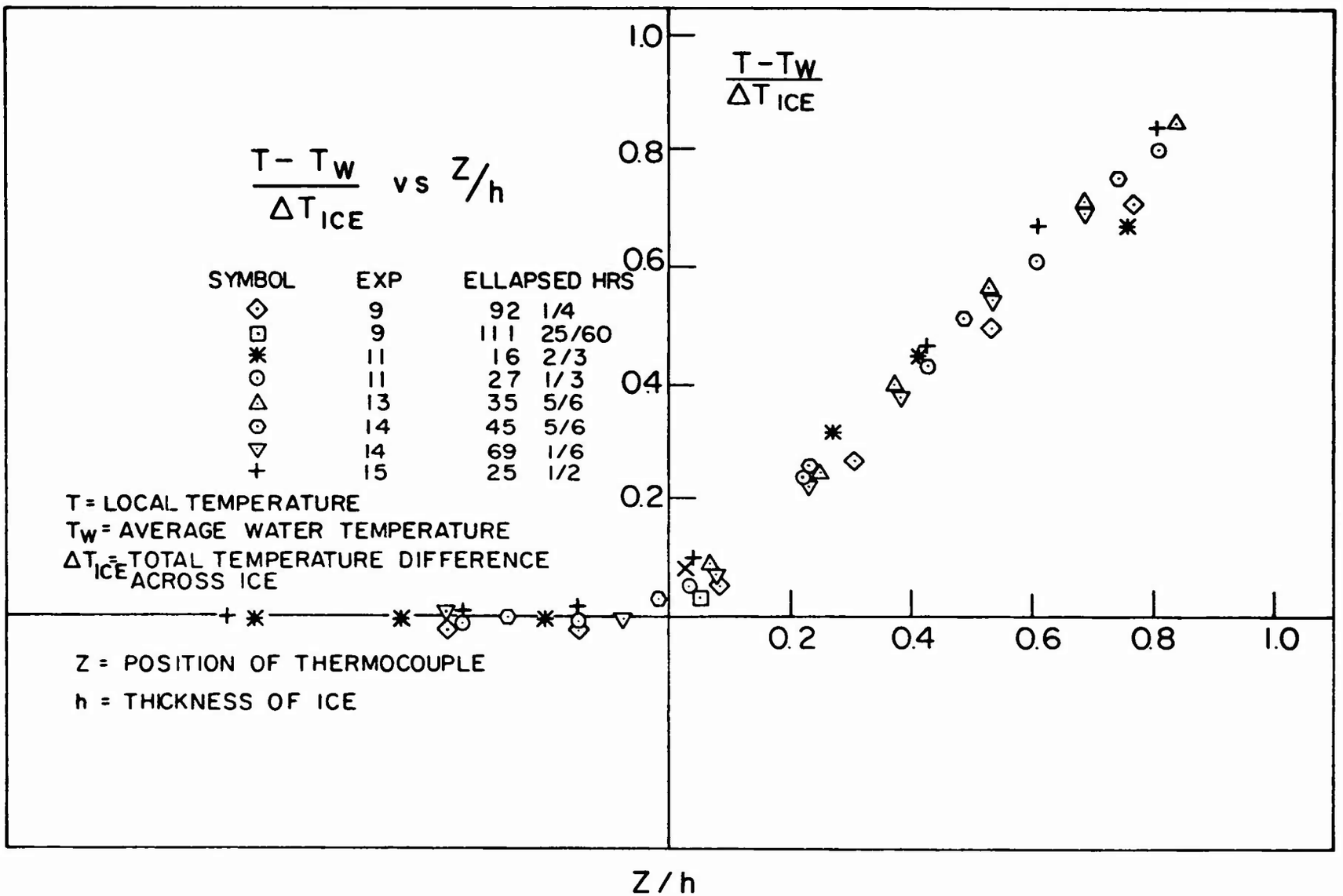

FIGURE 3. DIMENSIONLESS TEMPERATURE PROFILES.

flux out through the ice as predicted by Eq. (2).

$$Q/A = \frac{k_{ice}(\Delta T)_{ice}}{h_{ice}} \qquad (2)$$

This dimensionless growth rate is plotted as a function of the heat of formation and growth velocity product, ρLV, divided by the calculated heat gain per unit area through the walls of the tank and is displayed in Fig. 4. Note that the value of the dimensionless parameter $\rho LV/[k(\Delta T)/h]$ drops noticeably below unity when the ratio $\rho LV/(Q_{gain}/A)$ is about 150/1. The area of the tank walls is about 15 times the area of the cold plate. As expected, the growth velocity deviates significantly from Eq. (1) when the ratio of ρLV to the total heat gain is about 1/10. The large error bars on each data point are due primarily to the large uncertainty in the measurement of the rate of growth.

3.2 Mode of Oil Entrapment

The actual method by which the crude and diesel oils are trapped in the sea ice is a combination of modes (A) and (C) shown in Fig. 1. The bulk of the oil is pocketed in a pool below the original ice sub-surface while more sea ice proceeds to grow under it. A small amount of oil does rise into the pores of the skeletal layer, and into small, vertical shafts which rise from the lower surface of the ice. These shafts may be air bubbles similar to those that form in fresh water ice due to the inability of air entrained in the water and rejected upon freezing to escape beyond the advancing ice front (Weeks

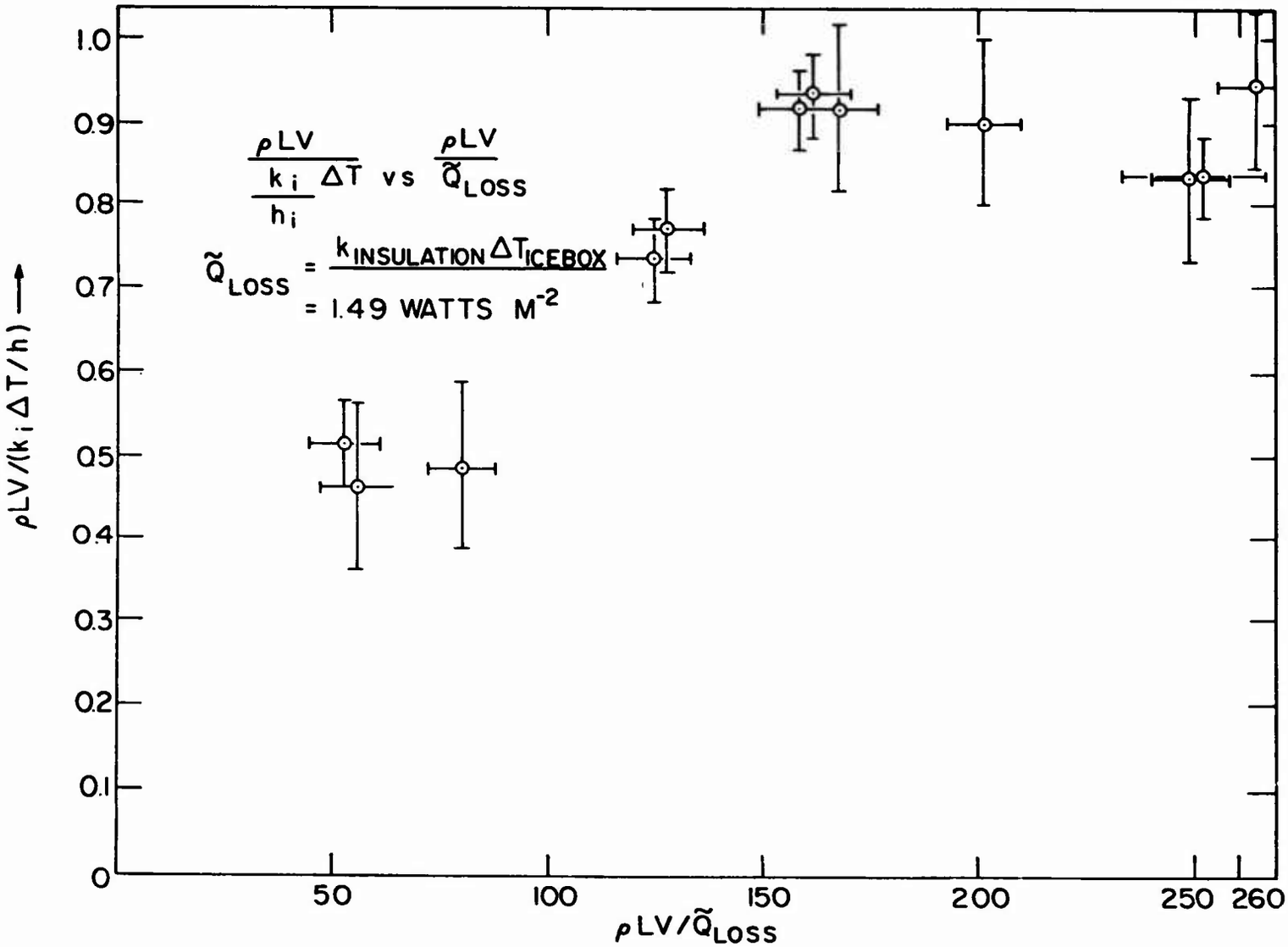

FIGURE 4. DIMENSIONLESS GROWTH VELOCITY TO HEAT FLUX RATIO AS A FUNCTION OF GROWTH VELOCITY TO HEAT GAIN RATIO.

and Assur, 1969, p. 8). The total amount of oil contained in these air bubbles is small in comparison to the amount of oil that adheres to the lowermost inch of the ice (see below). During the ice melting experiment, a considerably greater amount of oil rose into the ice, especially into the air shafts. In some instances it reached as high as 8 cm above the lower surface of a 13 cm thick block, yet the volume of oil trapped in this manner was still small, amounting to no more than $1/150^{th}$ of the volume of the ice.

The presence of the oil pool has a significant effect upon the heat transfer through the ice. The simple model of heat transfer through sea ice described above is a uniform solid of constant conductivity between two constant temperature regions, one at the liquidus temperature of seawater and the other at the ambient temperature of the air, or in the experimental case, the cold plate. As the oil has a thermal conductivity that is considerably lower than that of the ice, its presence acts as an insulating layer, impeding the flow of heat and reducing the temperature drop across the ice.

The temperature data obtained after the oil was placed under the ice may be nondimensionalized in the same manner as was done for the data taken with ice only. The origin for the vertical axis remains at the lower surface of the original ice block. As a result temperature measurements in the oil and below are expressed as negative numbers. The thickness of the ice before the oil was added is used to normalize distance, but the total temperature drop across the ice and oil is used to normalize temperature. The normalized temperature distribution are shown plotted in Fig. 5 for all temperature measurements taken after

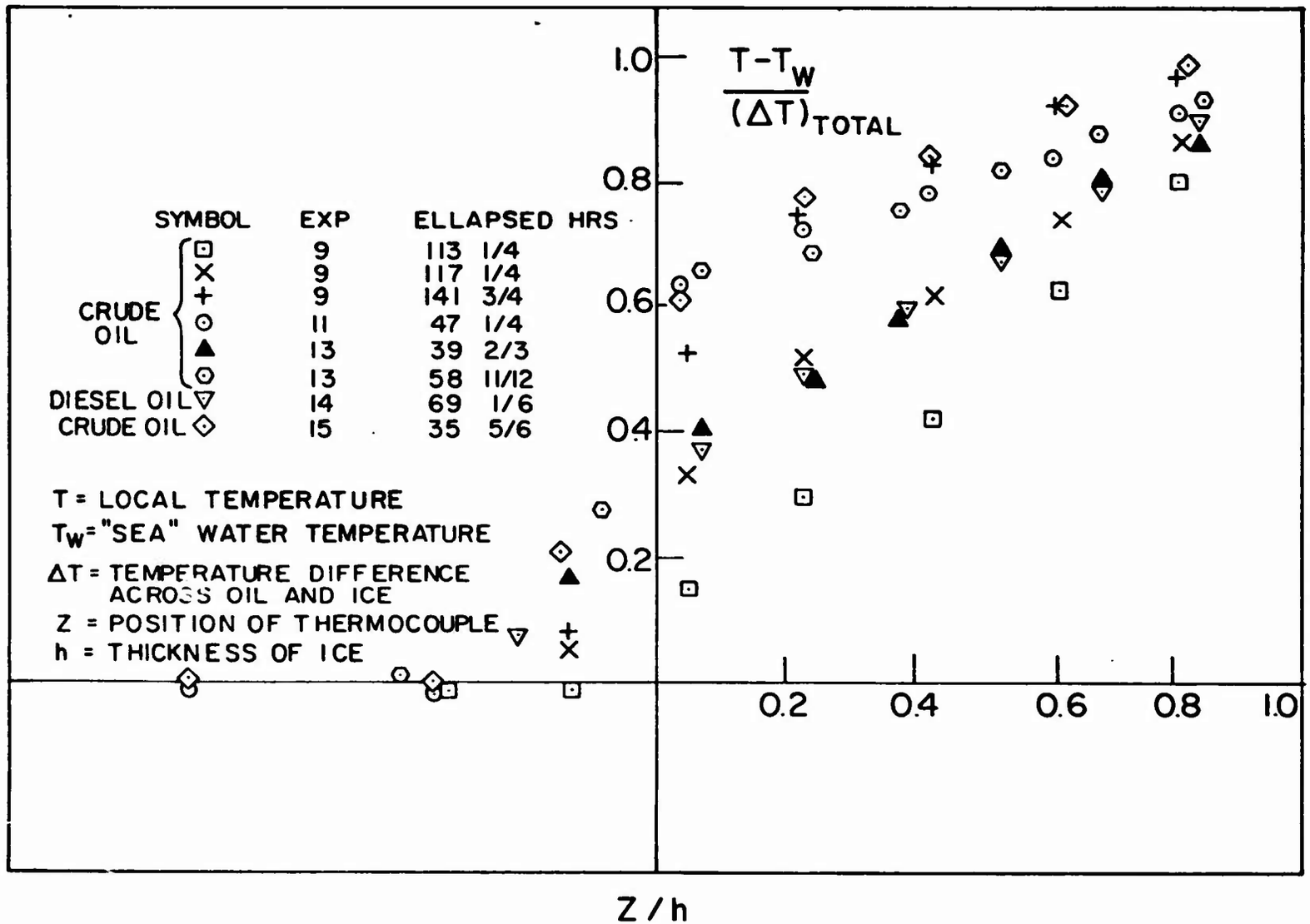

FIGURE 5. DIMENSIONLESS TEMPERATURE DISTRIBUTION AFTER OIL INSERTION.

the oil was in place.

As can be seen in Fig. 5, the temperature in the ice is linear at all times after the addition of the oil except for the case of Experiment 9, in which the temperature of the plate was high enough that the heat gain by the tank caused the water temperature to rise continuously. In the four other cases in which temperature profiles were measured, the temperature gradient in the ice remained constant, but decreased in magnitude from its initial value as shown in Fig. 3 through intermediate values to the final value. The temperature distribution in the oil could not be determined directly, since the oil layer was between 1.3 and 2.5 cm thick and the thermocouples were spaced 2.54 cm (one inch) apart in the bridge. It is clear that temperature gradients in the oil were much larger than in the ice.

Whereas clearly the heat transfer through the ice is that of solid body conduction, the mode of heat transfer in the oil pool is not obvious. It should be noted in Fig. 5 that for all of the crude oil experiments, the ratio of the temperature drop across the oil to that across the oil and ice is the same, 0.6. This ratio is independent of the thickness of the oil pool, which varies between 1.3 and 2.5 cm (in dimensionless units, (z/h), -0.097 and -0.189). For the diesel oil the ratio of the temperature drop across the oil to the total temperature drop across the oil and ice is 0.3. This behavior is not in accordance with the theory of static heat conduction. The thermal conductivity of most petroleum distillates is only a very weak function of temperature, and over the range of temperatures considered, the thermal conductivity

of the liquid fractions of petroleum changes less than 3%. (Wolfe, 1972, Appendix I). Within the limits of precision of this experiment, it may be considered constant. For constant thermal conductivity, the thermal resistance of a solid conducting heat in one direction is h/k, and thus the temperature drop across the solid is proportional to its thickness. For two solids conducting in series, the ratio of the temperature drop across one to the temperature drop across the other is $(h_1/h_2)(k_2/k_1)$. This is clearly not the case for the ice block and oil pool.

It is not proper to assume that the mode of heat transfer in the oil pool is by conduction alone. At the temperature involved, the crude oil is indeed highly viscous, but further examination is necessary to determine if it may be considered a solid body. The diesel fuel is quite fluid; it is entirely possible that convection cells could form and reduce the thermal resistance of the oil layer below that predicted by static conduction theory. The Nusselt number is the dimensionless ratio which compares the ratio of the convective heat transfer coefficient, $\underline{K}$, to the conductive heat transfer coefficient, k/h. For free convection between plane, horizontal surfaces, the Nusselt modulus may be defined as

$$Nu \equiv \underline{K}\, h/k \qquad (3)$$

The Nusselt modulus can be shown to be a function of the Grashof number and the Prandtl number, defined

by relations,

$$Gr \equiv \frac{q\beta(\Delta T)\, h^3}{\nu^2} \tag{4}$$

$$Pr \equiv c\,\mu/k \tag{5}$$

provided that the mode of heat transfer is free convection only (Kreith, 1965, p. 333). When a normal fluid whose density decreases with increasing temperature is placed between plane surfaces and cooled from above, convection results. This convection is commonly described in terms of the Rayleigh number which is the product of the Grashof and Prandtl numbers, GrPr. When this dimensionless variable is less than about 1700, no convection results, and heat is transferred by static conduction only. When GrPr is between 1700 and 42,000 convection is in the peculiar cellular manner known as Bénard cell convection. Irregular turbulence results at values of GrPr Higher than 42,000 (Eckert and Drake, 1959, p. 328). For values of GrPr less than 1700, the Nusselt modulus is by definition, unity. Bénard cell convection may be adequately correlated as a function of Nusselt modulus by Eq. (6), (Eckert and Drake, 1959, p. 328).

$$Nu = 0.107\,(GrPr)^{0.3} \tag{6}$$

The Nusselt number for the oil pool, can be expressed in terms of the measured parameters of the experiment. For one dimensional heat flow, the ratio of the thermal resistances of the oil to the ice is equal to the ratio of the temperature drops across the ice and across the oil, respectively. Since the value of the thermal resistance of the oil, $\underline{K}_{oil}$, is expressible in terms of known parameters, $(\Delta T)_{ice}$, $(\Delta T)_{oil}$, k_{ice}, the Nusselt number of Eq. (3) may be evaluated by Eq. (7).

$$Nu = \frac{k_{ice}\, h_{oil}\, (\Delta T)_{ice}}{k_{oil}\, h_{ice}\, (\Delta T)_{oil}} \qquad (7)$$

The Rayleigh number shown above has been evaluated for each of the experiments in which temperature profiles were measured. The Rayleigh number for the diesel oil measurement was about 22,000 while GrPr for the crude oil data ranged between 770 and 9700. A log-log plot of the Nusselt number as a function of Rayleigh number is shown in Fig. 6. The data conforms reasonably well to the standard relationship of Eq. (6) which is sketched. Although the data could be fitted better with another power law, it would be unwise to do so, since so few measurements have been made. The deviation from Eq. (6) may simply be due to errors in measurement since the data from which it was derived exhibits substantial scatter for relatively low Rayleigh numbers (Eckert and Drake, 1959, p. 331). Furthermore, Nusselt numbers less than unity must be attributable to errors in measurement.

As temperature measurements could not be made for all experiments, the heat flux through the ice after the

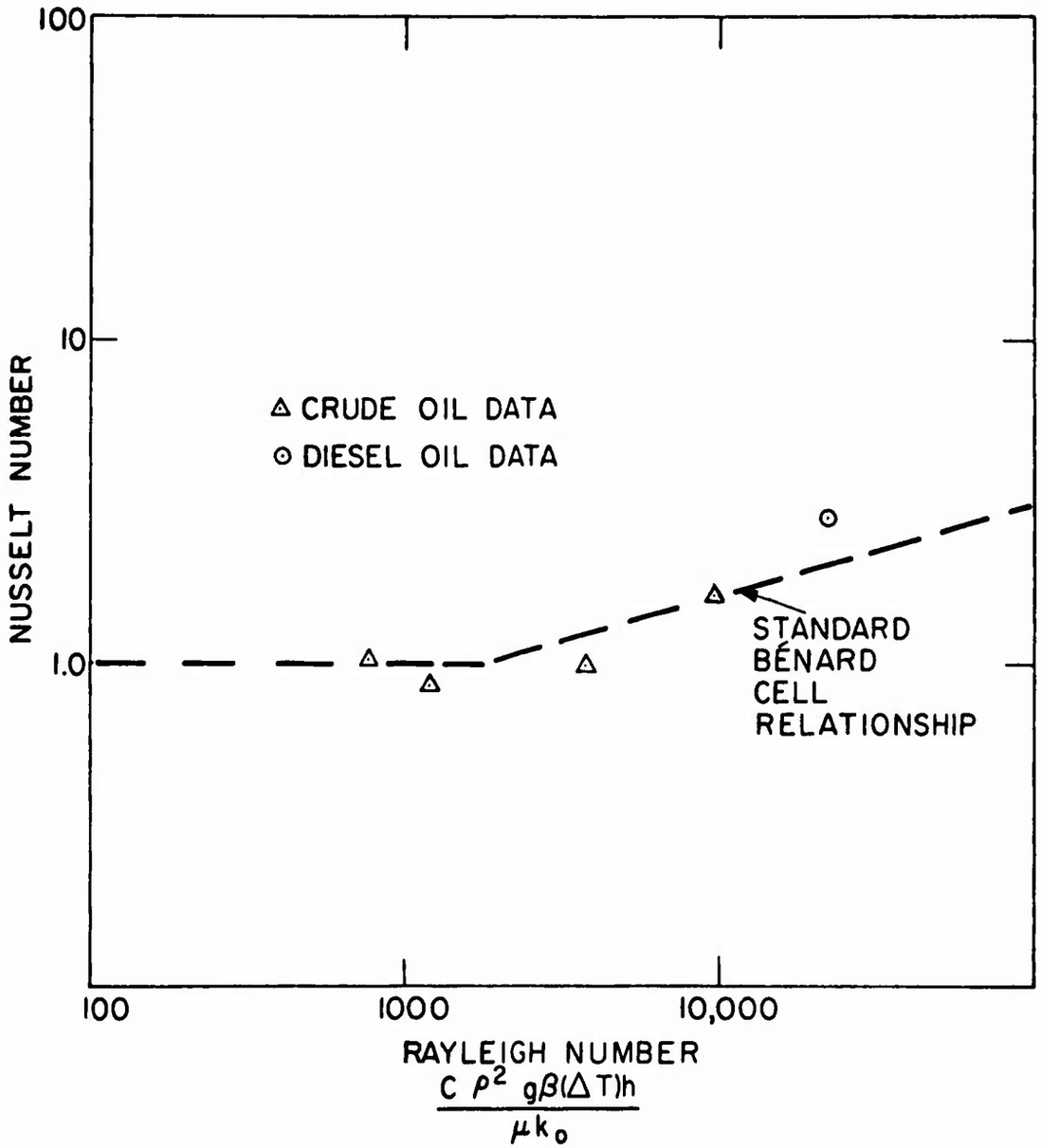

FIGURE 6. NUSSELT MODULUS AS A FUNCTION OF RAYLEIGH NUMBER FOR BÉNARD CELL CONVECTION IN THE OIL POOL.

oil is in place must be estimated from the temperature of the cold plate only. It was observed that the temperature drops across the oil and ice were constant fractions of the total temperature drop between the cold plate and the sea water, irrespective of the thickness of the ice or of the oil but dependent upon the type of oil. That this is expected can be shown from the equations for one dimensional heat conduction. The expressions for the flow of heat through the ice and oil can be written in terms of the thermal resistences and temperature drops in the system.

$$\frac{k_{ice}}{h_{ice}} (\Delta T)_{ice} = \frac{(\Delta T)_{total}}{\frac{h_{ice}}{k_{ice}} + \frac{1}{K}} \tag{8}$$

The linear temperature gradient in the ice is expressible in terms of the Nusselt number by substituting Eq. (3) into Eq. (8) and rearranging.

$$(\Delta T)_{ice} = \frac{(\Delta T)_{total}}{1 + \frac{k_{ice}}{k_{oil}} \frac{h_{oil}}{h_{ice}} \frac{1}{Nu}} \tag{9}$$

The expression for the Rayleigh number is

$$GrPr = \frac{c\rho^3 g\beta (\Delta T) h_o^3}{\nu k} \tag{10}$$

For constant properties of the oil and for small variations in (ΔT), the Rayleigh number is proportional to the cube of the oil thickness. Equation (6) shows the Nusselt number is proportional to the 0.3 power of GrPr. Therefore, for small variations in (ΔT) and in the fluid properties, the approximate equality Nu = Constant . (h_{oil}) is valid. Substituting this in Eq. (10)

$$(\Delta T)_{ice} = \frac{1}{1 + \frac{k_{ice}}{(k_{oil})} h_{ice} \cdot \text{Constant}} \qquad (11)$$

It can be seen that for small variations in h_{ice}, $(\Delta T)_{ice}$ is a nearly constant fraction of $(\Delta T)_{total}$. The thickness of the ice in the experiments ranged between 13 and 17 cm. It is therefore reasonable to consider that the ratio of the temperature drops $(\Delta T)_{ice}/(\Delta T)$ is the same for all experiments as it was for those in which the temperature profiles were measured. In all subsequent calculations involving the heat flux through the ice after the oil is present, $(\Delta T)_{ice}/(\Delta T)$ will be taken to be 0.4 for the crude oil experiments and 0.7 for the diesel oil experiments.

3.3 Thickness of Oil Adhering to the Ice

Upon removal of the ice block from the tank, some of the oil remained with the ice, either trapped in the porous ice structure or adhering to the lower surface, while the bulk of the oil remained in the original oil pool. The coating of diesel oil was fairly uniform but, the crude

oil was quite uneven in its adherence to the ice. It sometimes coated the ice in a continuous layer of uneven thickness, but in other cases it separated from the ice in patches, which were clean of oil (except for the oil in the interstices of the sketetal layer). A photograph of an ice block after removal from the tank following a typical crude oil experiment is shown in Fig. 7. Although the oil does not adhere to the ice in an even layer, an equivalent thickness of the oil layer may be calculated by dividing the total volume of oil measured after melting the ice sample by the area of the subsurface of the ice sample. It was difficult to determine visually to what extent the oil was trapped in the interstices of the ice and to what extent it simply adhered to the outside. Most of the oil appeared to be confined to the lowermost 0.5 cm, although a section of ice this thin could not be sliced. it is certain that all but slight traces of the oil was contained within the lowermost 2.5 cm of the ice. The traces above this level were due exclusively to the presence of the air bubbles.

The details of the mechanism by which oil adheres to the ice are neither simple nor obvious. From physical considerations it is possible to infer that the process of oil adhesion is both local and steady state. The adhesion phenomenon can not reasonably be expected to depend directly on any properties of the ice far away from the ice-oil interface. Thus the thickness of the ice or of the oil pool, the absolute temperature of the cold plate, the rate of growth of ice below the oil pool or the flow field within the oil pool can not be expected to influence the thickness of the adhering layer of oil, δ.

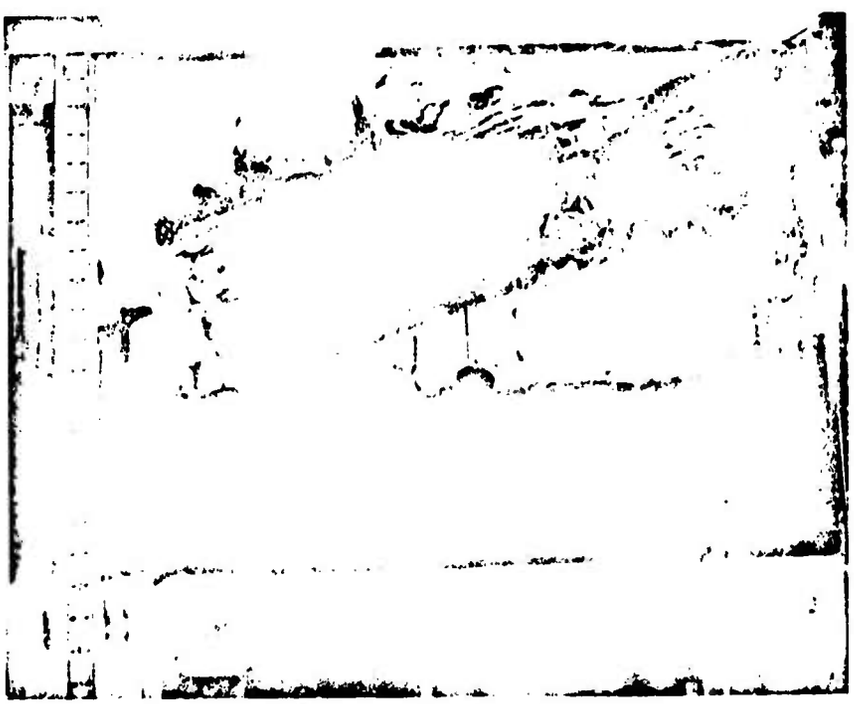

FIGURE 7. PHOTOGRAPH OF AN ICE BLOCK UPON REMOVAL FROM THE TEST CELL AFTER A TYPICAL CRUDE OIL EXPERIMENT.

The oil thickness may depend upon the geometry of the ice subsurface, the bulk properties of the ice and oil at the interface, the surface energy of the interface, and the heat flux through the interface.

That the adhesion process is steady state may be inferred from the fact that there were no transient effects taking place upon removal of the ice from the tank. At this time, all temperatures were in accordance with those predicted by static, one dimensional heat conduction. There was no discernable advance of the ice front after the oil was placed under the ice, and there was no observable change in the amount of oil entrapped after the steady state temperatures were reached. There was no trend in the adhesion thickness measured as a function of the time it remained under the ice.

The properties of the ice and oil at the interface which might be of significance are the viscosity of the oil, the buoyancy of the oil, the mechanical properties of the ice and the interfacial energy of the ice and oil. Since the ice does not fracture or deform as a result of the oil adhesion, its mechanical properties could be of no effect on δ. Since the oil is not in motion when the lower surface is removed, the viscosity of the oil could not be of influence on δ. The heat flux through the interface is a function of the steady state thermal conductivities of the ice and oil, but not of the thermal diffusivity which specifies the transient conduction properties of the materials. The interfacial energies of the ice and oil can be described in terms of a bulk property known as the adhesion coefficient.

In the simple theory of adhesion, the work necessary to create an additional unit surface may be expressed in terms of an adhesion coefficient, w, which has the same dimensions as surface tension. The simplest theory for adhesion coefficients relates them directly to surface tension, σ.

$$w = \sigma_{a/v} + \sigma_{s/v} - \sigma_{a/s} \qquad (12)$$

in which $\sigma_{a/v}$ and $\sigma_{s/v}$ are the common surface tensions usually measured for liquids or solids, i.e. the energy needed to create a unit surface in a vacuum, and the term $\sigma_{a/s}$ is a measure of the interfacial energy per unit surface of interface between the adhesive and the substrate (Skeist, 1962, p. 38). Although such quantities are simple to state in principle, they are not easy to measure. However, it is true for both water and petroleum derivatives that the surface tensions do not vary appreciably over the range of temperatures encountered in this experiment. Therefore, a preliminary estimate of the surface tensions may be found by using the tabulated values for the surface tension between oil and air, and water and air for $\sigma_{a/v}$ and $\sigma_{s/v}$ respectively, and the tabulated values for the interfacial tension between oil and water for $\sigma_{a/s}$. (Wolfe, 1972, Appendix I). Whether this value is accurate or not does not preclude its use in evaluating the importance of the adhesion coefficient. Surface tension is a strong function of the materials interfacing each other and only a weak function of the local temperature. Care

was taken to insure that the sea ice and oil used in the experiments were of the same composition as they would be in the Arctic. Thus, no matter what the actual value of w, it can be expected to be the same value in the field that it was in the laboratory.

Elementary physical considerations have reduced the list of parameters which may be of influence on δ to the buoyancy, $\rho\Delta g$, the adhesion coefficient, w, the heat flux through the ice, Q/A, and the geometric properties of the interface characterized by the interstitial spacing of the dendrites. (Weeks, 1966, p. 175). The interstitial spacing is a function of the velocity of growth of the ice before the oil is in place and is specified by Eq. (13)

$$a_o = 3.95 \times 10^{-5}/\sqrt{dh/dt} \qquad \text{(SI units)} \qquad (13)$$

(Assur and Weeks, 1963, pp. 97-98). Since the diameter of the pores of the skeletal layer is roughly constant, the volume of the skeletal layer filled with water can be expected to get larger as a_o becomes smaller. Any entrapment phenomenon that is dependent on filling the pores of the skeletal layer with oil would be expected to produce larger values of δ, as the growth velocity of the ice before the oil is added becomes larger. In fact just the opposite occurred. Less oil adhered at higher growth velocities.

Dimensional analysis can be used to determine the relationship between the heat flux through the ice, the buoyant forces on the oil and the adhesive forces on the

oil. If the thickness of the adhering oil is presumed to be a function of heat flux and buoyancy only, the Buckingham Pi Theorem indicates that only one dimensionless grouping can be formed, and that is invariant for all values of density and heat flux. That dimensionless variable is $\delta[(\rho\Delta g)^2 g/(Q/A)^2]^{1/3}$. Since density is the same in the Arctic as in the laboratory, the experimental values of δ should be extrapolated to field conditions by considering δ to be a linear function of $(Q/A)^{2/3}$. By similar reasoning if the adhesion thickness is considered to be a function of the adhesion coefficient, the heat flux through the ice and oil, and the acceleration of gravity, the only dimensionless grouping possible is $\delta(Q/A)^2/w^2 g$, and it must be invariant. Since w is the same in the Arctic as in the experiment, the experimental values of δ are expected to be directly proportional to $(Q/A)^{-2}$.

A dimensional log-log plot of the adhesion thickness, δ, as a function of (Q/A) was made in order to reveal which power law predominates. (See Fig. 8). As can be seen from the plot, within the limits of precision of the experiment, the data conforms to a power law of the form

$$\delta = C(Q/A)^{-2} \qquad (14)$$

This indicates that within the limits of precision of this experiment, the data correlates as a function of the dimensionless parameter $\delta(Q/A)^2/w^2 g$, and is therefore dependent upon the heat flux through the ice and oil, and the value of the adhesion coefficient alone. The limits

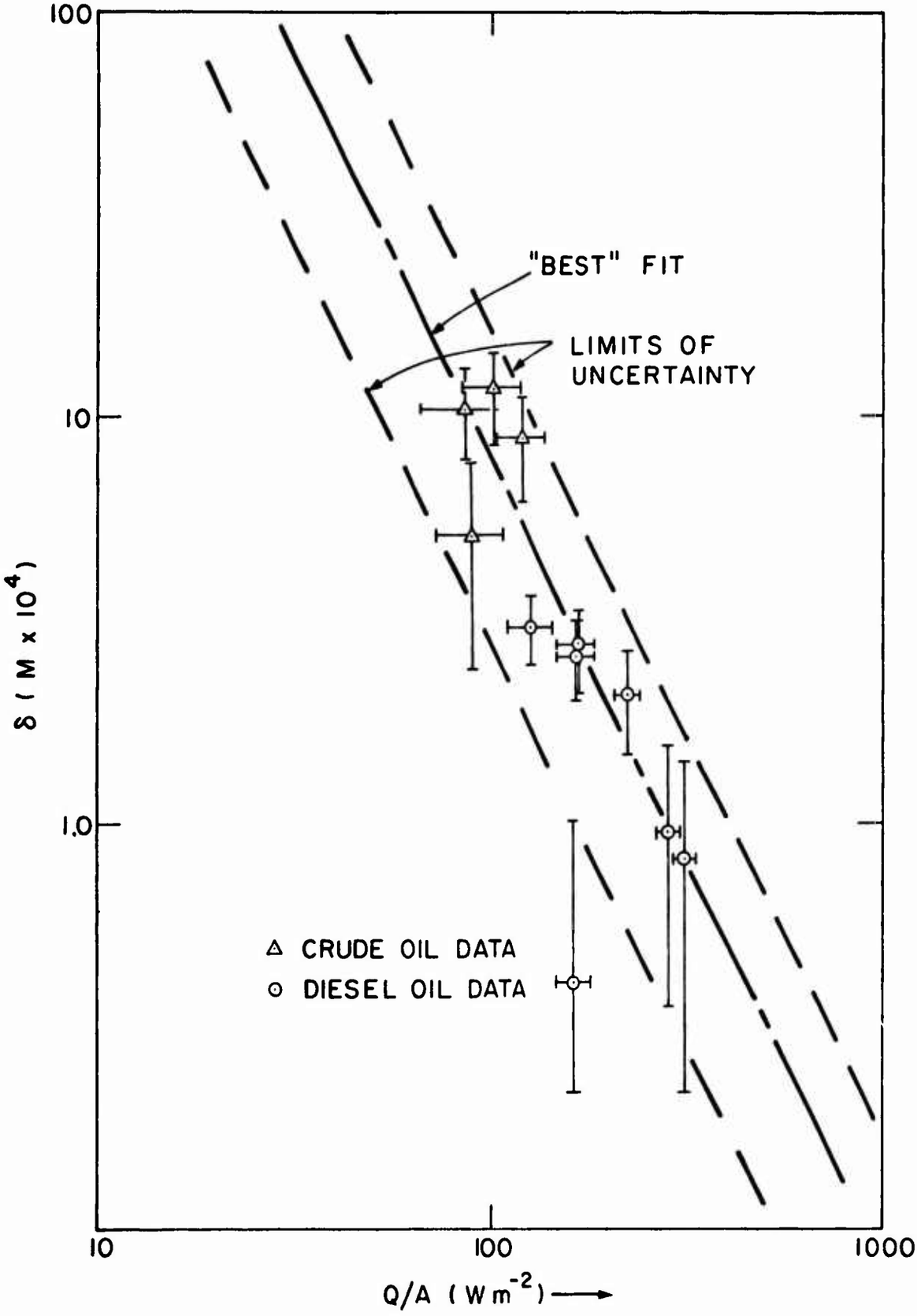

FIGURE 8. THICKNESS OF ADHERING OIL AS A FUNCTION OF THE HEAT FLUX THROUGH THE ICE AND OIL.

of precision of the experiment are not very good. The coefficient, C, of Eq. (14) may be evaluated within a factor of 2 or 3 at best. The "best" power law approximation to the data shown in Fig. 8 was drawn freehand and yields a value of C which is 8 $m^3 w^{-1}$. The equations for the limits of uncertainty of the data are also of the form of Eq. (14) and yield maximum and minimum values of C which are 16 and 3 $m^3 w^{-1}$, respectively. Equation (14) may be rewritten in dimensionless form

$$A = \frac{(Q/A)^2}{w^2 g} \qquad (14a)$$

The dimensionless constant A has a best value of 330 and may vary between 110 and 660 due to the uncertainty of the data. The adhesion coefficient, w, has been taken to be 0.05 n m^{-1}.

Equation (14) may be used to extrapolate the measurements of this experiment to actual Arctic conditions with an error factor of between 2 and 3. As shown below, such extrapolation can be used to give an upper bound to the extent to which an oil spill can spread in the Arctic. The correlation of the experimental data shown above does not yield a great deal of insight into the physical mechanism by which the oil adheres to the ice. It does indicate that the mechanism is related to the interfacial energies of the oil and the ice, rather than to the geometry of the surfaces or the other bulk properties of the oil. In general, the phenomenon of adhesion is poorly understood, and a detailed examination of the actual mechanism involved

is beyond the scope of this work.

It remains to explain the fact that almost no oil was observed to adhere to the ice during one of the crude oil experiments. This occurred during the coldest experiment run with a crude oil sample in which the steady state temperature gradient in the ice after oil injection was 86.6 deg m^{-1} and the mean temperature of the crude oil was -14.5°C., (well below the pour point for North Slope crude oil of approximately -4°C). Upon removal of the ice block, the oil sheared neatly away from the ice at the ice-oil interface. The oil appeared to be frozen, and was the consistency of ice cream. It may be that when the oil freezes, the mechanism of oil adhesion is altered because the oil behaves as a solid, instead of a liquid. If the block of oil is sufficiently heavy, its weight could cause it to break away from the ice at the ice-oil interface, because this is the weakest point in the composite ice and oil structure. Such an observation is not of much practical significance since temperature gradients of this magnitude rarely occur in natural sea ice.

4. CONCLUSIONS AND PRACTICAL APPLICATIONS

Three important conclusions can be drawn from these experiments concerning the behavior of crude oil when trapped under sea ice. First, the mode of entrapment of the oil has been conclusively determined. Second, the effect of the presence of an oil pool upon the growth rate of the ice and upon its temperature distribution has been determined. Third, an order of magnitude estimate of the maximum extent to which oil can spread under Arctic ice can be deduced from the measurements

of the thickness of the adhering oil layer.

The experiments have conclusively determined the mode by which oil is entrapped under a growing sheet of ice. The extent of the oil's entrapment in the ice-brine matrix has been shown to be negligible. Even when the porosity of the ice increases markedly during premelt conditions, the volume of oil entrapped remains small. Also, it has been shown that the ice does not in any way grow through the oil. The oil is neatly pocketed by the ice as more ice proceeds to form under it. In the absence of currents under the ice, even the large pockets of oil which might form in the larger recesses of the ice subsurface can be expected to be entrapped as a whole. Knowledge of this behavior should have significant impact on the design of equipment and procedures to clean up oil spills under ice.

The presence of an oil pool under the ice causes a marked change in the temperature distribution in the ice because the oil pool acts as an insulating layer between the cold air and the relatively warmer sea water. The temperature distribution in the ice can be calculated by a one dimensional analysis for oil pools whose widths are large in comparison with their depths. The exact procedure for such a calculation would depend upon the quantities which are easily measurable in a given oil spill. If, for example, the temperature distribution in the ice above the oil were desired, and the known parameters were the thickness of the ice before the spill, h_{icel}, the thickness of the oil pool, the thickness of the ice under the oil pool, h_{ice2}, and the temperature of the upper ice surface, then by presuming the heat flux uniform, the temperature difference across h_{ice2} could be calculated by the following relation

$$(\Delta T)_{icel} = \frac{(h_{icel}/k_{ice})\ (\Delta T)_{total}}{\frac{h_{icel}}{k_{ice}} \quad \frac{1}{K} \quad \frac{h_{ice2}}{k_{ice}}} \qquad (15)$$

The difficulty with this procedure is that the thermal resistance of the oil, $1/\underline{K}$, is dependent upon the temperature drop across it in accordance with Eqs. (3) through (6), and is thus dependent on $(\Delta T)_{ice}$ and $(\Delta T)_{total}$. Since Eq. (15) is non-linear and not explicit in $(\Delta T)_{ice}$ it must be solved by some sort of iterative procedure, such as simple trial and error, but it can be solved, since all the necessary governing relations have been defined. The distribution of temperature in the ice block is linear, so the temperature gradient may be readily calculated to determine the rate of growth under the ice. Also, this approach may be extended to cover cases in which additional thermal resistances, such as those due to snow cover or the thermal boundary layer of the air, are present. The effects of radiative heat transfer from the ice surface also may be included. In a converse procedure, the thickness of an oil pool under the ice may be inferred from measuring the thickness of the ice and the temperature gradient within it. Whether such calculations are of practical import remains to be seen.

The experiments which measured the effective thickness of adhering oil layer, δ, can be used to give an upper bound estimate of the extent to which an oil spill under ice can spread. It can be shown that the acceleration applied to the oil layer by currents under the ice is much smaller than the acceleration due to gravity applied to the oil layer when it is lifted from the tank prior to slicing. The shear stress applied to a plane surface in turbulent flow can be expressed in terms of the fluid density, the free stream velocity, and a friction factor which is a function of the surface roughness and nearly independent of Reynolds number. (Rohsenow and Choi, 1961, pp. 76-78).

$$\tau = C_f \frac{\rho}{2} U^2 \equiv \rho U^{*2} \qquad (16)$$

The acceleration applied to the fluid can be defined in terms of the friction velocity, U^*, as follows

$$g_{drag} = \frac{U^{*2}}{\varepsilon} \tag{17}$$

Where the mean roughness height, ε, is the approximate eddy size at the surface. For a roughness height of 0.5 m, a current velocity of 0.5 m s^{-1} (approximately 1 knot) and a friction factor of 0.04, the effective acceleration is calculated by Eqs. (16) and (17) to be 0.01 m s^{-2}, which is very small in comparison with the acceleration due to gravity. Thus, attempts to calculate the maximum area over which the oil spreads by using the effective oil thickness measured in these experiments will be quite conservative.

The effective thickness of the oil adhering to the ice, δ, determines the extent to which a given volume of oil will spread according to the relation

$$A = \frac{\text{Volume of oil}}{\delta} \tag{18}$$

It has been shown that δ is a function of the heat flux through the ice in accordance with Eq. (14). Thus from knowledge of the growth conditions of the ice and the volume of oil spilled, the area over which the oil spreads can be determined. For example, typical mid-winter conditions for the Northern Slope would be characterized by the presence of first year sea ice approximately 1.5 m thick with an air temperature of $-15^{o}C$.

(SEV Data Package, 1970, p. 11). Ignoring the effects of convective and radiative heat transfer at the ice-air boundary and assuming that no snow cover is present, the heat flux through the ice can be calculated to be approximately 35 watts m^{-2}. Since this calculation is performed to determine the maximum spread of the oil, the thickness of the oil, and thus its thermal resistance, will be very small in comparison with that of the 1.5 m thick ice. The heat flux through the oil and the ice can be considered to be the same as for the ice alone, 35 watts m^{-2}. From Eq. (14), δ is calculated to be 6.5 mm with a maximum value of 13 mm and a minimum of 2.5 mm. If crude oil spilled is from a supertanker of 100,000 metric tons capacity, the total volume of oil will be 113,000 m^3, and from Eq. (18) the total area over which it will spread will be a maximum of 45 km^2 (17 square miles), a minimum of 9 km^2 (4 square miles) and a "best" estimate of 17 km^2 (6 square miles). Even the largest of these values is considerably smaller than the area over which such a spill would spread in temperate waters. Similar calculations can be performed for the conditions of a particular spill, in accordance with the local ice thickness and temperature conditions.

It should be pointed out that all of the above conclusions apply to conditions typical for first year sea ice. Multi year ice is generally of much lower salinity and different composition due to the fact that brine drains from it. Because it is older, its history is less certain and because it occurs primarily in the permanent ice pack, it has often been deformed and distorted by the large forces within the ice cap. Yet from the physical analysis of the oil adhesion phenomenon, none of the above differences between new and old ice should affect the ultimate thickness to which the oil can spread. In mid-winter

the lowermost edge of the old ice will be composed of new ice which has just formed. The heat flux will be substantially lower because the old ice is thicker, and thus Eq. (14) will predict larger values of δ than would occur for new ice under similar weather conditions.

REFERENCES

American Petroleum Institute,, 1966, Technical Data Book, American Institute, New York.

Anderson, D.L., 1960, "The Physical Constants of Sea Ice", Research, 13, pp. 310-318.

Anonymous, November, 1970, SEV Arctic Environment Data Package, Cold Regions Research and Engineering Laboratory, Corps of Engineers, U.S. Army.

Assur, A., and Weeks, W.F., 1963, "Growth, Structure and Strength of Sea Ice", Extract of Publication No. 61, International Association of Scientific Hydrology, Berkeley, pp. 95-108.

Blumer, M., 1969, "Oil Pollution of the Ocean". (In Hoult, D.P., ed., Oil on the Sea), Plenum Press, New York.

Eckert, E.R.G., and Drake, R.M., 1959, Heat & Mass Transfer, 2nd Ed., McGraw-Hill, New York.

Kreith, F., 1965, Principles of Heat Transfer, International Textbook Company, Scranton, Pennsylvania.

Lofgren, G., and Weeks, W.F., 1969, "Effect on Growth Parameters of Substructure Spacing in NaCl Ice Crystals", in Journal of Glaciology, Vol. 8, No. 52, pp. 153-164.

National Research Council, 1926, International Critical Tables, McGraw-Hill, New York.

Rohsenow, W.M., and Choi, H.Y., 1961, Heat, Mass and Momentum Transfer, Prentice-Hall, Englewood Cliffs, New Jersey.

Sabersky, R.H., and Accosta, A.J., 1964, Fluid Flow, The Macmillan Company, New York.

Skeist, I., 1962, Handbook of Adhesives, Reinhold Publishing, New York.

Weeks, W.F., and Assur, A., September, 1969, Fracture of Lake and Sea Ice, Research Report 269, Cold Regions Research and Engineering Laboratory, Corps of Engineers, U.S. Army.

REFERENCES

(continued)

Weeks, W.F., March, 1962, "Tensile Strength of NaCℓ Ice", in Journal of Glaciology, Vol. 4, No. 31, pp. 25-52.

Weeks, W.F., and Anderson, D.L., August, 1958, "A Theoretical Analysis of Sea Ice Strength", in Transactions of the American Geophysical Union, Vol. 39, No. 4, pp. 632-639.

Weeks, W.F., 1966, "Understanding the Variations of the Physical Properties of Sea Ice", in Symposium on Antarctic Oceanography, Cold Regions Research and Engincering Laboratory, Corps of Engineers, U.S. Army, Hanover, N.H., pp. 173-190.

APPENDIX B

EXPERIMENTAL DETERMINATION OF THE EXTENT OF AN OIL SPILL ON ARCTIC ICE

1. INTRODUCTION

In 1968, oil was discovered on the North Slope of Alaska. Since the world supplies of oil are dwindling and the prices rising, this oil must be used if the present standard of living is to be maintained at a reasonable cost. This means that the crude oil must be shipped to a place where it can be refined, and whether supertanker or pipeline is used, the oil will have to travel over the rough surfac s of the Arctic. A small fraction of all oil shipped is spilled. In order to deal with this environmental problem it appears necessary to gain an understanding of how oil spreads on or under ice. This understanding must come in two parts: first, the process of spreading must be understood and the time for spreading determined; and second, the final size of the oil pool must be determined.

Initially, an inertial spreading law was proposed to explain the first problem. Using this theory the rate of spread could be scaled using the volume released and a gravity term. The spread would be independent of the surface characteristics. In order to solve the second problem, one must take into account the characteristics of the ice surface, namely its roughness and the random nature of this roughness. If this is done, the answer to the problem will be determined in a statistical way. This problem was studied by Patureau. The purpose of this thesis is to test the above theories by conducting experiments on a laboratory scale model and comparing these results with field data. Since the inertial theory was unable to correlate all

the data, another theory was derived from the results of known data.

The experimental apparatus and procedure will be studied in detail in Section 2. Since the results of Patureau are expressed in terms of parameters derived from the power spectrum of the surface, this section also described the apparatus and procedure used to determine the power spectrum of the experimental surface. In Section 3, the details of Patureau's final size theory and the spreading theory derived from the experimental results will be discussed, along with the assumptions and limitations. Section 4 will present the results in the form of correlations between theory and experiment, an explanation of the derivation of the spreading theory, sources of error, and the conclusions of the study.

2. EXPERIMENTS

In planning the experiments, the characteristics of Arctic ice were first studied. Since earlier work indicated that the spreading was gravity-inertia dominated it was decided to construct an apparatus that could dump a known volume of 'oil' at a fast rate.

To obtain dynamic and geometric similarity, certain parameters were then established and values determined. These are:

$$\mathrm{Re} = \frac{(\Delta g \langle \bar{h} \rangle)^{1/2} \langle \bar{h} \rangle}{\nu} > 500$$

$$\beta = \frac{\langle \bar{h} \rangle}{T} \approx \begin{cases} 1/80 \text{ above ice} \\ 1/20 \text{ below ice} \end{cases}$$

N = number of pockets >> 1

Δ = density ratio <.2 (under only)

With the exception of Re, the conditions are all well met. In the case of the Reynolds number, a desire to use fluids that could be used easily, would not destroy plexiglas and would provide agreement with the other parameters led to a relaxation of the restriction. Water for the over ice experiments provides an Re of a little more than 400 and kerosene for the under ice case provides an Re of about 100. This is believed to provide sufficient turbulence to satisfy the theory.

A schematic of the spreading experiment apparatus is shown in Fig. 1. This figure should be referred to if any questions arise.

The rough surface itself was built by epoxying various sizes of rocks to a plywood board in a random fashion. The surface was then painted white with black concentric circles. When used in conjunction with a dyed fluid, the spread is easily observed and photographed. The size of the surface, and therefore the size of the tank, is 4' x 4'. It was felt that this size tank would offer a large enough surface to be statistically significant and yet small enough to be easily handled.

In order to scale the laboratory model to a real spill, one should consider that a real spill would be on the order of 10^5 cubic feet and the Arctic roughness height is on the order of 1'. The roughness height of the experimental surface is about 1/10 inch. This means that the 4' x 4' surface corresponds to about 500 x 500 in the Arctic.

The tank is made of plexiglas to allow the spread to be easily observed and photographed. The frame was designed to allow for rotation of the tank when conducting under ice experiments. This was necessary because if the tank were filled in a horizontal position the pockets in the surface would trap air and make the experimental results meaningless.

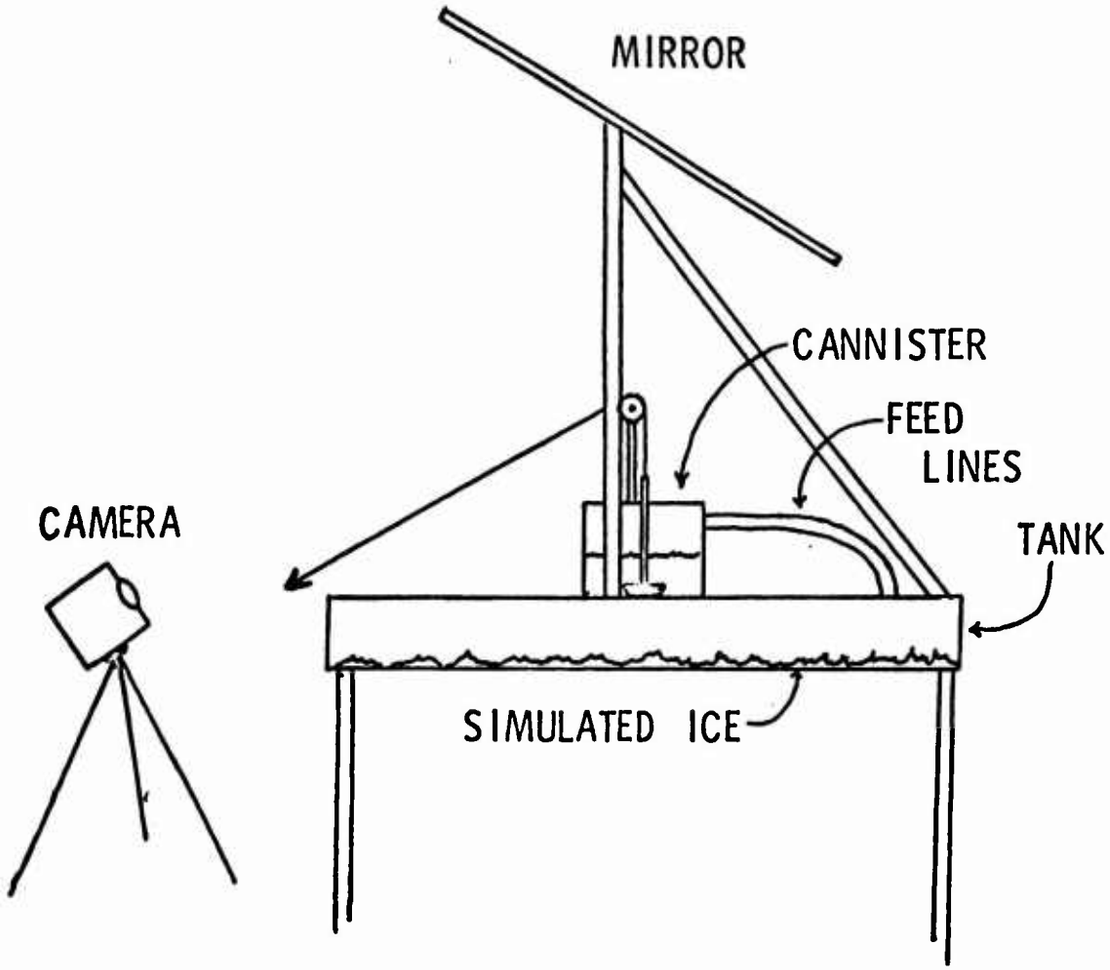

FIG. 1 SCHEMATIC OF SPREADING APPARATUS (OVER ICE SPREAD)

To record the progress of each experiment a Bolex 16mm camera with a 10mm lens and a variable time base was used. Since this lens needs a focal length of around nine feet to get a large enough field to cover the apparatus, it was decided to use a mirror. The camera was then run at a known speed, usually 20 fps, to record the spread. The developed film was then examined frame by frame to determine radius versus time and the final size.

To measure the surface a frame was made from 1" x 1" angle iron (see Fig. 2) and marked in 1/4" increments. The elevation of the surface was then measured every 1/4" with an accuracy of 1/32". The distance below a fixed line, the frame, was recorded by hand and then transferred to computer cards. The variance and the power spectrum were then calculated by the program shown in Fig. 3. The quarter inch spacings were chosen as a compromise between accuracy and ease of measurement.

To test the isotropy assumption, traces were taken in perpendicular directions and then their power spectra compared. This is explained in Section 4.

The frame is believed to affect the spectrum only in the wavelength range greater than ten inches. If this is true, and there are no indications otherwise, then the imperfections in the frame will have no effect on the results.

For the over ice experiments, the fluid used was water dyed with food coloring. Soap was added to reduce the surface tension and the 'oil' was placed in the cannister. The apparatus was then leveled very carefully to prevent the fluid from running off to one side. Problems were encountered in this area. Once the experiment was ready to start, the camera was started and the stopper pulled. This released the oil at a

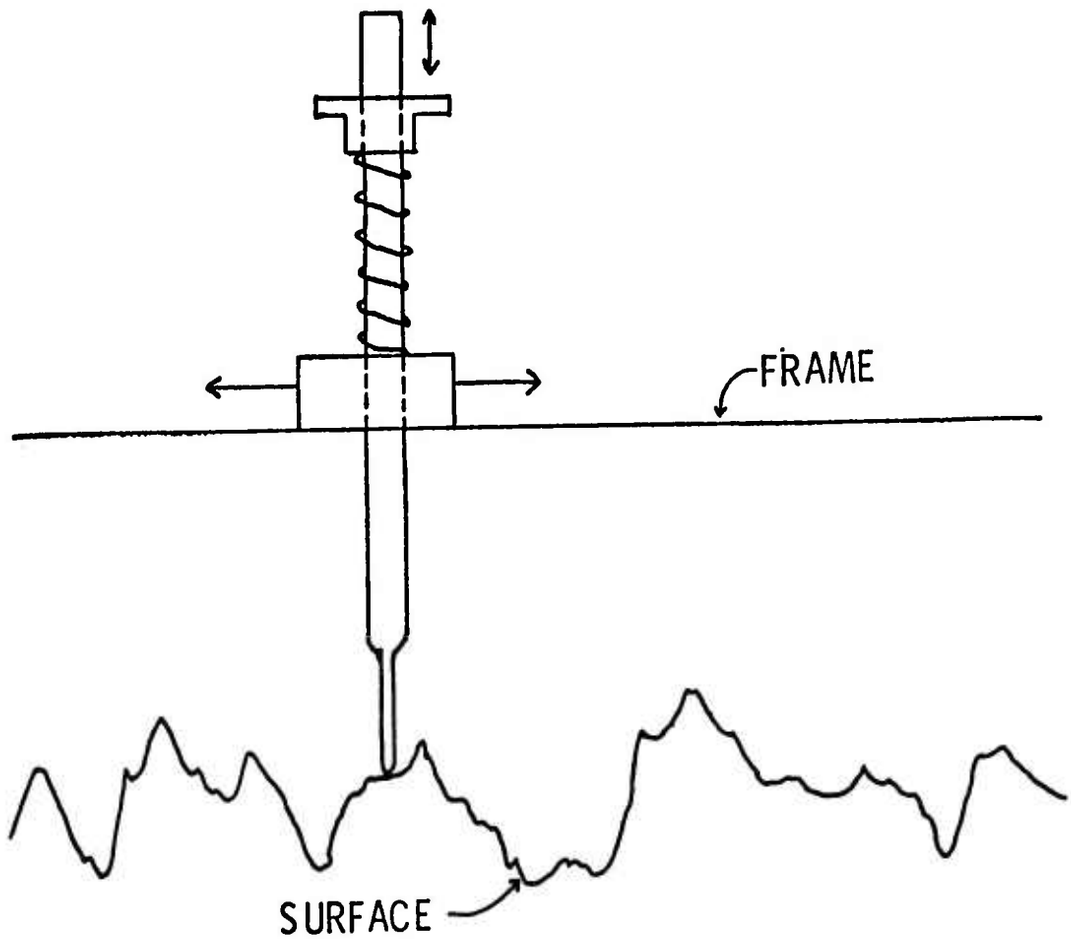

FIG. 2 SCHEMATIC OF APPARATUS TO MEASURE SURFACE

```
10    T(1)=0.
      S(1)=0.
      DO 11 I=1,NTOT
      T(1)=T(1)+H(I)
11    S(1)=S(1)+H(I)*H(I)
      LGMXP1=LGMX+1
      F(1)=T(1)
      G(1)=S(1)
      DO 12 LAG=2,LGMXP1
      KK=NTOT-LAG+2
      T(LAG)=T(LAG-1)-H(LAG-1)
      F(LAG)=F(LAG-1)-H(KK)
      S(LAG)=S(LAG-1)-H(LAG-1)*H(LAG-1)
12    G(LAG)=G(LAG-1)-H(KK)*H(KK)
      DO 15 LAG=1,LGMXP1
      C(LAG)=0.
      KK1=NTOT-LAG+1
      DO 13 I=1,KK1
      IPLLAG=I+LAG
13    C(LAG)=C(LAG)+H(I)*H(IPLLAG-1)
      RLTMLG=NTOT-LAG+1
      W(LAG)=C(LAG)/RLTMLG
14    AUTOCO(LAG)=(RLTMLG*C(LAG)-F(LAG)*T(LAG))/ SQRT((RLTML
     1G*G(LAG)-F(LAG)*F(LAG))*(RLTMLG*S(LAG)-T(LAG)*T(LAG)))
15    CONTINUE
      WRITE(IWRIT,903)AUTOCO
      DO 17 LAG=1,LGMXP1
      SPECES(LAG)=0.
      DO 16 I=2,LGMX
      RLGMX=LGMX
      ANG1=(LAG-1)*(I-1)
      ANG1=ANG1*3.1416/RLGMX
16    SPECES(LAG)=SPECES(LAG)+2.*W(I)*COS(ANG1)
      ANG2=LAG-1
      ANG2=ANG2*3.1416
17    SPECES(LAG)=SPECES(LAG)+W(1)+W(LGMXP1)*COS(ANG2)
      WRITE(IWRIT,903)SPECES
      SMSPEC(1)=.54*SPECES(1)+.46*SPECES(2)
      SMSPEC(LGMXP1)=SPECES(LGMX)*.46+.54*SPECES(LGMXP1)
      DO 18 LAG=2,LGMX
18    SMSPEC(LAG)=(SPECES(LAG-1)+SPECES(LAG+1))*.23+.54*SPEC
     1ES(LAG)
      WRITE(IWRIT,903)SMSPEC
```

FIG. 3 COMPUTER PROGRAM TC DETERMINE POWER SPECTRUM

fairly fast rate. In order to determine the amount released, the fluid level in the cannister was measured before and after the release.

The underwater experiments were considerably more difficult. The experiment had to be set up in such a way that no air pockets remained in the tank and no kerosene escaped the feed lines connecting the tank to the cannister. To do this, water was first placed in the cannister to a level that would prevent the kerosene from getting into the feed lines. Then, enough kerosene, which was dyed using enamel paint, is added to fill the cannister. The rough surface was then placed on the tank and the tank was almost completely filled and then tilted to allow the air to escape from the pockets. The filling of the tank was completed in this position. When all the air escaped out the top and the tank was full, it was rotated back to a horizontal position and leveled. Since there was sufficient pressure in the tank to cause the surface to deflect at the center, water was bled off in an attempt to ensure that the surface was flat. Some degree of error was probably caused by this deflection. Once the tank was leveled and the pressures equalized, the experiments proceeded in the same way as the over ice experiments.

To check for the presence of viscous effects, experiments were run with glycerin-water and kerosene-oil mixtures. These experiments are described in the Sub-Appendix.

3. THEORY

The theory that governs the spreading was developed as a result of data from the experiments described in the last section and the available field data. The steps taken in deriving the theory are described in Section 4. In this section

the theories will be explained in simple terms and the analytical expressions derived.

In determining what will happen to oil spilled in the Arctic, two cases must be considered. In the case of a pipeline breakage, the oil will spread over ice and tundra. In the case of a supertanker accident, the oil will probably spread under the ice. This happens because Arctic ice has a specific gravity of about 0.8 and North Slope crude has a specific gravity of about 0.9. Therefore, at an ice-water interface the oil will, on hydrostatic considerations, tend to spread under the ice. The spreading in both cases follows the same theory and the results differ only by a factor determined by the density ratio of water and oil. For either a pipeline break or a supertanker accident, the maximum rate of oil released will be about 1.5×10^5 cubic feet per day.

Patureau's theory states that pockets in the ice are filled to the roughness height, $\langle \bar{h} \rangle$, and it was shown experimentally that the value of the viscosity is not important (see Sub-Appendix B-1). This means that as pockets in the ice are filled additional fluid flows over the filled pockets frictionlessly and the drag can act only at the edge over an area proportional to the radius multiplied by the roughness height. When attempting to correlate the laboratory data for over and under ice and the field data, it was found that the data would not scale with the volume released. By forming dimensional plots described in the next section, it was shown that the rate of spread for a given surface could be scaled using the rate of oil release, Q. Since the size of the final pool depends upon various statistical parameters, one can see that for a given volume and surface there will be an average pool size and an associated variance. In order to determine the accuracy of the averages, Patureau

developed an expression relating the standard deviation of the size with the average size.

Figure 4 shows a sketch of oil being released on a rough surface with a roughness height $\langle \bar{h} \rangle$. The driving force is gravity, which causes a pressure at the outside edge of the spill. Thus,

$$F_g \sim \rho A \sim (\rho \Delta g h) hr \tag{1}$$

Since

$$h^2 \sim \frac{(Qt)^2}{r^4} \tag{2}$$

the gravitational force from Eq. (1) can be expressed as

$$F_g \sim \rho \Delta g \frac{(Qt)^2}{r^3} \tag{3}$$

The pressure drop caused at the outer edge as the oil flows will be

$$dp \sim C_f \rho U^2 \tag{4}$$

where C_f is a friction coefficient of order one. Since the area over which the drag acts is the roughness height, $\langle h^- \rangle$, times r the retarding force becomes

$$Fr \sim \rho U^2 r \langle h^- \rangle \tag{5}$$

Replacing U in Eq. (5) with r/t and setting Eq. (5) equal to Eq. (3) gives

$$\rho \Delta g \frac{(Qt^2)}{r^3} \sim \rho \frac{r^3}{t^2} \langle h^- \rangle \tag{6}$$

After some algebra, this becomes

$$r \sim \left(\frac{gQ^2}{\langle h^- \rangle} \right)^{1/6} t^{2/3} \tag{7}$$

This can be non-dimensionalized by defining a scaling length

$$r^* = \langle h^- \rangle \tag{8a}$$

and a scaling time

$$t^* = \left(\frac{\langle h^- \rangle^7}{gQ^2} \right)^{1/4} \tag{8b}$$

To obtain an expression for the final size and the associated standard deviation additional assumptions must be made. The first of these assumptions equates the average of a sample from the surface with the ensemble average over the whole surface. This assumption has no real relevance to experimental procedure. Next it is assumed that the elevation of points on the surface are normally distributed about some mean. This assumption is in fair agreement with the experimental surface (and good agreement with the real ice surface) which actually is closer to a lag-normal distribution. Under this assumption, the roughness height, $\langle \bar{h} \rangle$, and the variance of the height, σ_h, can be related by the simple equation:

$$\langle \bar{h} \rangle = \left(\frac{\sigma_h}{2\pi} \right)^{1/2} \tag{9}$$

Thirdly, it is assumed that pockets in the ice surface are filled to the roughness height (see Fig. 5). The level assumption has no real justification save that it eases the calculations. The accuracy of this assumption can only be determined by experiment. The fourth main assumption is that the number of pockets filled is always large enough to give a statistically meaningful result. This assumption is well satisfied. It was further assumed that the pockets assumed a rectangular shape (square in the case of an isotropic surface). This was done strictly for computational reasons. For the purpose of this thesis the surface will be assumed isotropic and the spill will be circular. The isotropy assumption will be shown to be a good assumption by comparing the power spectra along perpendicular paths of the experimental surface. Lastly, it was assumed that a two-dimensional power

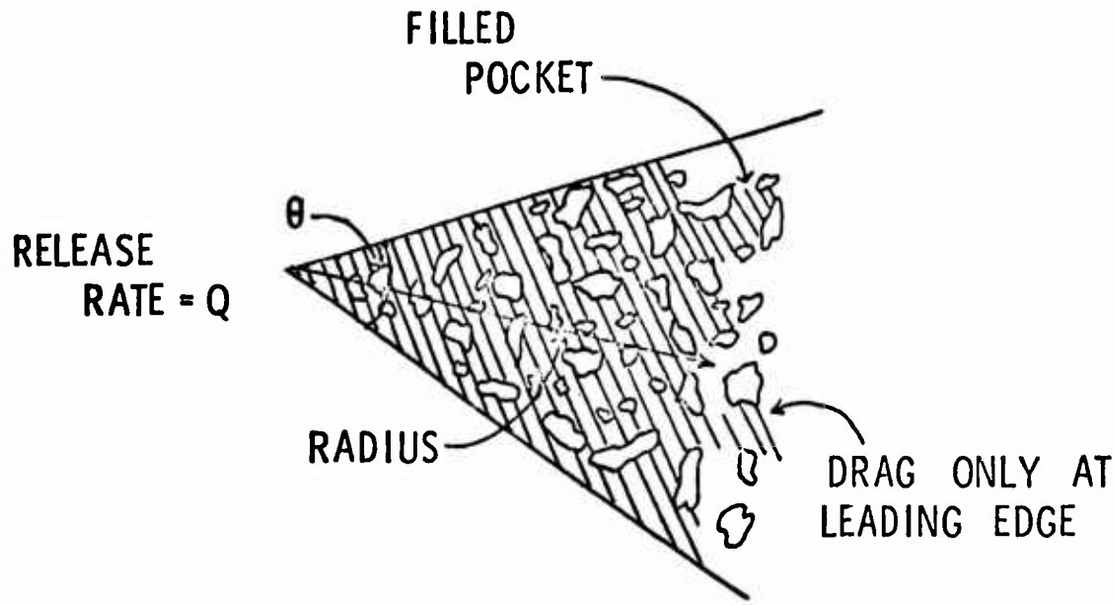

FIG. 4 SECTION OF OIL SPREADING ACROSS A ROUGH SURFACE

(ONLY θ OUT OF 2π SHOWN FOR EASE)

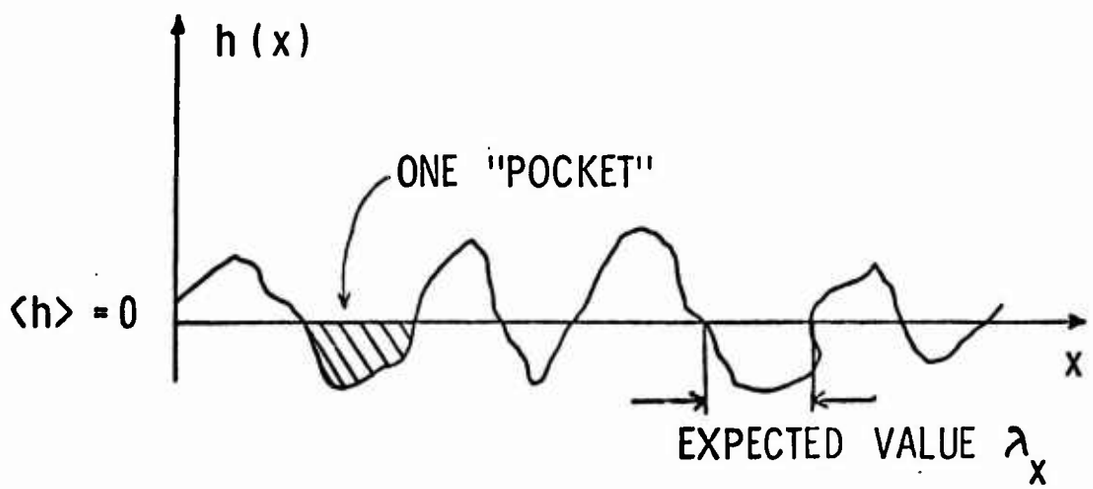

FIG. 5 AVERAGE LONGITUDINAL DIMENSION OF A POCKET

spectrum could be formed as the product of two-dimensional spectra. This assumption has no mathematical justification, but even if it were poor, no real error in the results would appear. The procedure for determining the power spectrum, which is done by computer, is explained in the experimental section.

The final results of the theory are expressed in terms of parameters which are derived from the statistics of the ice surface. The first of these is the variance of the roughness, σ_h. Next are two parameters k and T derived from the power spectrum of the surface. For a one-dimensional spectrum, T is the wavelength of the peak of the spectrum and k is determined from the following equation:

$$P(\frac{1}{T}) = \frac{2\pi h}{k^{1/2}} \exp\left(\frac{-2\pi}{Tk^{1/2}}\right) \cosh\left(\frac{2\pi}{Tk^{1/2}}\right) \tag{10}$$

To meet the requirements of the theory, the product kT^2 should be greater than 50, or, in the two-dimensional case $(kT^2)^2$ should be greater than 2500. From $(kT^2)^2$, an additional parameter, Θ, can be determined from Fig. 6. (See eq 22)

Following the assumpcion that the oil fills the pockets to the roughness height on the average, we get the equation

$$\langle V \rangle = \langle S_{max} \rangle \langle \bar{h} \rangle \tag{11}$$

or, for a normal distribution

$$\langle V \rangle = \langle S_{max} \rangle \left(\frac{\sigma_h}{2\pi}\right)^{1/2} \tag{12}$$

from Eq. (8).

To non-dimensionalize the results, Patureau introduced the concept of the 'most probable pocket' size,[7], that is, the most common size for a pocket on the ice. Defining the surface area of a most probable pocket as

$$S_{mp} = T^2 \tag{13}$$

and the volume of a most probable pocket as

$$V_{mp} = \frac{T^2 \, 2(2\sigma_h)^{1/2}}{\pi^2} \tag{14}$$

we find the following dimensionless equation from Eq. (12):

$$\frac{\langle S_{max} \rangle}{S_{mp}} = \left(\frac{4}{\pi^{3/2}}\right) \frac{V}{V_{mp}} \tag{15}$$

To provide a measure of the accuracy of the above equation, an expression for the variance of the surface area, σ_s, was derived. This expression is obtained by considering the pockets in the ice to be filled sequentially and independently. For ease of understanding, the derivation will be for the one-dimensional case. This can then be easily extended to the two-dimensional case.

Since the pockets each have a volume variance, $\sigma_{V_{mp}}$, and a length variance $\sigma_{X_{mp}}$ and since they are filled independently, the total variance σ_V will be expressed as the sum of the

variances of the pockets filled:

$$\sigma_V = N\sigma_{V_{mp}} \tag{16}$$

The total length of the average one-dimensional spill, $\langle X_{max} \rangle$, is equal to the length of a mean pocket, X_{mp}, multiplied by the number of pockets filled, N.

$$\langle X_{max} \rangle = NX_{mp} \tag{17}$$

$$\sigma_V = \left(\frac{V_{mp}}{X_{mp}} \right)^2 \sigma_x \tag{18}$$

Using Eq. (16)

$$\sigma_x = \left(\frac{X_{mp}}{V_{mp}} \right)^2 N\sigma_{V_{mp}} \tag{19}$$

or

$$\sigma_x^{1/2} = \left(\frac{X_{mp}}{V_{mp}} \right) N^{1/2} \sigma_{V_{mp}}^{1/2} \tag{19a}$$

In dimensionless form, this becomes, using Eq. (16):

$$\frac{\sigma_x^{1/2}}{X_{mp}} = \left(\frac{\langle X_{max} \rangle}{X_{mp}} \right)^{1/2} \cdot \frac{\sigma_{V_{mp}}^{1/2}}{V_{mp}} \tag{20}$$

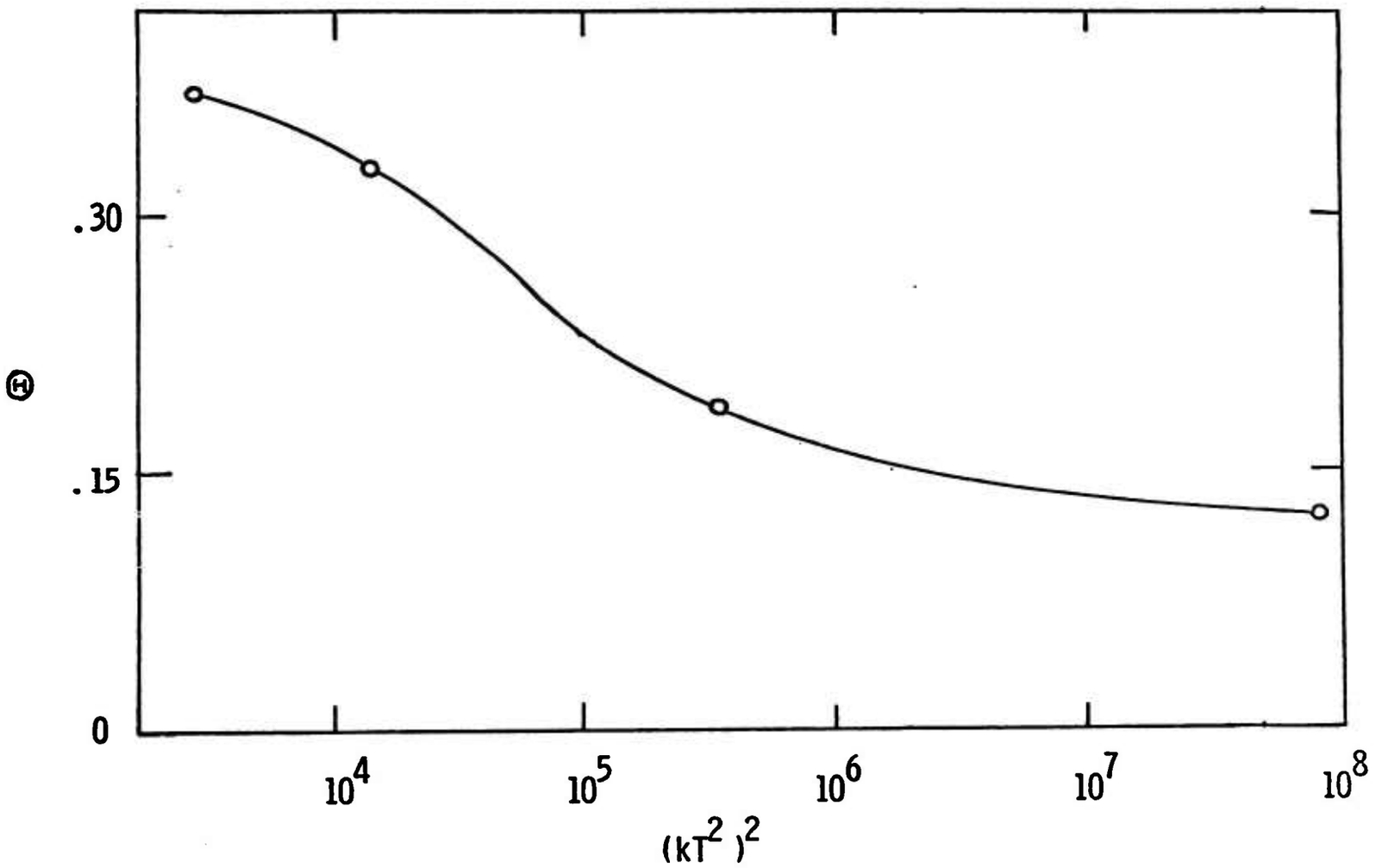

FIG. 6 Θ vs DIMENSIONLESS GROUP $(kT^2)^2$

In the two-dimensional case, one finds

$$\frac{\sigma_s}{S_{mp}}^{1/2} \left(\frac{\langle S_{max} \rangle}{S_{mp}}\right)^{1/2} \tag{21}$$

Where the proportionality constant can be defined as

$$\Theta = \left(\frac{\sigma_{V_{mp}}}{V_{mp}}\right)^{1/2} \tag{22}$$

with Θ as shown in Fig. 6. It is seen that Θ depends only upon the product kT^2. This yields

$$\frac{\sigma_s}{S_{mp}}^{1/2} = \Theta\left(\frac{\langle S_{max} \rangle}{S_{mp}}\right)^{1/2} \tag{23}$$

which is the result presented by Patureau.

4. RESULTS

Figures 7 and 8 show the power spectra for surfaces 1 and 2 respectively. The isotropy assumption can be checked by comparing the spectral points determined from paths taken perpendicularly. The two directions are distinguished by the use of open and closed symbols. By noting that there is little difference between the two directions, one can see that the isotropy assumption is a good one. Also shown on these figures are σ_h, k, T and Θ.

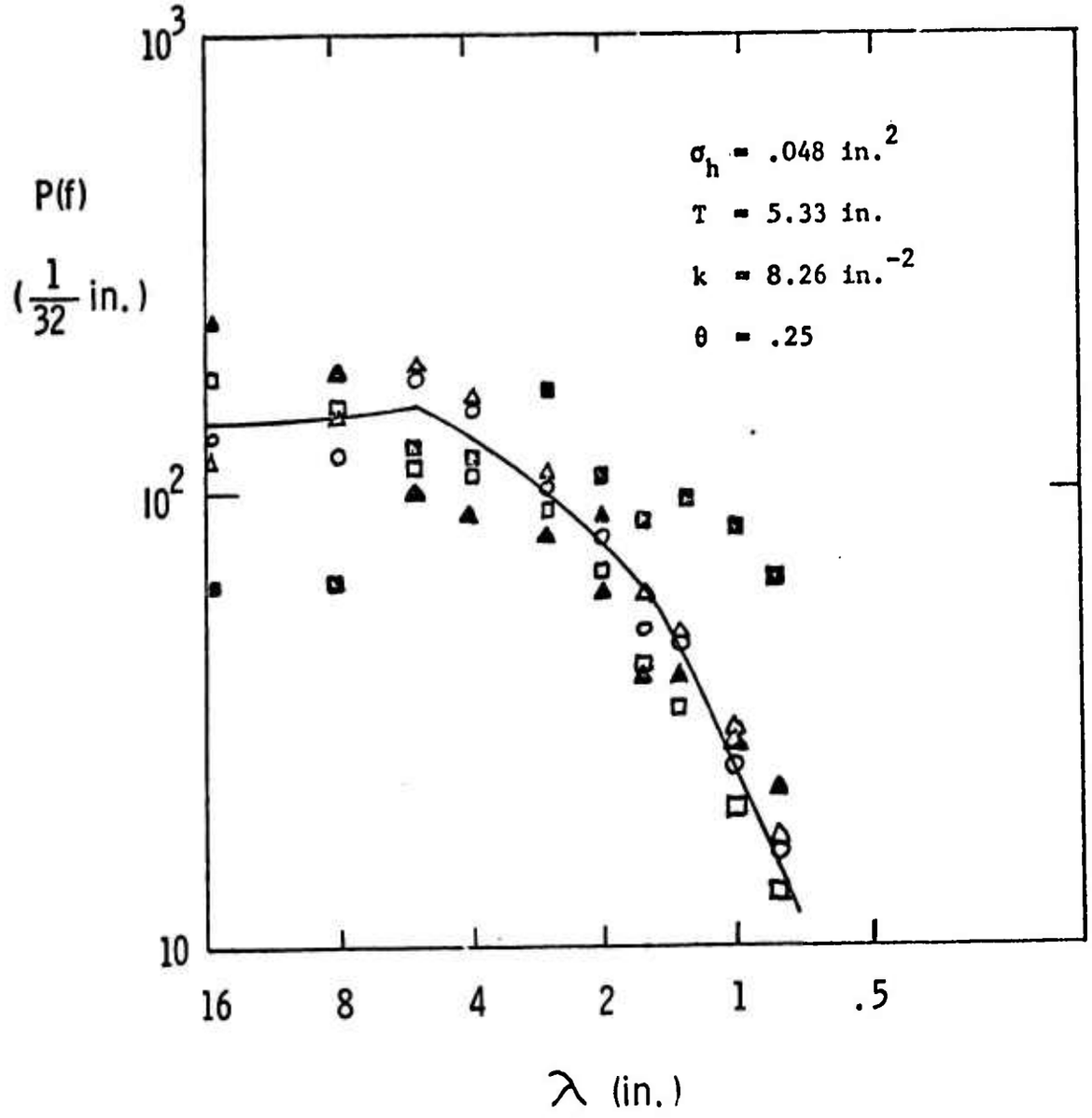

FIG.7 POWER SPECTRUM vs WAVELENGTH FOR SURFACE 1

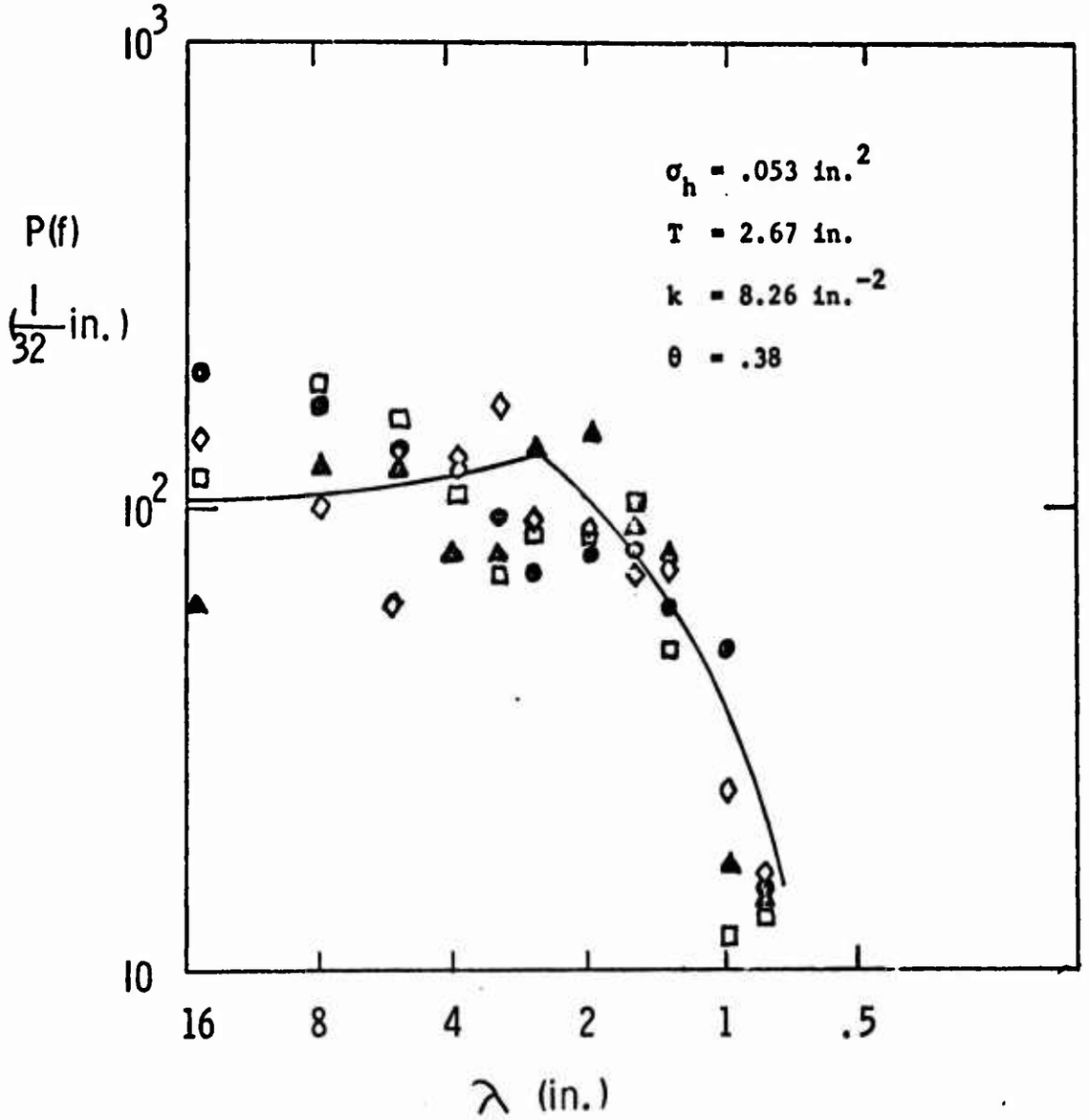

FIG. 8 POWER SPECTRUM vs WAVELENGTH FOR SURFACE 2

Figures 9 and 10 show that the data for the final pool size for surfaces 1 and 2 respectively is in good agreement with Patureau's theory. The values of the scaling area and scaling volume are shown on the figures, where S_{mp} and V_{mp} are as calculated in Eqs. (13) and (14). The solid lines on the graphs are the average of the final size from Eq. (15). The dashed lines on either side represent one standard deviation on each side of the average and were determined from Eq. (23). On these graphs, the open symbols represent over ice runs and the filled symbols indicate under ice runs. It appears that the under ice pools are slightly smaller. This could be within experimental error or could be caused by a slight deflection of the rough surface caused by water pressure. Water was bled from the tank in an attempt to remove the deflections, but some error is anticipated.

Using the inertial theory to correlate the laboratory data led to two distinct groups, over and under ice, with intercepts differing by about a factor of two. Additionally, the over ice data did not correlate well with the data from Glaeser and Vance. In order to determine the proper scaling laws, a series of dimensional graphs were made. Since the radius in the laboratory data appeared to grow approximately as the time to the one-half power, it was decided to calculate $r/t^{1/2}$ for all laboratory and field data. These values were then plotted against volume released, release rate, gravity, and roughness height. Figure 12 shows $r/t^{1/2}$ as a function of volume on the left side and release rate on the right. It can be seen that $r/t^{1/2}$ cannot be described as a function of volume but that $r/t^{1/2}$ does vary approximately as the release rate to the one-third power. Once a rough power law for release rate was known, additional correlations were tried. Using the results of these crossplots and the viscosity experiments, the theory described in Section III was derived.

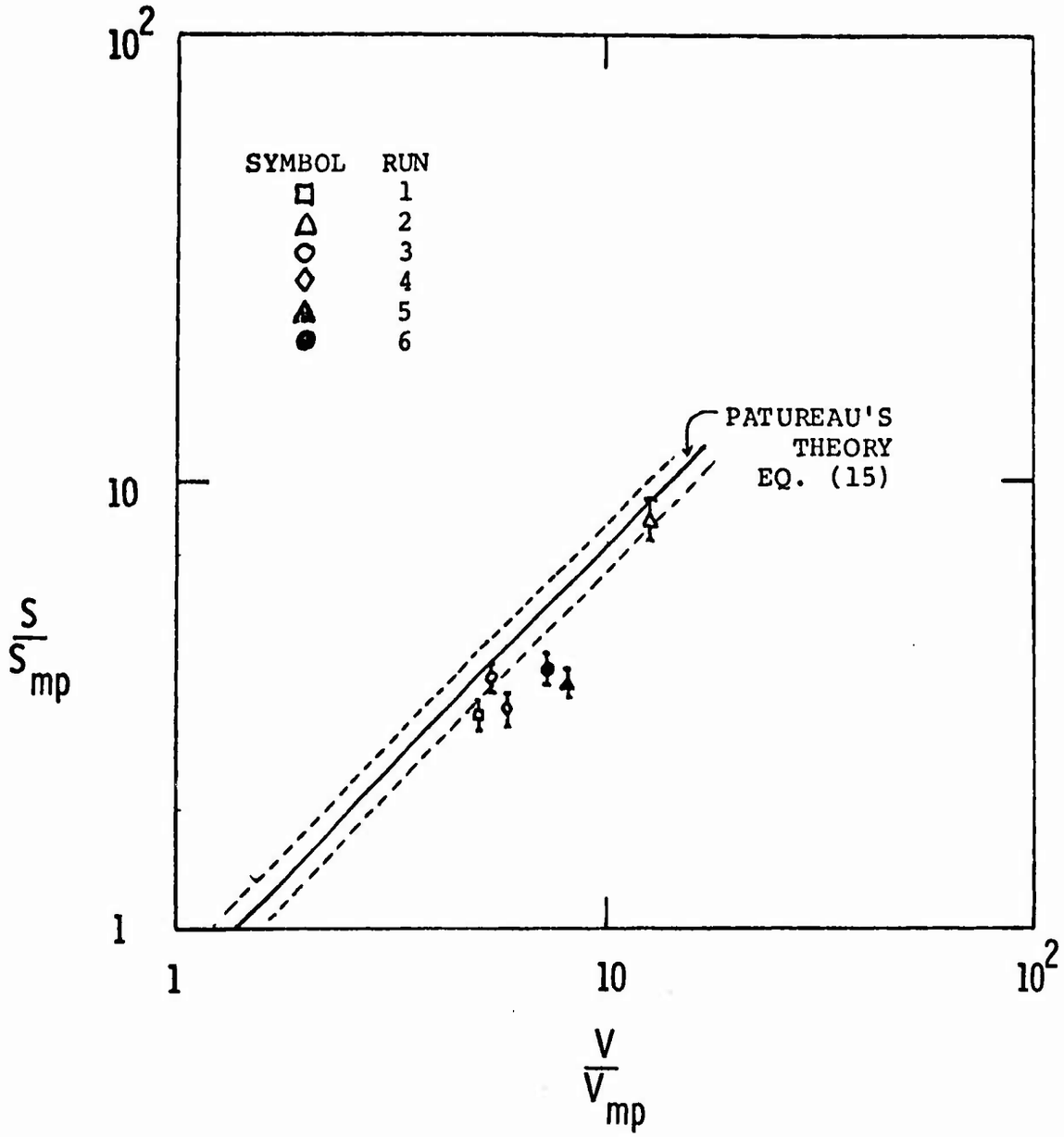

FIG. 9 DIMENSIONLESS VOLUME RELEASED vs SURFACE AREA FOR SURFACE 1

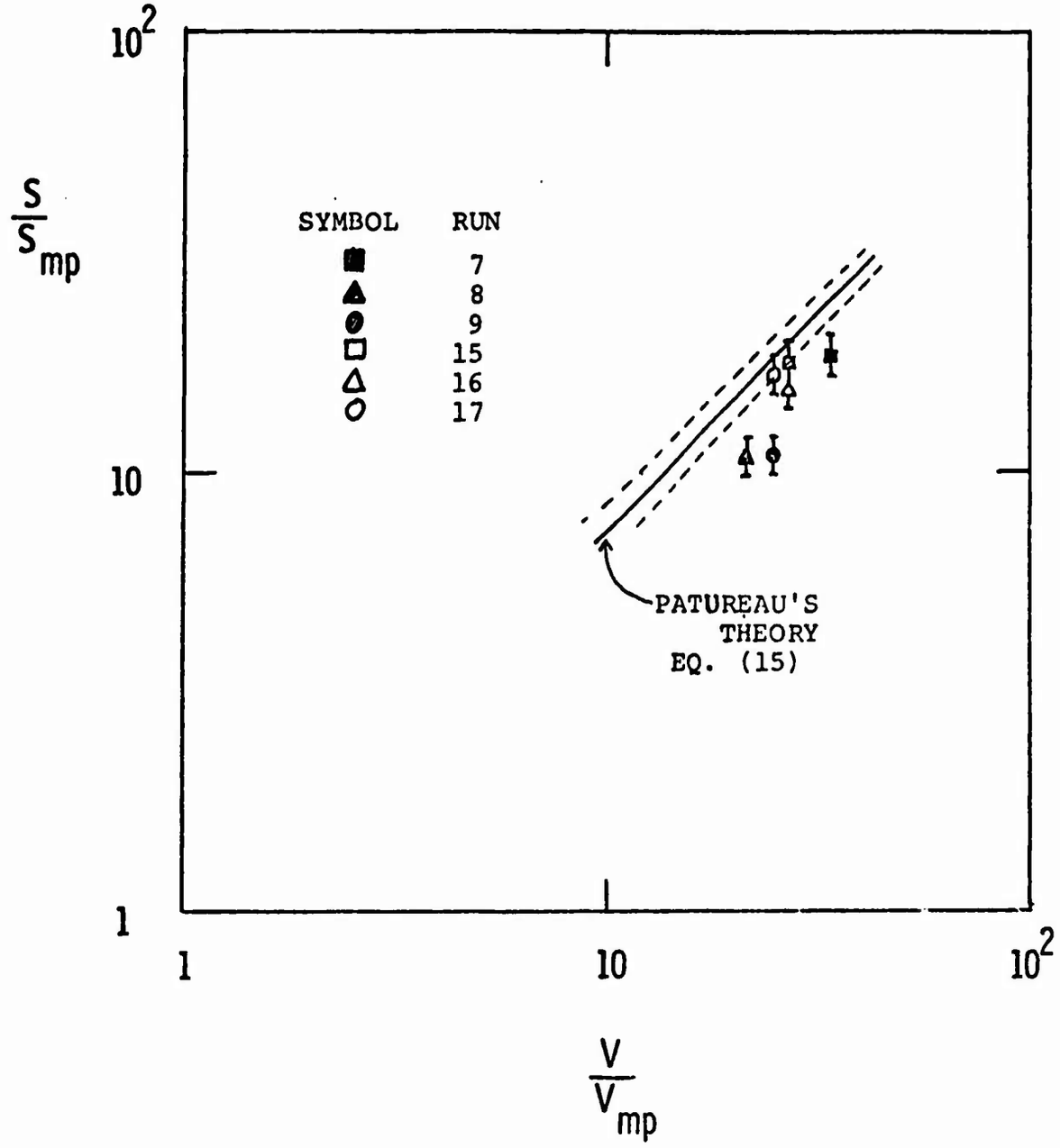

FIG. 10 DIMENSIONLESS VOLUME RELEASED vs SURFACE AREA FOR SURFACE 2

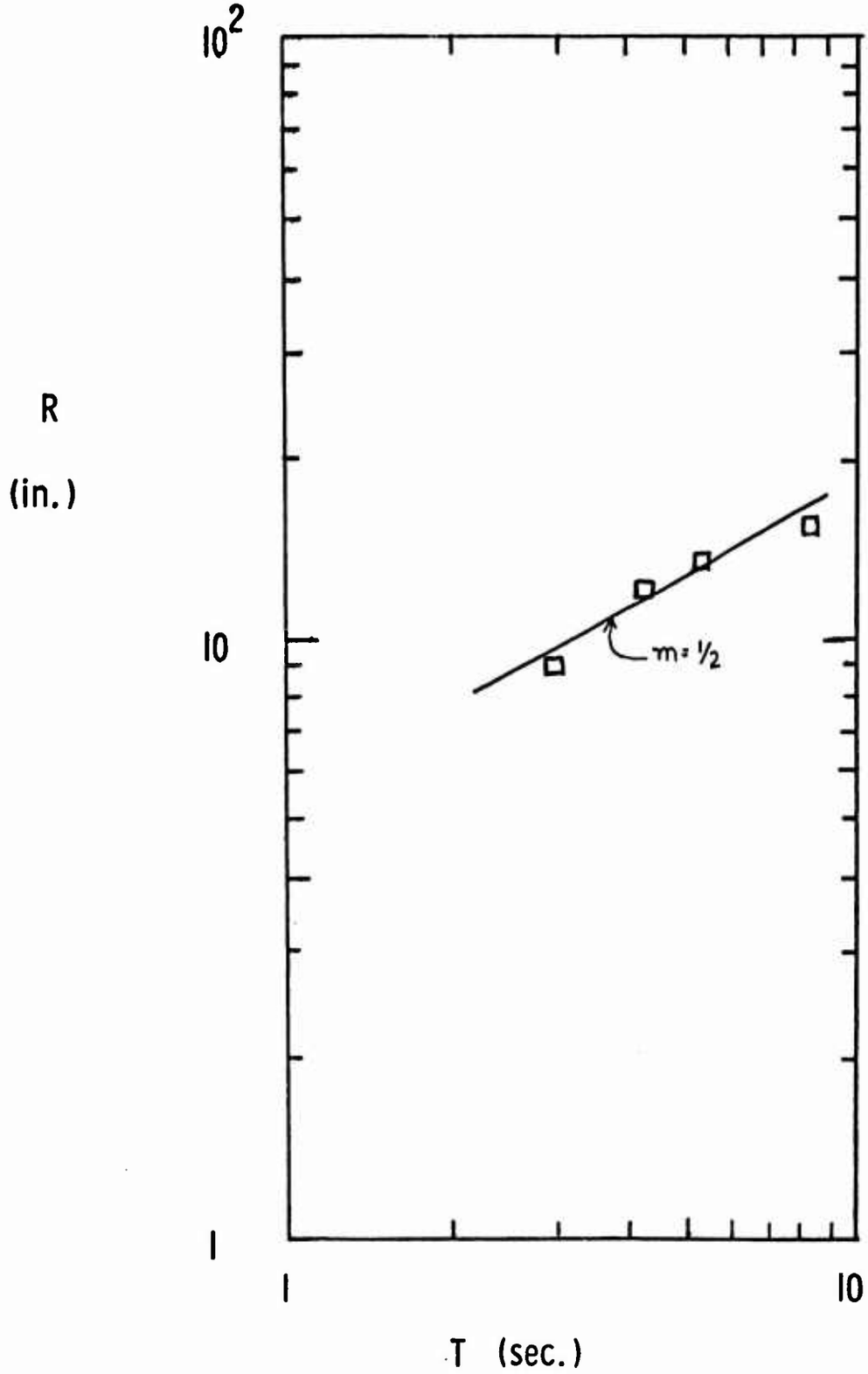

FIG. II RADIUS vs TIME FOR RUN 6

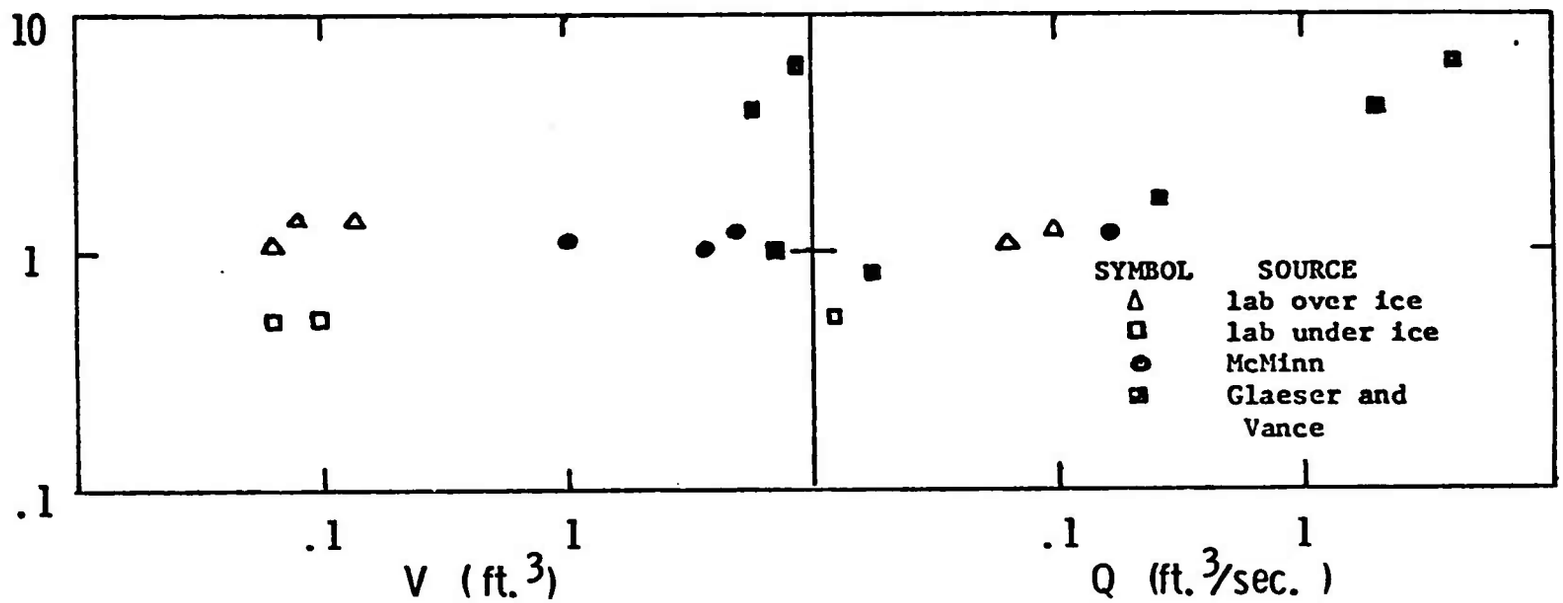

FIG. 12 $R/T^{1/2}$ vs REPRESENTATIVE VOLUMES AND RELEASE RATES FOR FIELD AND LAB DATA

Figure 13 shows the dimensionless radius versus dimensionless time for both over and under ice cases using the results of Section 3. Also shown on this graph is field data from Glaeser and Vance[3] and McMinn[6]. The raw laboratory data that make up this figure is given along with the dimensionless values in Sub-Appendix B-3. The equation that best describes the line in Fig. 13 is:

$$r = .25(\Delta g Q^2/\langle h^- \rangle)^{1/6} t^{2/3}$$

The under ice data shown in Fig. 13 is plotted after allowing for a starting time. It was found that in the under ice case there was a significant lag between the time the stopper was pulled and the actual beginning of the spread. This was due to the time for the kerosene to float up through the water to the surface. This starting time was found to be about 1.5 seconds (see Sub-Appendix B-2).

For the field data, the roughness heights are not known. Thus, the field data was fit to the solid line in Fig. 13 by adjusting the value of the roughness height. In some cases, this led to a value of the roughness height that appears either too large or too small.

However, the experiments were run in small areas with different kinds of surfaces (snow covered, windswept ice, etc.), so effective roughness heights for these experiments could vary greatly.

To expand the results of the laboratory experiments, one must know the characteristics, particularly the roughness height, of the Arctic ice. From laser profilometer traces taken in areas of high spill potential it has been determined that the rough-

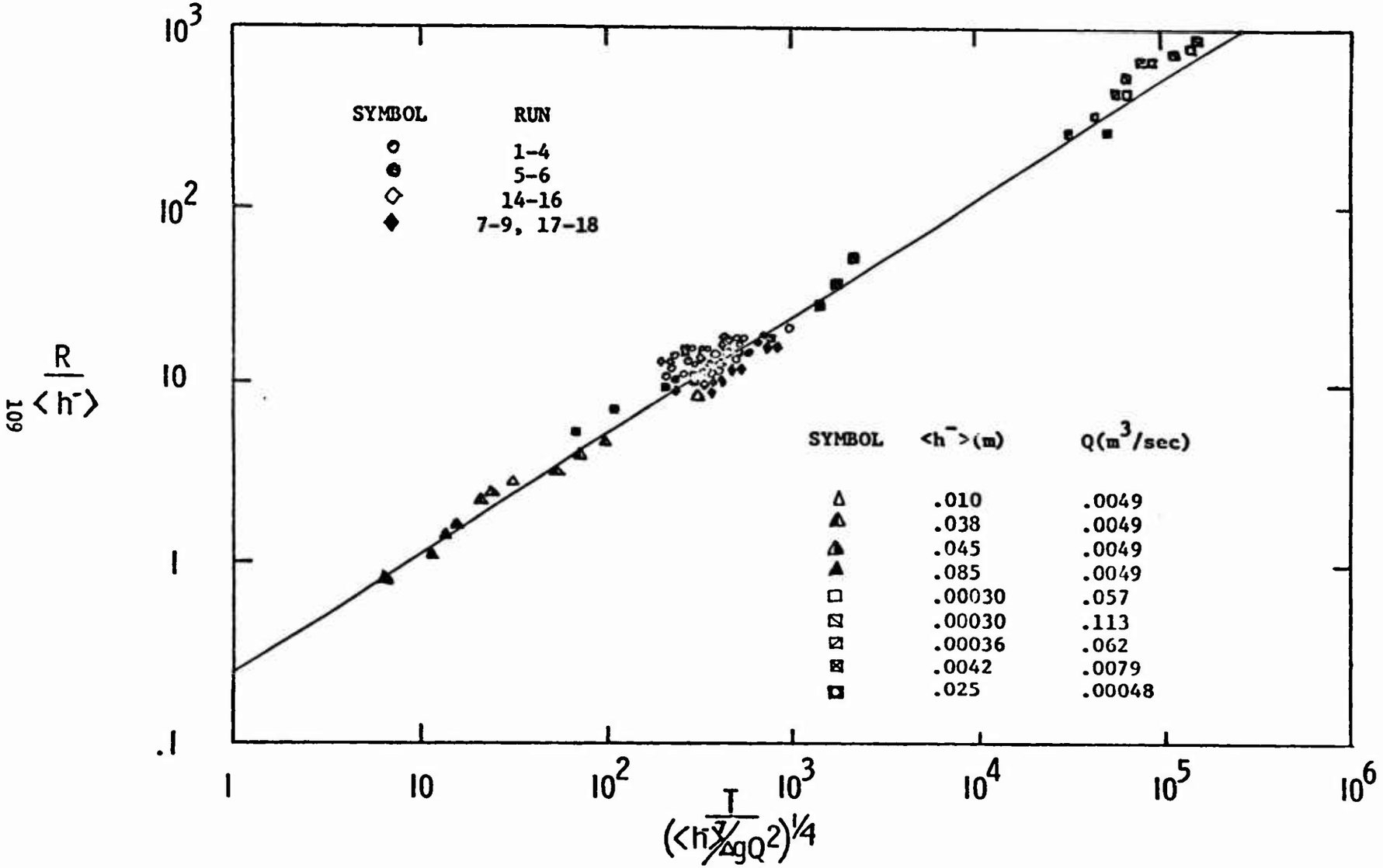

FIG. 13 DIMENSIONLESS RADIUS vs TIME FOR LABORATORY AND FIELD DATA

ness height varies greatly but is seldom less than three centimeters or greater than 60 centimeters. The size of a spill would be on the order of 10^4 cubic meters. Figure 14 shows how the final radius of a spill varies with the roughness height and the total volume released. For an average volume and roughness height the final radius will be on the order of 300 meters.

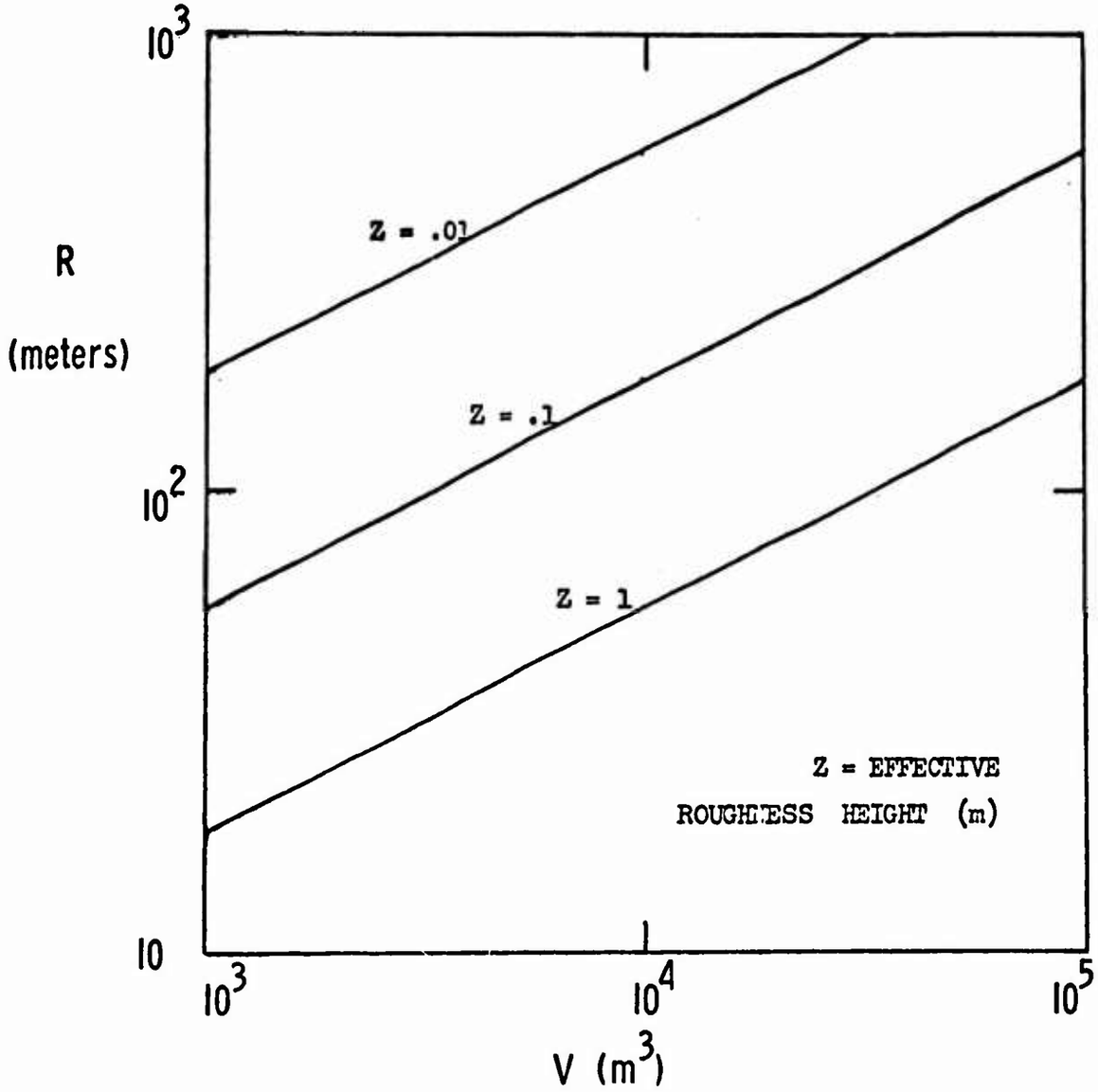

FIG. 14 AVERAGE AREAL COVERAGE vs VOLUME RELEASED FOR A SPILL ON ARCTIC ICE

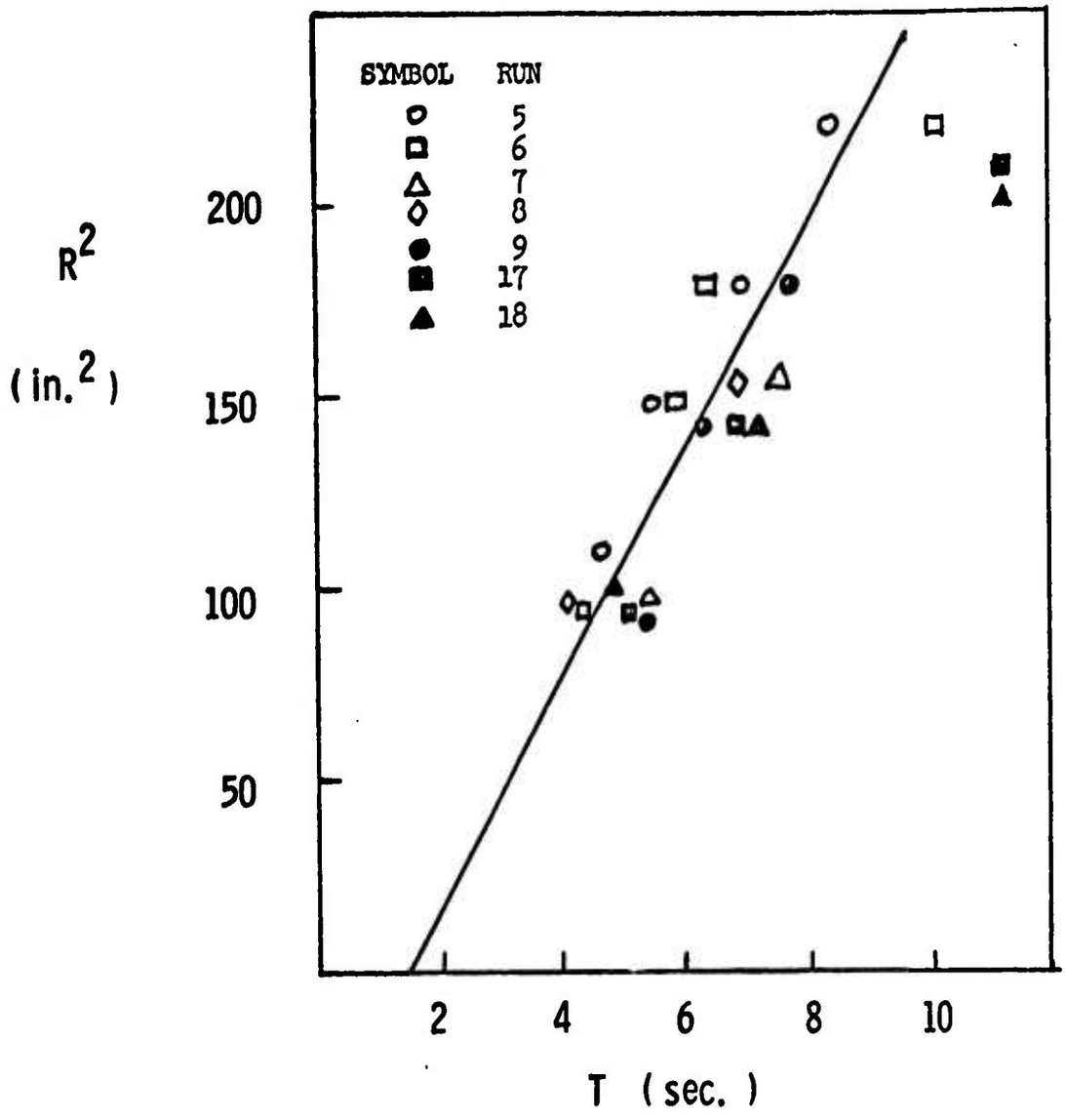

FIG. 15 EXTRAPOLATION OF R^2 vs T TO DETERMINE STARTING TIME

SUB-APPENDIX B-1

Since the Reynolds Numbers of the under ice and over ice experiments differ by a factor of about five and the starting time of the under ice and over ice data differ by about 60%, it was decided to test for viscosity effects. This was done by increasing the viscosity of the over ice fluid (soap and water) by the addition of glycerin and by increasing that of the under ice fluid (kerosene) with SAE 30 wt. oil. The viscosity of the new fluids was measured on a Tag Saybold viscometer. The figures for the viscosities of the various experiments are shown in the table below. Changing the viscosity of the water by a factor of five and the viscosity of kerosene by factors of two and four had no real effect on the fluid spread.

The Reynolds number below is defined as:

$$Re = \frac{\sqrt{g\Delta Z_o}\, Z_o}{\nu}$$

For the over ice experiments with just water, the Reynolds number was about 400 and for the kerosene only under ice experiments, the Reynolds number was about 80.

SUB-APPENDIX B-1
(continued)

Fluid	Exp. No.	Saybolt Viscosity (Seconds)	Kinematic Viscosity (Centistokes)	Temp. (°F)	Re
Water & Glycerin	15,16	42.8	5.1	78	80
Kerosene & Oil	17	44.0	5.5	65	40
Kerosene & Oil	18	57.8	10.0	68	20

SUB-APPENDIX B-2

In the case where the kerosene was released under the rough surface, there was a delay between the time the stopper was pulled and the time that the fluid started to spread. This 'starting time' was found by extrapolating the radius versus time curve to zero radius. Since the radius varies approximately as the square root of the elapsed time, a graph was constructed using the radius as the ordinate and the time squared as the Absissa (see Fig. 15). By extrapolating, the starting time was found to be about 1.5 seconds.

SUB-APPENDIX B-3

Below is the raw data for the laboratory experiments along with the non-dimensionalized values: (in cgs units)

Run 1 Over Surf. 1
Q = 88 V = 90 r_{max} = 16.5

r	$\tilde{r}$	t	$\tilde{t}$
10.5	121	.70	2550
12	138	1.1	4005
14	161	1.5	5460

Run 2 Over Surf. 1
Q = 270 V = 218 r_{max} = 24

r	$\tilde{r}$	t	$\tilde{t}$
12	138	.5	2595
13	150	.65	3375
15	173	1.0	5190
17	196	1.45	7525
19	219	2.0	10.380

Run 3 Over Surf. 1
Q = 190 V = 99 r_{max} = 18

r	$\tilde{r}$	t	$\tilde{t}$
11	127	.65	2840
13	150	.80	3490
15	173	1.3	5680

Run 4 Over. Surf. 1
Q = 123 V = 104 r_{max} = 17

r	$\tilde{r}$	t	$\tilde{t}$
10	116	.60	2110
13	150	.85	2980
14	162	1.05	3690

Run 5 Under Surf. 1
Q = 22.5 V = 144 r_{max} = 18

r	$\tilde{r}$	t	$\tilde{t}$
10.5	121	3.1	2890
12	138	4.3	4010
13	150	5.5	5130
15	172	7.0	6525

Run 6 Under Surf. 1
Q = 21.7 V = 126 r_{max} = 18.5

r	$\tilde{r}$	t	$\tilde{t}$
9.3	110	3.0	2800
12	138	4.3	4015
13	150	5.1	4765
15	172	8.5	7940

SUB-APPENDIX B-3
(continued)

Run 7 Under Surf. 2
Q = 21.9 V = 153 r_{max} = 19.5

r	$\tilde{r}$	t	$\tilde{t}$
10	105	3.7	3030
12	126	5.6	4585
15	158	8.8	7207

Run 8 Under Surf. 2
Q = 20.6 V = 99 r_{max} = 16

r	$\tilde{r}$	t	$\tilde{t}$
9.0	95	2.8	2210
12	126	5.3	4185
15	158	8.8	6952

Run 9 Under Surf. 2
Q = 22.5 V = 117 r_{max} = 16

r	$\tilde{r}$	t	$\tilde{t}$
9	95	3.8	3155
12	126	4.2	3490
14	147	5.9	4900

Run 14 Over Surf. 2
Q = 180 V = 126 r_{max} = 20

r	$\tilde{r}$	t	$\tilde{t}$
12	126	.6	2230
14	147	1.0	3710
15	158	1.25	4640

Run 15 Over Surf. 2
Q = 180 V = 135 r_{max} = 19

r	$\tilde{r}$	t	$\tilde{t}$
10	105	.4	1480
13	137	.75	3180
15	158	1.1	4660

Run 14 Over Surf. 2
Q = 180 V = 126 r_{max} = 19

r	$\tilde{r}$	t	$\tilde{t}$
10	105	.4	1460
12	126	.55	2040
14	147	1.05	3900

Run 17 Under Surf. 2
Q = 14.4 V = 126 r_{max} =

r	$\tilde{r}$	t	$\tilde{t}$
10	105	3.5	3600
12	126	4.9	5080
15	158	6.5	6730

Run 18 Under Surf. 2
Q = 20.0 V = 180 r_{max} =

r	$\tilde{r}$	t	$\tilde{t}$
10	105	2.8	3540
12	126	3.8	4810
15	158	5.8	7340

BIBLIOGRAPHY

1. Blackman, Ralph B., and Tukey, J.W., The Measurement of Power Spectra, Dover, N.Y., 1959.
2. CRREL, SEV Arctic Environment Data Package, Corp of Engineers, Hanover, N.H., 1970.
3. Glaeser, John L., and Vance George P., A Study of the Behavior of Oil Spills in the Arctic, U.S. Coast Guard, Washington, D.C., 1971.
4. Granger, C.W.J., Spectral Analysis of Economic Time Series, Princeton University Press, Princeton, N.J., 1964.
5. Hoult, David P., ed., Oil on the Sea, Plenum Press, N.Y., 1969.
6. McMinn, T.J., Crude Oil Behavior on Arctic Winter Ice, U.S. Coast Guard, Washington, D.C., 1972.
7. Patureau, Jean-Pierre, Statistical Approach for Determining the Extent of an Oil Spill Over a Rough Surface, M.I.T. Master's Thesis, 1972.
8. Suchon, Walter, An Experimental Investigation of Oil Spreading Over Water, M.I.T. Master's Thesis, 1970.

APPENDIX C

STATISTICAL APPROACH FOR DETERMINING THE EXTENT OF AN OIL SPILL OVER A ROUGH SURFACE

1. INTRODUCTION

As one seriously thinks of using the crude oil discovered in the Arctic Slope, no matter which means of transportation will be adopted, it appears that some understanding of how oil would spread on the ice is of major importance.

This problem cannot be dealt with as a classical oil spill on a plane surface because the characteristic feature of an Arctic Ocean ice surface is its roughness. Moreover, field observations show that such a surface can be regarded as formed of "pockets" of different sizes, some of them being interconnected. One can easily see that the oil will stop spreading abruptly after having filled a certain number of pockets. The goal of this work is to determine the final size of the pool as a function of the amount of oil released.

It is clear that the geometry of the "pockets" previously introduced is entirely related to the local variations in the ice surface altitude; it can therefore be determined by functions $h(x,y)$ defined in an arbitrary plane coordinate system xy as the elevation of the ice surface above a reference level; most often in the rest of this work, these functions will be referred to as roughness height. A simple way to record information about these variations in the elevation is to take airborne laser profilometer traces[†]. Such data were obtained by the U.S.

[†]A profiler operating from a plane records the phase delay between transmitted to the ground and reflected laser beam light, thus measuring the altitude variations along straight lines and yielding a random output signal.

Navy in the Beaufort and Chuckchi Seas. There is no doubt, when examining any of these traces, that the major character of the ice roughness is its randomness (Ref. [3]). Releasing the same amount of oil V at different locations on a randomly rough ice surface would result in different values for the measurement of the oil pool final size. Clearly, we must then formulate our problem in a statistical way, namely: the extent to which oil would spread has to be determined in terms of a certain number of statistical parameters characterizing the ice surface where the spill occurs. An analytical treatment of the profilometer traces can provide us with $\bar{h}$[†], the mean value of the roughness height h, σ_h, the variance of h, equal to $(h - \bar{h})^2$, and the auto-correlation function of h. We will see in the course of this work that these quantities are sufficient to give an answer to our problem, provided certain simplifying assumptions are made.

With no more field data than those just introduced, it is unlikely, however, that we should end up with an elaborate and complete description of the oil spreading phenomenon. This paper will only aim at determining the first two statistical moments of the oil pool final size - i.e., its average value and its variance - both in cases when the spreading follows a privileged direction (so called "one-dimensional") and when it doesn't (two-dimensional).

Section 2 will introduce and discuss the basic assumptions necessary to set up a simplified model of the phenomenon, whereas Section 3 will give a general mathematical expression for these quantities in terms of the field data available, namely: h, σ_h and the auto-correlation of h.

[†]The bar denotes an average over a sample.

In Section 4, we will be concerned with applying the previous results to certain ice surfaces where field data is available, thereby involving the modelling of the auto-correlation function of h or, more exactly of its cosine Fourier transform. Finally, in those specific cases examined in Section IV, a simple power law will be derived, relating the first two statistical moments of the final size of the oil pool in a dimensionless form.

2. BASIC ASSUMPTIONS

If the ice surface where the spill occurs is being considered as randomly rough, it is clear that we cannot have a complete definition of the function h relevant to that specific spill, which is what would be necessary to yield a single, definite value for the oil pool size in that case.

A way of overcoming this difficulty is to retain a certain number of statistical properties of h met by different possible "realizations"[†] of the ice surface. These properties are then regarded as "ensemble averaged" over all those realizations and generally consist of a certain number of locally defined statistical moments and correlation functions of h. These quantities provide a certain amount of information common to any ice surface realization that belongs to the ensemble. Obviously, the smaller this number, the more random is the surface and, when the number of such properties goes to infinity, the ice surface tends to be perfectly defined and therefore no longer random. In other words, since we are talking about ensemble averages, all

[†]A "realization" of the ice surface verifying certain statistical conditions is an actual, observed surface such that it meets the previous conditions.

the realizations are becoming identical. The idea is thus to have locally defined functions that give statistical information on a whole ensemble of possible realizations of the ice surface.

In the present case, the only statistical data we have is $\bar{h}$, $\sigma_h = \overline{(h - \bar{h})^2}$ and $\overline{h(P)h(P')}$ where the bar denotes an average over a specific "realization" of the ice surface and where P and P' denote any two different points of that surface. Since these data are "space averaged" and therefore not locally defined, we are lead to make an ergodic hypothesis, assimilating $\bar{\cdot}$ and $\langle . . \rangle$[†] averages. Our random surface is now characterized by $\langle h \rangle$, $\sigma_h = \langle [h - h]^2 \rangle$ and $h(P)h(P')$ but clearly, this is not sufficient since nothing is said about the aspect of the surface.

There appears our second assumption, related to the statistics of the roughness height h: we will suppose h is normally distributed. If $\delta(h)$ denotes this distribution, we have immediately:

$$\delta(h) = \frac{1}{\sqrt{2\pi\sigma_h}} \exp\left\{ - \frac{(h - \langle h \rangle)^2}{2\sigma_h} \right\} \qquad (1)$$

$\delta(h)dh$ represents the fraction of time that h will be found between h and h + dh. It does not seem possible to prove this assumption by any physical argument since the natural processes that make the ice grow are extremely intricate and not thoroughly known. Therefore, we have to verify in each case that this is not too far from the observed distribution; this was done as

[†] i.e., ensemble and space averages are equal.

an example on Fig. 3 where the Gaussian curve $\int_{-\infty}^{h} \delta(\tau)d\tau$ is plotted against h and is compared to corresponding data points measured on a real surface. It appears that the Gaussian approximation is in relatively good agreement with observations.

The third assumption concerns the way the oil would fill the "pockets" of which the ice surface is formed and more precisely, up to what level. Since the ice relief is random, the answer to this question is unlikely to be unique. Most probably, a large number of different levels would appear, corresponding to more or less "open" or "closed" pockets. However, to keep the problem feasible, we have to account only for an average uniform level of the oil pool, which is another way to say that all the "pockets" are interconnected. Moreover, it seems a reasonable assumption - at least most simplifying - to say that this uniform level is the same as that of <h>. No observations exist so far to confirm such a point and the reason why we chose this level is that any other one would have been even more arbitrary and would have lead to more intricate mathematical derivations.

The fourth hypothesis reads as follows: we will always assume throughout this study that the number of "pockets" involved in an oil slick is very large; in other words, the ratio of the volume V released to the mean volume of a pocket is large; this will allow us to give a statistical answer for the final size of the oil pool. This assumption may be considered as valid in so far V is generally large (10,000 to 50,000 m^3 for the crash of a supertanker) and also the ice roughness is such that a big pocket contains many small ones and so on; therefore, even if the slick occurs in a big one, the numbers of pockets involved will always be large.

These four assumptions obviously cannot lead to a sophisticated model since they mainly reflect our lack of information about ice topography in the Arctic Slope. Moreover, the general mathematical results obtained from this model won't be the unique approximate solution to the oil spreading problem since, for instance, another frequency distribution for h could have been selected - log-normal particularly -, or another height of the oil pool level could have been chosen. Nevertheless, the simple model we can thus build provides us with a first understanding of how oil spreads over a statistical surface.

3. MATHEMATICAL ANALYSIS

The first four subsections will be concerned with a two-dimensional study whereas subsection 3.5 will briefly state the results for a one-dimensional case.

3.1 Problem

We suppose no privileged direction in the ice surface, at least for the scale of the roughness we are interested in[†]. Therefore, the ice topography is determined by a two-dimensional function $h(x,y)$ describing the variations of the surface altitude with respect to a reference plane. The origin of the coordinates x and y is taken at the point of oil release and the reference level is chosen so that:

$$\langle h(x,y) \rangle = 0 \qquad (2)$$

[†]It has been shown that big pressure ridges do appear with certain definite orientations.

There again, $\langle h(x,y) \rangle$ denotes the ensemble average of h(x,y) where the averaging ensemble consists of the many ice surface realizations that can be observed in the region one considers. From our hypothesis, $\langle h(x,y) \rangle$ does not depend on x and y and therefore has to be identified to the space average $\overline{h(x,y)}$ of h(x,y) over the realizations of the ice surface themselves.

By the same token, $\sigma_h = \langle h^2(x,y) \rangle$ is the variance of h(x,y) calculated over the whole ensemble. Hence, the frequency distribution of h(x,y), assumed to be Gaussian, is independent of any direction and is given by Eq. (1).

A proper investigation of the actual ice topography can† provide us with a two-dimensional auto-correlation function defined as:

$$\Psi(\xi,\eta) = \langle h(x + \xi, y + \eta)\, h(x,y) \rangle \qquad (3)$$

We can thus pose the two-dimensional problem in the following terms: in a region of the Arctic Ocean where we know $\sigma_h = \langle h^2(x,y) \rangle$ and $\Psi(\xi,\eta)$, a volume V of oil is released at point x = y = 0. What will be the total area covered with oil and also, what will be the final geometrical aspect of the pool?

The general mathematical answer will consist of the first two statistical moments of the oil pool size in

†By building a two-dimensional grid of laser profilometer traces.

terms of V, σ_h and $\Psi(\xi,\eta)$, along with a dissymmetry factor expressing the most probable ratio of the longest dimension of the pool to the smallest one.

3.2 Dissymmetry of the Final Oil Pool

As we do not allow any dissymmetry in the frequency distribution of h(x,y), the final shape of the slick will be influenced by the aspect of the "pockets" themselves in the plane xy. In general, the ice surface is not isotropically rough. It follows that if λx and λy are the ensemble averages of a pocket dimensions in the x and y directions respectively, the ratio μ of λx to λy can be called "dissymmetry factor" since it provides a rough idea about the final pool aspect.

From Sub-Appendix C-1, it appears that μ is given by:

$$\mu = \left\{ \frac{\partial^2 \Psi}{\partial \eta^2}(0,0) \Big/ \frac{\partial^2 \Psi}{\partial \xi^2}(0,0) \right\}^{1/2} \qquad (4)$$

Now, let us imagine how oil would spread from point of release. Since the volume V is supposed to be very large, the shape of the pockets is not important at the beginning and the slick would propagate circularly. But, after this initial phase, one can assume that the geometrical aspect of the pockets would influence the final shape of the oil slick.

Considering a laser profilometer trace that passes through the origin of the coordinates x and y, it is clear from our ergodic hypothesis that the statistics of the

roughness height remain the same all along the trace. It follows that the origin of the coordinates is a geometric center of symmetry for the pool shape. Moreover, in order to simplify further calculations, we assume that the resulting oil pool is rectangular, x_{max} and y_{max} being the x-direction and y-direction dimensions respectively.

Therefore, it follows that:

$$\frac{x_{max}}{y_{max}} = \mu \neq \text{unity, in general}$$

Obviously, when the ice surface is truly isotropic, μ is unity and the final pool is a square in our assumption.

3.3 First Two Statistical Moments of the Oil Pool Final Size

As was suggested at the end of the last sub-section, the oil pool is likely to be symmetric with respect to the point of release i.e., the origin of the coordinates. Hence, defining $h^+(x,y)$ and $h^-(x,y)$ such that $h = h^+ + h^-$ and:

$$h^-(x,y) = 0 \qquad \text{when} \quad h(x,y) \geq 0$$

$$h^-(x,y) = h(x,y) \quad \text{when} \quad h(x,y) < 0 \qquad (5)$$

we can introduce $v(x,y)$ as the volume held by the ice surface - under the third assumption of Section 3 - within a

rectangle of dimensions x and y. Then:

$$v(x,y) = -\int_{-x/2}^{+x/2}\int_{-y/2}^{+y/2} \bar{h}(x,y)\, dx\, dy \qquad (6)$$

This is a mathematic definition and, evidently, it does not account for the fact that the oil-air interface must be horizontal when edge pockets are not completely filled up to the average uniform level; this fact is illustrated on the sketch, Fig. 1 for the one-dimensional spreading. It follows that the mathematical extent of the oil is only slightly different from the real one: at most within a pocket. Since we made the assumption of a large number of pockets, we can define x_{max} and y_{max} as the x-direction and y-direction maximum extents of the final pool when a volume V of oil is being released over a specific realization of the ice surface; namely:

$$V = -\int_{-x_{max}/2}^{x_{max}/2}\int_{-y_{max}/2}^{y_{max}/2} \bar{h}(x,y)\, dx\, dy \qquad (7)$$

Or, introducing the area S_{max} defined as:

$$S_{max} = x_{max}\, y_{max} \qquad (8)$$

Relation (7) becomes:

$$V = -\int_{S_{max}} \bar{h}(x,y)\, dx\, dy \qquad (9)$$

As the function $\bar{h}$ is everywhere continuous, we can also write relation (9) as:

$$V = -\int_{\langle S_{max}\rangle} \bar{h}(x,y)\, dx\, dy - [S_{max} - \langle S_{max}\rangle]\bar{h}(\mu,\rho) \qquad (10)$$

where point (μ,ρ) belongs to the surface $(S_{max} - \langle S_{max}\rangle)$; $\bar{h}(\mu,\rho)$ is exactly the average of $\bar{h}$ taken over the surface $(S_{max} - \langle S_{max}\rangle)$.

We now assume that:

$$\bar{h}(\mu,\rho) \doteq \langle \bar{h}(\xi,\eta)\rangle \qquad (11)$$

This cannot be justified in general. Therefore, Eq. (11) is more valid as this surface becomes large since, when the averaging sample gets large enough, the average of $\bar{h}$ approaches $\overline{\bar{h}(\xi,\eta)}$, hence $\langle \bar{h}(\xi,\eta)\rangle$ from our ergodic hypothesis. An "a posteriori" verification will thus be possible.

Then, taking the ensemble average of (10) and making use of the previous approximation, we obtain the first

statistical moment of the pool size, namely:

$$\langle S_{max} \rangle = - \frac{V}{\langle h^{-}(\xi,\eta) \rangle} \tag{12}$$

To determine the second moment, let us first notice that σ_s, the variance of S_{max} and σ_ν the variance of $\nu(\langle x_{max} \rangle, \langle y_{max} \rangle)$ are related. By definition:

$$\sigma_s = \langle (S_{max} - \langle S_{max} \rangle)^2 \rangle \tag{13}$$

$$\sigma_\nu = \left\langle \left[\nu(\langle x_{max} \rangle, \langle y_{max} \rangle) - \langle \nu(\langle x_{max} \rangle, \langle y_{max} \rangle) \rangle \right]^2 \right\rangle \tag{14}$$

From relations (10) and (11), it comes out that:

$$\left\langle \left[\int_{\langle S_{max} \rangle} h^{-}(x,y) - V \right]^2 \right\rangle = \langle (S_{max} - \langle S_{max} \rangle)^2 \rangle \langle h^{-}(\xi,\eta)^2 \tag{15}$$

Or:

$$\sigma_\nu = \sigma_s \langle h^{-}(\xi,\eta)^2 \rangle \tag{16}$$

Therefore, computing σ_U in Sub-Appendix C-2, we end up with:

$$\sigma_s = \frac{16}{\langle \bar{h}(\xi,\eta)^2 \rangle} \int_0^{\langle x_{max} \rangle/\sqrt{2}} \int_0^{\langle y_{max} \rangle/\sqrt{2}} \left[\frac{\langle x_{max} \rangle}{\sqrt{2}} - \xi \right] \left[\frac{\langle y_{max} \rangle}{\sqrt{2}} - \eta \right] \left[\bar{\Psi}(\xi,\eta) - \frac{\sigma_h}{2\pi} \right] d\xi \, d\eta \qquad (17)$$

From all previous calculations, especially relations (12) and (17), it appears that knowing $\langle \bar{h}(\xi,\eta) \rangle$ and $\bar{\Psi}(\xi,\eta)$ enables us to derive the average value $\langle S_{max} \rangle$ and the standard deviation $\sigma_s^{1/2}$ of the total area covered with oil, in terms of the amount V released. Furthermore, an idea about the dissymmetry in the aspect of the pool can be gotten from coefficient μ. This will constitute our answer to the two-dimensional problem posed in Sub-section 3.1, provided we can relate $\langle \bar{h}(\xi,\eta) \rangle$ and $\bar{\Psi}(\xi,\eta)$ to the available statistical data i.e., σ_h and $\Psi(\xi,\eta)$. This is the purpose of the next sub-section.

3.4 Determination of $\bar{h}(\xi,\eta)$ and $\bar{\ }(\xi,\eta)$

We now go into more detail about the distribution function $\delta(h)$ that was first mentioned in the Introduction. This function tells us that the probability h will lie between γ and $\gamma + d\gamma$ is $\delta(\gamma)d\gamma$ and therefore:

$$\int_{-\infty}^{+\infty} \delta(\gamma) d \quad = \quad 1 \qquad (18)$$

Assuming, as in our second hypothesis, that this frequency distribution is Gaussian with mean value 0 implies that h will be negative as many times as it is positive. Since γ is the value taken by a stochastic function h, it is also a stochastic variable. Therefore, as we know its frequency distribution function $\delta(\gamma)$, it is clear that the average of a stochastic quantity Q uniquely related to γ is expressed by:

$$\langle Q \rangle = \int_{-\infty}^{+\infty} Q(\gamma)\delta(\gamma)d \tag{19}$$

If now we identify Q to the value of $\bar{h}(x,y)$, it follows from relations (5):

$$Q = \gamma \quad \text{when} \quad \gamma \leq 0$$

$$Q = 0 \quad \text{when} \quad \gamma > 0 \tag{20}$$

Then, substituting into Eq. (19) for $\delta(\gamma)$ and $Q(\gamma)$:

$$\langle \bar{h}(\xi,\eta) \rangle = \int_{-\infty}^{0} \frac{\gamma}{\sqrt{2\pi\sigma_h}} \exp\left(-\frac{\gamma^2}{2\sigma_h}\right) d\gamma \tag{21}$$

Or, performing the integration:

$$\langle \bar{h}(\xi,\eta) \rangle = -\sqrt{\frac{\sigma_h}{2\pi}} \tag{22}$$

Now, to determine $\Psi^-(\xi,\eta)$, we have to extend what we previously did for a one-dimensional distribution of h to a joint two-dimensional frequency distribution. We end up with the following relation (see Sub-Appendix C-3 for details):

$$\Psi^-(\xi,\eta) = \left[\frac{(\Psi_o - \Psi)^3}{\pi(\Psi_o + \Psi)}\right]^{1/2} \left\{ \int_0^\infty (u^2 - \tfrac{1}{2}) \operatorname{erf}(u) \exp\left(-u^2 \frac{\Psi_o - \Psi}{\Psi_o + \Psi}\right) du + \frac{\Psi_o + \Psi}{4\sqrt{\pi}\Psi_o} \right\} \quad (23)$$

where we have set for convenience:

$$\Psi_o = \Psi(0,0)$$

$$\Psi = \Psi(\xi,\eta) \quad (24)$$

It appears (see relation (7) in Sub-Appendix C-4) that $\Psi^-(0,0) = \frac{1}{2}\Psi(0,0)$ which is consistent with the physical conditions at $\Psi = \Psi_o$ namely:

$$\Psi(0,0) = \langle h^2 \rangle = \langle (h^+ + h^-)^2 \rangle = \langle h^{+2} \rangle + \langle h^{-2} \rangle + 2\langle h^+ h^- \rangle = 2\langle h^{-2} \rangle \quad (25)$$

When assuming the statistics of h^- and h^+ are the same as suggested by a normally distributed h. The product h^+h^- must always be zero as can be seen by Eq. (5).

Furthermore, when ξ or η tends to infinity, $\Psi^-(\xi,\eta)$ tends to $\frac{\sigma_h}{2\pi}$, in compliance with the fact that $h^-(x,y)$ and $h^-(x + \xi, y + \eta)$ are then no longer correlated. Therefore, according to relation (22):

$$\langle h^-(x,y)h^-(x + \ ,y + \ )\rangle = \langle h^-(x,y)\rangle\langle h^-(x + \xi, y + \eta)\rangle$$

$$= \langle h^-(\xi,\eta)\rangle^2 = \sigma_h/2\pi \qquad (26)$$

We have therefore provided a means of deriving the statistical quantities we need in Sub-section 3.3, i.e., $\Psi^-(\xi,\eta)$ and $\langle h^-(\xi,\eta)\rangle$, from the field data generally available, namely: $\sigma_h = (h - \bar{h})^2$, the variance of the roughness height and $\Psi(\xi,\eta)$, its auto-correlation function.

3.5 One-Dimensional Case

We can imagine that in a particular region, the statistics of the ice roughness are almost one-dimensional; that is to say, the averaging ensemble consists here of traces parallel to this privileged direction we denote by x. Therefore, the ensemble $\langle h\rangle$ and auto-correlation function are only functions of x. And, if h(x) denotes the elevation (positive or negative) above the mean value of h taken along the trace (see Fig. 1), we have from our ergodic hypothesis:

$$\langle h(x) \rangle = \bar{h}(x) = 0$$

$$\langle h^2(x) \rangle = \overline{h^2(x)} = \sigma_h \quad \text{variance of } h \tag{27}$$

and, $\psi(\tau)$ being the auto-correlation function of $h(x)$:

$$\psi(\tau) = \langle h(x)h(x+\tau) \rangle = \overline{h(x)h(x+\tau)} \tag{28}$$

From the previous considerations, it follows that any actual surface profile parallel to x will be described by the statistical properties (27) and (28).

Now, suppose an oil spill occurs in such a zone, a volume V being released per unit width perpendicular to x; if the spill is wide enough, we can regard the spreading of oil as one-dimensional in the direction of x. This is not completely unrealistic since narrow water leads bounded by large floes are fairly frequent in the Arctic Slope. Under these conditions, a large oil spill would first spread rapidly on water, thus creating this wide spill (V per unit width) that would further spread over ice almost in a single direction perpendicular to the lead.

We can then put our problem this way: a volume of oil V per unit direction perpendicular to x is released at point $x = 0$. What will be the maximum abscissa x_{max} reached by the oil when it has come to a standstill?

We will just state the one-dimensional results since their derivation is quite similar to that of the two-dimen-

sional study in the previous sub-sections. A more detailed analysis is given in Sub-Appendix C-5. The first statistical moment $\langle x_{max} \rangle$ of the oil pool final size is found to be:

$$\langle x_{max} \rangle = - \frac{V}{\langle \bar{h}(\xi) \rangle} \tag{29}$$

whereas the second moment σ_x defined as:

$$\sigma_x = \left\langle \left[x_{max} - \langle x_{max} \rangle \right]^2 \right\rangle \tag{30}$$

appears to be:

$$\sigma_x = \frac{4}{\langle \bar{h} \rangle^2} \int_0^{\langle x_{max} \rangle / \sqrt{2}} \left[\frac{\langle x_{max} \rangle}{\sqrt{2}} - \tau \right] \left[\bar{\psi}(\tau) - \frac{\sigma_h}{2\pi} \right] d\tau \tag{31}$$

Here again, $\bar{\psi}(\tau)$ and $\langle \bar{h} \rangle$ are related to $\psi(\tau)$ and σ_h through the relations:

$$\langle \bar{h} \rangle = - \sqrt{\frac{\sigma_h}{2\pi}} \tag{32}$$

$$\bar{\psi}(\tau) = \sqrt{\frac{(\psi_o - \psi)^3}{\pi(\psi_o + \psi)}} \left\{ \int_0^\infty (u^2 - \tfrac{1}{2}) \operatorname{erf}(u) \exp\left(- u^2 \frac{\psi_o - \psi}{\psi_o + \psi} \right) du + \frac{\psi_o + \psi}{4\sqrt{\pi}\, \psi_o} \right\} \tag{33}$$

where: $\psi_o = \psi(0)$

$\psi = \psi(\tau)$

3.6 General Mathematical Results

In this section, we have been able to give an analytical expression for the first two statistical moments of the oil slick final size, resulting from a spill of volume V. Thus, when the oil spreading is either one-dimensional (with a privileged direction) or two-dimensional (no privileged direction), the assumptions made in Section 2 enabled us to derive the ensemble average value of the pool size and its standard deviation, as well as a "dissymmetry factor" μ characterizing the aspect of the slick (in the two-dimensional case only).

These quantities are all determined in terms of σ_h, the variance of the roughness height h, and the auto-correlation function of h (either $\Psi(\tau)$ or $\Psi(\xi,\eta)$.

Namely:

$$\left.\begin{aligned} \langle x_{max} \rangle &= \frac{V\sqrt{2\pi}}{\sqrt{\sigma_h}} \\ \sigma_x &= \langle [x_{max} - x_{max}]^2 \rangle = \frac{8\pi}{\sigma_h} \int_0^{\langle x_{max} \rangle/\sqrt{2}} \left[\frac{\langle x_{max} \rangle}{\sqrt{2}} - \tau\right] \left[\psi^-(\tau) - \frac{\sigma_h}{2\pi}\right] d\tau \end{aligned}\right\} \text{1-dim. case} \qquad (34)$$

where $\psi^-(\tau)$ is obtained by equation (15) of Sub-Appendix C-3.

$$\left.\begin{aligned}
&\langle S_{max}\rangle = \frac{V\sqrt{2\pi}}{\sqrt{\sigma_h}} \\
&\sigma_s = \langle [S_{max} - \langle S_{max}\rangle]^2\rangle = \frac{32\pi}{\sigma_h} \int_0^{\langle x_{max}\rangle/\sqrt{2}} \int_0^{\langle y_{max}\rangle/\sqrt{2}} \\
&\left[\frac{\langle x_{max}\rangle}{\sqrt{2}} - \xi\right] \cdot \left[\frac{\langle y_{max}\rangle}{\sqrt{2}} - \eta\right] \left[\Psi^-(\xi,\eta) - \frac{\sigma_h}{2\pi}\right] d\xi\, d\eta \\
&\mu = \frac{\partial^2}{\partial\eta^2}(0,0) \Big/ \frac{\partial^2}{\partial\xi^2}(0,0)
\end{aligned}\right\} \text{2-dim. case} \qquad (35)$$

where Ψ^- is obtained by Eq. (18) of Sub-Appendix C-3.

However, we have to point out again that these results do not constitute the unique answer to the general problem of oil spreading over an ice surface since the basic assumptions made in Sub-section 3.2 are quite limiting. Nevertheless, they can provide us with a first understanding of the possible effects of an oil slick in an Arctic environment.

4. APPLICATION - SAMPLE CALCULATIONS

In this section, the general mathematical results of the last section will be applied to a certain number of specific cases of ice topography where the corresponding statistical field data is available.

Both in the one and two-dimensional cases (for privileged and no privileged direction of spreading respectively), the statistics, i.e., the first and second moments of the final size of the oil pool, have been determined in terms of σ_h, the variance of the roughness and ψ, its auto-correlation function. We recall here that h stands for the variations in altitude of the ice surface with mean value 0.

$$\sigma_h = \langle h^2 \rangle \tag{36}$$

$$\psi(\tau) = \langle h(x)h(x+\tau) \rangle \quad \text{in the 1-dim. case} \tag{37}$$

$$\Psi(\xi,\eta) = \langle h(x,y)h(x+\xi, y+\eta) \rangle \quad \text{in the 2-dim. case} \tag{38}$$

Then within a certain region of the Arctic Slope that can generally be regarded as large compared to the area of an eventual oil slick, the ice topography obeys the statistics expressed either by Eqs. (36) and (37) or by Eqs. (36) and (38) when the oil spreading phenomenon is one and two-dimensional respectively.

Now, in order to give a numerical answer to a specific oil slick problem, we have to know σ_h and either ψ or Ψ characterizing that part of the Arctic Slope where the spill occurs, and that are the results of field observations. However, the statistical properties of the permafrost relief are generally given in the form of a power density spectrum of the ice surface (Ref. [3]). We must therefore use that kind of field data instead of the auto-correlation function itself.

From the Wiener theorem in generalized harmonic analysis, it appears that the auto-correlation function and the power density spectrum are related by a Fourier cosine transformation. Thus, if P denotes the power density spectrum of h, it follows that:

$$\left.\begin{aligned} \psi(\tau) &= \int_{-\infty}^{+\infty} P(F) \cos 2\pi f\tau \, df \\ P(f) &= \frac{1}{2\pi} \int_{-\infty}^{+\infty} \psi(\tau) \cos 2\pi f\tau \, d\tau \\ \psi(0) &= \sigma_h = \int_{-\infty}^{+\infty} P(f) \, df \end{aligned}\right\} \text{in the one-dimensional case} \qquad (39)$$

And:

$$\left.\begin{aligned} \Psi(\underline{X}) &= \int_{-\infty}^{+\infty} P(\underline{U}) \cos (2\pi \underline{U}.\underline{X}) \, d\underline{U} \\ P(\underline{U}) &= \frac{1}{4\pi^2} \int_{-\infty}^{+\infty} \Psi(\underline{X}) \cos (2\pi \underline{U}.\underline{X}) \, d\underline{X} \\ \Psi(\underline{0}) &= \sigma_h = \int_{-\infty}^{+\infty} P(\underline{U}) \, d\underline{U} \end{aligned}\right\} \text{in the two-dimensional case} \qquad (40)$$

where $\underline{U}$ is a frequency vector of components U_1 and U_2 and $\underline{X}$ any vector of the plane xy of components ξ and η.

Therefore, it is clear that the information we need about the ice surface statistics, i.e., σ_h and the auto-correlation function of h, is contained in the power density spectrum P. The problem is now to build a continuous function P fitting the observed power spectrum as well as possible. This is the object of the next sub-section.

4.1 Modelling of the Power Spectra

In order to make the mathematical analysis of Section 2 applicable to any part of the ice in the Arctic Ocean, we have to determine the parameters necessary to describe the most important features of the ice surface statistics. A general answer to this modelling problem cannot be given here, even by increasing the number of such parameters since the actual data is far from being complete and reliable. Moreover, another problem is raised by the two-dimensional case of oil spreading since no corresponding field data - two-dimensional functions $\Psi(\xi,\eta)$ - is available to date. Therefore, in order to obtain numerical orders of magnitude, we have assumed that a two-dimensional auto-correlation function $\Psi(\xi,\eta)$ can be regarded as the product of two one-dimensional auto-correlation functions. Namely:

$$\Psi(\xi,\eta) = \sigma_h \, \psi_1(\xi) \, \psi_2(\eta) \qquad (41)$$

There is no evidence at all that this is correct and it only appears as a fair and indispensable assumption to treat the two-dimensional case. Therefore, since the latter can be derived from one-dimensional field data, this sub-section will only be concerned with the modelling of the one-dimensional power spectra that directly come out by Fourier analyzing laser profilometer traces such as those mentioned in the Introduction. The two-dimensional model will only be stated following the above assumption.

There is no doubt that modelling $P(f)$ or $\psi(\tau)$ is equivalent since the power density spectrum and the autocorrelation function are uniquely related through a Fourier transformation. In fact, from the few data examined - both ψ and P -, it turns out that the shape of the spectra is quite varying thereby making the choice of parameters difficult, whereas the form of $\psi(\tau)$ seems to remain pretty much the same; it is, therefore, easier and perhaps more reliable to propose a model for $\psi(\tau)$ and then take its Fourier transform. Since this function presents observed damped oscillations around a zero value and starts at $\psi(0) = \sigma_h$ (by definition of ψ), we think that two parameters k and T are sufficient to set up a consistent model. Namely:

$$\psi(\tau) = \frac{\sigma_h}{1 + k\tau^2} \cos 2\pi \frac{\tau}{T} \qquad (42)$$

where k is the inverse of a length squared and T has the dimension of a length.

However, as we mentioned at the beginning of this section, this is not the form under which field measurements generally appear. Thus, we have to derive a model for the power spectrum P(f). This can be done by taking the inverse Fourier transform of the model for ψ and evaluating k and T from the power spectra. It follows that:

$$\left.\begin{aligned} P(f) &= \frac{\pi\sigma_h}{\sqrt{k}} \exp\left(-\frac{2\pi f}{\sqrt{k}}\right) \cosh\left(\frac{2\pi}{T\sqrt{k}}\right) : \; f > 1/T \\ P(f) &= \frac{\pi\sigma_h}{\sqrt{k}} \exp\left(-\frac{2\pi}{T\sqrt{k}}\right) \cosh\left(\frac{2\pi f}{\sqrt{k}}\right) \quad f < 1/T \\ P(f) &= P(-f) \end{aligned}\right\} \tag{43}$$

There exists a symmetry with respect to the origin and it is therefore sufficient to consider only the positive frequencies for which a peak in the power spectrum appears at F = 1/T. In that case, the normalization of the spectrum is such that:

$$\int_0^\infty P(f)\, df = \sigma_h \tag{44}$$

which is equivalent to multiplying P(F) by a factor two in relation (43).

This relation constitutes the two-parameters model[†] we propose for the one-dimensional power spectra. When considering specific ice surface statistics, the parameters k and T can be determined by having the model fit exactly the observed intensity and frequency position of the peak on the power spectrum. In other words, if f_{no} is observed position of the peak, we have:

$$T = 1/f_{no} \tag{45}$$

and k is the solution of the following transcendental equation:

$$P(f_{no}) = \frac{2\pi\sigma_h}{\sqrt{k}} \exp\left(-\frac{2\pi}{T\sqrt{k}}\right) \cosh\left(\frac{2\pi}{T\sqrt{k}}\right) \tag{46}$$

Figures 4 to 6 show one-dimensional spectra modelled in this way. Each figure is relevant to different ice surface statistics, i.e., different k's and T's; the solid line shows the proposed model whereas the black squares represent the corresponding field measured spectrum. It appears that the decaying of the spectrum is acceptably verified but, unfortunately, the lower frequency region, beyond the peak is not very well matched. As the peaks of the power density spectra play a central role in our analysis, a point pertaining to their exact definition has to be raised here.

[†] σ_h is not a parameter in that model since $\int_0^\infty P(F)\, df = \sigma_h$ for any k's and T's

As a matter of fact, the behavior of the power spectra for very low frequencies (where the peaks lie most often) remain unclear. These data generally come out by Fourier analyzing field measurements of the ice surface variations in altitude. We must notice that the recording device does not have an infinite analyzing band-width and that in order to remove the variations in altitude of the plane which carries the recorder the data signal is filtered through a hagh-band pass filter. Therefore, we cannot rely on the information at low frequencies provided by such methods, and it would be necessary to set up a physical argument to account for the general aspect of the power spectra in the low frequencies. This requires a thorough understanding of the ice formation and life and has not been done to date. Our modelling is therefore restricted to such field measured power spectra that exhibit a well defined single predominant peak, almost regardless of their behavior for frequencies less than the peak frequency.

Let us now state the resulting model for a two-dimensional statistics. Following the assumption we made earlier, we write:

$$\Psi(\xi,\eta) = \sigma_h \, \psi_1(\xi) \, \psi_2(\eta) \qquad (47)$$

where ψ_1 and ψ_2 are one-dimensional auto-correlation functions, hence modelled by relation (42) with parameters k_1, T_1 and k_2 respectively. It follows that the corresponding

two-dimensional power spectrum is $P(\underline{U})$ such that:

$$P(\underline{U}) = \sigma_h P_1(U_1) P_2(U_2)$$

where U_1 and U_2 are the components of the frequency vector $\underline{U}$ and P_1 and P_2 are the two one-dimensional models corresponding to the parameters k_1, T_1 and k_2, T_2 respectively. Namely:

$$\left.\begin{aligned} P_1(U_1) &= \frac{\pi}{\sqrt{k_1}} \exp\left(-\frac{2\pi U_1}{\sqrt{k_1}}\right) \cosh\left(\frac{2\pi}{T_1\sqrt{k_1}}\right) \\ P_2(U_2) &= \frac{\pi}{\sqrt{k_1}} \exp\left(-\frac{2\pi U_2}{\sqrt{k_2}}\right) \cosh\left(\frac{2\pi}{T_2\sqrt{k_2}}\right) \end{aligned}\right\} \text{ if } U_1, U_2 > 1/T \quad (48)$$

$$\left.\begin{aligned} P_1(U_1) &= \frac{\pi}{\sqrt{k_1}} \exp\left(-\frac{2\pi}{T_1\sqrt{k_1}}\right) \cosh\left(\frac{2\pi U_1}{\sqrt{k_1}}\right) \\ P_2(U_2) &= \frac{\pi}{\sqrt{k_2}} \exp\left(-\frac{2\pi}{T_2\sqrt{k_2}}\right) \cosh\left(\frac{2\pi U_2}{\sqrt{k_2}}\right) \end{aligned}\right\} \text{ if } U_1, U_2 < 1/T \quad (49)$$

$$P(-\underline{U}) = P(\underline{U})$$

Here again, $P(\underline{U})$ is symmetric with respect to the origin in the frequency plane. Hence, one needs only

consider a half-plane (for instance $U_1 > 0$), normalizing the power density spectrum so that:

$$\int_{U_1 > 0} P(\underline{U})\, d\underline{U} = \sigma_h \qquad (50)$$

which is equivalent to multiplying $P(\underline{U})$ as expressed in Eqs. (48) and (49) by a factor 2.

The overall aspect of such a power spectrum is given in Fig. 7. Two peaks appear, corresponding to the two peaks of $P_2(U_2)$. As was said earlier, no comparison with field data is possible due to the lack of the latter.

In this section, a simple two-parameters model has been proposed for the one-dimensional power spectra and is in good agreement with observations in so far as a real predominant peak appears in the measured spectra. The two-dimensional model has been purely hypothesized as being a cross product of two one-dimensional models. The next sub-section will use these models to develop a concept of "most probable pocket" in the ice relief.

4.2 Concept of Most Probable Pocket

In this sub-section, both in the one and two-dimensional cases, a "most probable pocket" will be defined as the "most apparent periodical relief" in the ice surface; mathematically, it will be identified with the negative part of the main term in the Fourier series expansion of the ice surface. Moreover, being the most characteristic feature of an ice

surface, this most probable pocket will be used to non-dimensionalize our further results.

As soon as we have the power density spectrum P(w) of the function h, from harmonic analysis[†] we know that:

$$h(x) = \int_0^{+\infty} F(w) \cos(wx)\, dw \qquad (51)$$

with $2P(w)\, dw = |F(w)|^2$

$w = 2\pi f$

It is then clear that we can approximate this function by an infinite Fourier cosine series which is nothing more than replacing the surface contained between the power spectrum curve and the frequency axis by an infinite number of rectangles of width Δw_n and height $P(w_n)$ where w_n is a circular frequency and $P(w_n)$ the value of the power spectrum at that frequency.

Thus:

$$h(x) \simeq \sum_0^{\infty} \sqrt{2P(w_n)\ \Delta w_n} \cos(w_n x - \psi_n) \qquad (52)$$

in the one-dimensional case

by the same token:

$$h(\underline{X}) \simeq \sum^{\infty} \sqrt{2P(\underline{U}_n)\ \underline{U}_n} \cos(\underline{U}_n . \underline{X} - \psi_n) \qquad (53)$$

in the two-dimensional case

[†]See Ref. 4.

In these equations, the "approximately equal" symbol tends to an "equal" symbol when $\Delta w_n - \Delta \underline{U}_n$ in the two-dimensional case - tends to zero, that is to say when the sum is replaced by an integral.

The amount of randomness characteristic of any given realization of the ice surface among a particular statistics appears in the set of phases ψ_n that are regarded as completely random variables.

Now, in so far as the power spectrum decays fast enough when the frequency increases and decreases from its value at the peak, there is no doubt that the term corresponding to the frequency position of the peak, $w_{no} - \underline{U}^1_{no}, \underline{U}^2_{no}$ † in the two-dimensional case - in the Fourier series is prevailing over the other ones.

Figures 4 to 6 show that such a fast decaying is confirmed by field data when w increases, but this is not the case when w decreases since, as was already mentioned, this low frequency part of the spectra is not quite reliable. However, it seems intuitively reasonable to expect that the zero frequency values of the spectra have to be zero; in other words, in the Fourier expansion of h, terms with an infinite wave length should have zero amplitude because otherwise, this would mean that there exists points infinitely far from the origin of the coordinates with non-zero roughness height. This is intuitively non-acceptable.

A rigorous argument can only come out from a detailed discussion of the ice relief formation and evolution. This is beyond the scope of this analysis and we must be content

---

† $\underline{U}^1_{no}, \underline{U}^2_{no}$ refer here to the two peaks of a two-dimensional spectrum.

with the assumption that a real peak exists in every spectra and its frequency position and intensity explicitly appear on the field data.

Thus, it follows that an even cruder approximation for h would be:

$$h(x) \simeq \sqrt{2\sigma_h} \cos (w_{no}x - \psi_{no}) \tag{54}$$

in the one-dimensional case

and

$$h(\underline{X}) \cong \sqrt{2\sigma_h} \left[\cos (\underline{U}^1_{no}.\underline{X} - \psi^1_{no}) + \cos (\underline{U}^2_{no}.\underline{X} - \psi^2_{no})\right] \tag{55}$$

in the two-dimensional case

For the one-dimensional case, we can look at Eq. (52) as expressing h in terms of a superposition of sinusoids of period $\frac{2\pi}{w_n}$ and intensity $\sqrt{2P(w_n)\ \Delta w_n}$. Each sinusoid will contribute - in proportion to its amplitude - to form the actual aspect of a typical one-dimensional profilometer trace verifying the statistics expressed in the power spectrum P. Then, Eq. (54) tells us that the greatest amplitude sinusoid, and therefore that which most influences the shape of the real pockets, corresponds to the frequency

of the peak. Hence the notation "most probable pocket" refers to this particular term of the Fourier expansion of h. This privileged pattern in the ice relief has a length Lmp equal to one period T of the sinusoid and a "volume" per unit width Σmp equal to the area contained between a negative arch of the curve and the axis, namely:

$$L_{mp} = \frac{2\pi}{w_{no}} = T \tag{56}$$

$$\Sigma_{mp} = -\int_{0}^{L_{mp}} \sqrt{2\sigma_h} \cos(w_{no}x)\, dx \tag{57}$$

negative integrand

Or, integrating:

$$\Sigma_{mp} = \frac{\sqrt{2\sigma_h}}{w_{no}} = \frac{T\sqrt{2\sigma_h}}{\pi} \tag{58}$$

By the same token, for the two-dimensional case, Eq. (53) is an expansion of the ice surface in terms of sinusoidal surfaces, the most apparent pattern corresponding to the two peaks of frequency vectors $\underline{U}^1_{no} = (U_{no1}, U_{no2})$ and $\underline{U}^2_{no} = (U_{no1}, -U_{no2})$ as in Eq. (55), (see Fig. 7). Analogous to the one-dimensional case, the "most probable pocket" has here a surface S_{mp} and a volume V_{mp} corresponding

to an increase of $(U_{no1})^{-1}$ in x and $(U_{no2})^{-1}$ in y.

Or more precisely:

$$Smp = \frac{4\pi^2}{U_{no1}\, U_{no2}} \tag{59}$$

$$Vmp = -\int_{\substack{1 \text{ period in} \\ 1 \text{ period in} \\ \text{negative integrand}}} \sqrt{2\sigma_h} \left[\cos \underline{U}^1_{no} \cdot \underline{X} + \cos \underline{U}^2_{no} \cdot \underline{X}\right] d\underline{X} \tag{60}$$

Upon integration, this yields:

$$Vmp = \frac{8\sqrt{2\sigma_h}}{U_{no1}\, U_{no2}} \tag{61}$$

Since they express the most important feature of the power density spectra - namely, their peak -, the "most probable pocket" dimensions will provide a good reference to non-dimensionalize our further results. This concept of most probable pocket has also the advantage of giving, in a simple way (through Eqs. (52) and (53), a rough estimate of what the ice surface looks like.

4.3 General Mathematical Results of Section 3 Using the Modelled Spectra of 4.1

With Eqs. (34) in the one-dimensional case (35) in the two-dimensional case, we have obtained a relation between the first and second statistical moments of the oil pool final size, the auto-correlation function of $\bar{h}$ and the parameter σ_h of the ice surface statistics. The purpose of this section is to derive more simple relations, using modelled spectra, and non-dimensionalize these results with respect to the "most probable pocket". Thus, it will be shown that in their dimensionless form, the second moment is proportional to the first one through a factor θ only dependent on the non-dimensional group kT^2 (or $k_1 k_2 T_1^2 T_2^2$ in the two-dimensional case) for suitable values of this group.

4.3.1 One-Dimensional Case

We recall here that if $\langle x_{max} \rangle$ is the final dimension of the oil pool and σ_x its variance, we have, from the mathematical analysis of Section 3:

$$\langle x_{max} \rangle = \frac{V\sqrt{2\pi}}{\sqrt{\sigma_h}} \tag{62}$$

$$\sigma_x = 8\pi \int_0^{\langle x_{max} \rangle/\sqrt{2}} \left[\frac{\langle x_{max} \rangle}{\sqrt{2}} - \tau \right] \left[\frac{\bar{\psi}(\tau)}{\sigma_h} - \frac{1}{2\pi} \right] d\tau \tag{63}$$

$\bar{\psi}(\tau)$ being obtainable from $\psi(\tau)$ defined as:

$$\psi(\tau) = \frac{\sigma_h}{1 + k\tau^2} \cos 2\pi \frac{\tau}{T} \tag{64}$$

Through the relation (see Sub-Appendix C-4).

$$\bar{\psi}(\tau) = \mathfrak{F}(\psi) = \frac{1}{2\pi(\psi_o^2 - \psi^2)^{1/2}} \iint_0^\infty ab \exp\left(-\frac{(a^2 + b^2)\psi_o - 2ab\psi}{2(\psi_o^2 - \psi^2)}\right) dadb \tag{65}$$

We can notice that, for k's and T's such that $\left[\frac{\bar{\psi}(\tau)}{\sigma_h} - \frac{1}{2\pi}\right]$ approaches zero within one period T - or one most probable pocket length Lmp - Eq. (63) becomes:

$$\sigma_x = 8\pi \int_0^{Lmp} \left[\frac{\langle x_{max} \rangle}{\sqrt{2}} - \tau\right] \left[\frac{\bar{\psi}(\tau)}{\sigma_h} - \frac{1}{2\pi}\right] d\tau \tag{66}$$

Since the integrand in relation (66) is a continuous function of τ, we can define τ_o such that:

$$\sigma_x = 8\pi \, Lmp \left[\frac{\langle x_{max} \rangle}{\sqrt{2}} - \tau_o \right] \left[\frac{\bar{\psi}(\tau_o)}{\sigma_h} - \frac{1}{2\pi} \right] \qquad (67)$$

Now, from Sub-Appendix C-4, it it clear that $\left[\frac{\bar{\psi}(\tau)}{\sigma_h} - \frac{1}{2\pi} \right]$ will be positive between $\tau = 0$ and $\tau = \frac{T}{4}$ and negative between $\tau = \frac{T}{4}$ and $\tau = \frac{T}{2}$; hence:

$$0 < \tau_o < T/4 \qquad (68)$$

In so far as $\langle x_{max} \rangle$ is large as compared to $\frac{T}{4}$, we can rewrite Eq. (67):

$$\sigma_x = \frac{8\pi}{\sqrt{2}} \, Lmp \, \alpha \, \langle x_{max} \rangle \qquad (69)$$

with $$\alpha = \frac{\bar{\psi}(\tau_o)}{\sigma_h} - \frac{1}{2\pi} \qquad (70)$$

Taking the square root of Eq. (69), it appears that the standard deviation of the oil pool final size is proportional to $\langle x_{max} \rangle^{1/2}$. This is in accordance with the following physical argument. Let V be the volume of a pocket per unit width, and let us split it into a "most probable pocket" volume plus a fluctuating quantity V':

$$\Delta V = Lmp \langle \bar{h} \rangle + V' \dagger \tag{71}$$

If $\sigma_{\Delta V}$ is the variance of ΔV and $\sigma_{V'}$ that of V', we have obviously:

$$\sigma_{\Delta V} = \sigma_{V'} \tag{72}$$

Now that the total volume V of a spill is such that:

$$V = N \Delta V \tag{73}$$

Furthermore, all these pockets are statistically independent if we assume that the correlation for $\bar{h}$ goes to zero within an interval Lmp.

---

†Lmp is defined in (56).

Therefore

$$\sigma_V = N \sigma_{\Delta V} = N \sigma_{V'} \tag{74}$$

where σ_V is the variance of the volume occupied by N pockets. Since $\langle x_{max} \rangle$ is always of the form

$$\langle x_{max} \rangle = N mp \tag{75}$$

we have from (74):

$$\sigma_V = \langle x_{max} \rangle \frac{\sigma_{V'}}{Lmp} \tag{76}$$

$\sigma_x^{1/2} = \left[\frac{\sigma_V}{\langle h^- \rangle^2}\right]^{1/2}$ is then proportional to $\langle x_{max} \rangle^{1/2}$ as expressed in Eq. (69).

Now, let us show that α defined in relation (70) is independent of $\langle x_{max} \rangle$ for sufficiently large values of $\langle x_{max} \rangle$.

Equation (66) can be rewritten:

$$\alpha = \frac{1}{L_{mp}} \int_0^{L_{mp}} \frac{[\langle x_{max} \rangle/\sqrt{2} - \tau]}{[\langle x_{max} \rangle/\sqrt{2} - \tau_o]} (\bar{\psi}(\tau)/\sigma_h - \frac{1}{2\pi}) \, d\tau \quad (77)$$

the ratio $\frac{\langle x_{max} \rangle/\sqrt{2} - \tau}{\langle x_{max} \rangle/\sqrt{2} - \tau_o}$ can be regarded as constant in so far $\tau - \tau_o$ remains small as compared to $\langle x_{max} \rangle$ when τ varies from 0 to L_{mp}. In other words, since τ_o is of order $mp/4$, α independent of $\langle x_{max} \rangle$ is a reasonable approximation when the number of "most probable pockets" involved in the oil spill is large (of order 10 or greater).

We can also show that, when kT^2 exceeds a number to be determined, α only depends on the non-dimensional group kT^2:

$$\bar{\psi}(\tau) = \mathcal{F}(\psi) = \frac{1}{2\pi(\psi_o^2 - \psi^2)^{1/2}} \int_0^\infty \int_0^\infty ab \exp\left(- \frac{(a^2 + b^2)\psi_o - 2ab\psi}{2(\psi_o^2 - \psi^2)} \right) da\,db \quad (78)$$

Furthermore, it appears that, setting

$$\tau_o = \gamma Lmp = \gamma T \tag{79}$$

γ is almost a constant within a few percent; this result comes out directly from a large number of numerical computations with different k's and T's and is not surprising since the overall shape of the functions $\left[\frac{\bar{\psi}(\tau)}{\sigma_h} - \frac{1}{2\pi}\right]$ does not change very much (see Fig. 9).

Then,

$$\psi(\tau_o) = \frac{\sigma_h}{1 + k\gamma^2 T^2} \cos 2\pi\gamma \tag{80}$$

is only a function of kT^2.

Hence, from Eq. (78)

$$\bar{\psi}(\tau_o) = \mathcal{F}(\psi(\tau_o)) = \text{function of } kT^2 \text{ only} \tag{81}$$

We have therefore shown that α depends on the non-dimensional group kT^2 only.

Non-dimensionalizing Eq. (69) with respect to the "most probable pocket" length Lmp, we obtain:

$$\frac{\sigma_x^{1/2}}{Lmp} = \theta\left(\frac{\langle x_{max}\rangle}{Lmp}\right)^{1/2} \tag{82}$$

with

$$\theta = \sqrt{\frac{8\pi\alpha}{\sqrt{2}}} \tag{83}$$

We now determine the universal curve θ versus kT^2 for k and T's that verify the assumptions we have made in the previous derivations.

The only one concerned with k and T tells us $\left[\frac{\bar{\psi}(\tau)}{\sigma_h} - \frac{1}{2\pi}\right]$ must decay to zero within a period[†] T = Lmp. From Sub-Appendix C-4, we know that this is equivalent to $\psi(\tau)$ going to zero within a period T; if we assume that $\psi(T) = \frac{\psi(0)}{50}$ is a good approximation for $\psi(T)$ equals zero, it follows that:

$$\psi(0)/\psi(T) \geq 50 \tag{84}$$

[†]We could have taken the same condition within two or more periods T; the dependence of α on kT^2 only would not have been changed, but α independent of $\langle x_{max}\rangle$ could be questioned. However, the decaying to zero within a period seems to be in good accordance with field data.

or:

$$kT^2 \geqslant 50 \tag{85}$$

We will therefore compute the curve θ (kT^2) for $kT^2 \geq 50$. This is represented on Fig. 11. We can notice that, when kT^2 goes to infinity, θ goes to zero. This is not surprising since, when $T = \infty$, α equals a constant divided by infinity and when $k = \infty$, α equals zero times a constant; in both cases, θ is therefore zero.

Knowing the k and T of a given ice surface statistics, we are now in a position to obtain the corresponding θ (on Fig. 11) and, with Eq. (82) have got a single relationship between the two first statistical moments of the oil pool size x_{max}, in their non-dimensional form.

4.3.2 Two-Dimensional Case

We recall that the two-dimensional size of the oil pool is S_{max} and its variance σ_s such that:

$$\langle S_{max} \rangle = \frac{V\sqrt{2\pi}}{\sqrt{\sigma_h}} \tag{86}$$

$$\sigma_s = 32\pi \int_0^{\langle x_{max} \rangle/\sqrt{2}} \int_0^{\langle y_{max} \rangle/\sqrt{2}} \left[\frac{\langle x_{max} \rangle}{\sqrt{2}} - \xi\right] \left[\frac{\langle y_{max} \rangle}{\sqrt{2}} - \eta\right] \left[\frac{\Psi^{-}(\xi,\eta)}{\sigma_h} - \frac{1}{2\pi}\right] d\xi d\eta \tag{87}$$

where $\Psi^{-}(\xi,\eta)$ is obtainable from $\Psi(\xi,\eta)$ defined as:

$$\Psi(\xi,\eta) = \frac{\sigma_h}{(1 + k_1\xi^2)(1 + k_2\eta^2)} \cos 2\pi\frac{\xi}{T_1} \cos 2\pi\frac{\eta}{T_2} \tag{88}$$

Going through the same kind of derivations as we did for the one-dimensional case, and under the same conditions for k's, T's and S_{max}, we will obtain comparable results.

Thus, for k_1, k_2, T_1 and T_2 such that $\bar{\Psi}(\xi,\eta)$ goes to 0 within the area $T_1 \times T_2$ and sufficiently large $\langle S_{max} \rangle$, we can write

$$\frac{\sigma_s^{1/2}}{Smp} = \Theta\left(\frac{\langle S_{max} \rangle}{Smp}\right)^{1/2} \qquad (89)$$

Θ being only a function of $k_1\ k_2\ T_1^2\ T_2^2$ (if we neglect $k_1\ T_1^2 + K_2\ T_2^2$ compared to $k_1\ k_2\ T_1^2\ T_2^2$). Θ versus dimensionless group has also been determined on Fig. 13, and one notices that for $\bar{\Psi}(\xi,\eta)$ to go to zero within the area $T_1 \times T_2$, $k_1\ k_2\ T_1^2\ T_2^2$ has to be greater than 2500 if we keep the same standards as in the one-dimensional case for the meaning of "goes to zero".

Therefore, knowing k_1, k_2, T_1 and T_2 of the two-dimensional statistics we are considering, we are in a position to obtain the corresponding Θ and thereby, we have got a simple $\frac{1}{2}$ power law relationship between the non-dimensional first and second statistical moments of the oil pool size.

4.4 Results

Having three experimental power density spectra coming from different parts of the Arctic Ocean, we have attempted to insert them in our parametered model described in Section 4.1. We obtained the following values for the parameters k and T[†] (see the modelled spectra on Figs. 4 to 6).

T	k	σ_h	
115 ft.	0.00378 ft.$^{-2}$	2.295 ft.^{2}	①
200 ft.	0.002786 ft.$^{-2}$	1.016 ft.^{2}	②
540 ft.	0.04075 ft.$^{-2}$	0.2033 ft.^{2}	③

(90)

Then, on Fig. 10, plotting the relationship between the two first moments of the oil pool size in the one-dimensional case for any of the three above statistics, we have compared the simple $\frac{1}{2}$ power laws given by Eq. (82) with the corresponding θ's (solid lines) to points obtained from the general mathematical model - Eq. (34) - for different volumes released V. The agreement is extremely good for any statistics, as well as it is on Fig. 12 for the two-dimensional case; in order to build two-dimensional statistics, we have made the following combinations of one-dimensional statistics: ① + ①, ② + ②, ③ + ③ and ① + ② of Table (90).

[†]We notice that kT^2 is always larger than 50 for all three statistics which allows us to use Section 4.3 analysis.

Therefore, in so far the conditions over k and T is verified ($kT^2 \geqslant 50$ for instance), this $\frac{1}{2}$ power law relationship between the oil pool final size and its standard deviation appears to be a very good approximation to solve our problem, both in the one and two-dimensional case.

It might be interesting to show a rough estimate of what these numerical results can be. Let us take a volume $V = 1000$ ft.^{3} per foot width in our one-dimensional case; this yields the following figures for each of the statistics of Table (90):

① ⟶ $\langle x_{max} \rangle = 1458$ ft. $\qquad \sigma_x^{1/2} = 304$ ft.

② ⟶ $\langle x_{max} \rangle = 2487$ ft. $\qquad \sigma_x^{1/2} = 480$ ft.

③ ⟶ $\langle x_{max} \rangle = 5560$ ft. $\qquad \sigma_x^{1/2} = 675$ ft.

As to the two dimensional case, let us take a volume $V = 5 \times 10^5$ ft.^{3} which appears to be a reasonable size, even in case of a supertanker crash, then, we obtain for the following combinations of one-dimensional statistics:

	1 + 1	2 + 2	3 + 3	1 + 2
$\langle S_{max} \rangle = \langle x_{max}\ y_{max} \rangle$	7.29×10^5 ft.^{2}	1.24×10^6 ft.^{2}	2.78×10^6 ft.^{2}	1.6×10^6 ft.^{2}
$\mu = (y_{max}/x_{max})^{-1}$	1	1	1	2.2
$\sigma_s^{1/2}$	37,000 ft.^{2}	72,000 ft.^{3}	116,000 ft.^{2}	146,000 ft.^{2}
Smp	13,200 ft.^{2}	40,000 ft.^{2}	290,000 ft.^{2}	23,000 ft.^{2}

(91)

Such results for σ_x and σ_s provide good evidence that our assumptions of Eqs. (11) and (7, in Sub-Appendix C5) are valid. We recall that in these assumptions, the average of $\bar{h}$ over a length $\sigma_x^{1/2}$ or area $\sigma_s^{1/2}$ was identified to $\overline{\bar{h}(\xi)}$, the average of $\bar{h}$ over the whole realization of the surface, on the ground that $\sigma_x^{1/2}$ or $\sigma_s^{1/2}$ was large enough.

Since the correlation for h approaches zero within one "most probable pocket" dimension, a length Lmp - or an area Smp in the two-dimension case - of the ice surface realization can be considered as containing all the statistical characteristics of the entire surface. Therefore, the average value of $\bar{h}$ over a length Lmp - or area Smp should not differ very much from $\langle \bar{h}(\xi) \rangle$.

Hence, it comes out that for V such that the standard deviation of the oil pool is much less than a "most probable pocket", the assumptions are no longer verified, thereby making the lower part of the curves σ_x versus $\langle x_{max} \rangle$ - or σ_s versus $\langle S_{max} \rangle$ - less trustworthy.

5. CONCLUSION - SUMMARY - DISCUSSION

In this study, the two first statistical moments of the oil pool resulting from a spill of volume V have been determined in terms of σ_h, the variance of the roughness height h and the auto-correlation function of h, both when the spreading is one-dimensional (one privileged direction) and when it is two-dimensional (no privileged direction).

These results have then been developed and simplified in compliance with a two-parameter (k,T) model proposed for one-dimensional statistics as long as their power spectrum exhibits a single predominant peak. If P(f) is the modelled spectrum, we have:

$$P(f) = \frac{2\pi\sigma_h}{\sqrt{k}} \exp\left(-\frac{2\pi f}{\sqrt{k}}\right)\cosh\left(\frac{2\pi}{T\sqrt{k}}\right) \text{if } f > 1/T$$

$$P(f) = \frac{2\pi\sigma_h}{\sqrt{k}} \exp\left(-\frac{2\pi}{T\sqrt{k}}\right)\cosh\left(\frac{2\pi f}{\sqrt{k}}\right) \text{if } f < 1/T \qquad (92)$$

T is nothing more than the inverse of the frequency position of the peak and k is determined by the intensity of the spectrum at that peak, through the transcendental equation:

$$P\left(\frac{1}{T}\right) = \frac{2\pi\sigma_h}{\sqrt{k}} \exp\left(-\frac{2\pi}{T\sqrt{k}}\right)\cosh\frac{2\pi}{T\sqrt{k}} \qquad (93)$$

Two-dimensional statistics have been regarded as characterized by a product of two one-dimensional power density spectra, therefore, their modelling is quite similar to that of the one-dimensional case.

A "most probable pocket" that could be physically defined as the "most apparent periodical relief" in the ice surface has been introduced both in the one and two-dimensional case. Mathematically, it is identified to the main term in the Fourier series expansion of the ice surface.

If $\frac{1}{T}$ is the frequency position of the peak in a one-dimensional spectrum and (U_{no1}, U_{no2}), $(U_{no1}, -U_{no2})$ the positions of the peaks in a two-dimensional spectrum (see Fig. 7), the dimensions of this "most probable pocket" are its size and volume:

$$\left.\begin{array}{lll} \text{Length} & \text{Lmp} = T & \\ \text{"volume"} & \Sigma\text{mp} = \dfrac{T\sqrt{2\sigma_h}}{\pi} & \end{array}\right\} \text{one dim. case} \qquad (94)$$

$$\left.\begin{array}{lll} \text{area} & \text{Smp} = T_1 T_2 = \dfrac{4\pi^2}{U_{no1}\, U_{no2}} & \\ \text{volume} & \text{Vmp} = \dfrac{8\sqrt{2\sigma_h}}{U_{no1}\, U_{no2}} & \end{array}\right\} \text{two dim. case} \qquad (95)$$

The first statistical moment of the final size of the oil pool - namely x_{max} in the one-dimensional case or S_{max} in the two-dimensional one - has been determined and then non-dimensionalised with respect to the "most probable pocket" size:

$$\left.\begin{aligned} \frac{\langle x_{max} \rangle}{Lmp} &= \frac{V}{Lmp}\sqrt{\frac{2\pi}{\sigma_h}} = \frac{V}{mp}\cdot\frac{2}{\sqrt{\pi}} \\ \frac{\langle S_{max} \rangle}{Smp} &= \frac{V}{Smp}\sqrt{\frac{2\pi}{\sigma_h}} = \frac{V}{Vmp}\cdot\frac{4}{\pi^{3/2}} \end{aligned}\right\} \qquad (96)$$

A simple $\frac{1}{2}$ power law relationship between the non-dimensional first and second moments of the pool size has been developed with a slope θ - in the two-dimensional case - depending only on the dimensionless group kT^2 - $k_1 k_2 T_1^2 T_2^2$ in the two-dimensional case - that characterized the modelled spectra. Namely, if σ_x is the variance of x_{max} and σ_s that of S_{max}:

$$\frac{\sigma_x^{1/2}}{L_{mp}} = \theta\left(\frac{\langle x_{max} \rangle}{mp}\right)^{1/2} \qquad \text{see Fig. (10) and (11)} \qquad (97)$$

$$\frac{\sigma_s^{1/2}}{Smp} = \ominus\left(\frac{\langle S_{max} \rangle}{Smp}\right)^{1/2} \qquad \text{see Figs. (12) and (13)} \qquad (98)$$

Therefore, suppose we are given the volume V of oil released and the parameters which characterize the region of the Arctic Ocean where the spill takes place: k and T in the one-dimensional case or k_1, k_2, T_1 and T_2 in the two-dimensional one, along with the variance σ_h of the roughness height; we are then

in a position to predict the final size of the oil pool as well as its standard deviation. Furthermore, in the two-dimensional case, an idea about the dissymetry of the pool can be gotten from the quantity μ, the ratio of the dimensions of the rectangle limiting the pool. With relation (4):

$$\mu = \left[\frac{(2\pi/T_2)^2 + 2\ k_2}{(2\pi/T_1)^2 + 2\ k_1} \right]^{1/2} \qquad (99)$$

We have to notice here that this rectangular shape x_{max} X y_{max} surely does not represent the real aspect of an oil pool. The latter is much closer to an ellipse - a circle in the case of a truly isotropic surface - and it follows that the size computed under this assumption can result in a 13% underestimation of $\langle x_{max} \rangle$ and $\langle y_{max} \rangle$. The computations relative to an ellipse, although quite intricate, can be performed but, in view of the precision obtained on the statistical field measurements, we did not deem it worthwhile.

The limitations for the use of these power law relationships between the first two moments of the pool size (Eqs. (97) and (98)) are concerned with the value of kT^2 and $\langle x_{max} \rangle - \langle S_{max} \rangle$ and $k_1\ k_2\ T_1^2\ T_2^2$ in the two-dimensional case - namely:

$$kT^2 \geqslant 50 \quad \text{or} \quad k_1\ k_2\ T_1^2\ T_2^2 \geqslant 2500 \qquad (100)$$

$$\frac{\langle x_{max} \rangle}{Lmp} \Big/ \frac{\langle S_{max} \rangle}{Lmp} \geq 10 \qquad (101)$$

These conditions, described in some detail in Sub-section 4.3 do not influence more general results as those of Eqs. (34) and (35) which are valid for any power spectra model.

Also, an important point to understand is the actual behavior of the power spectra at very low frequencies since it has been here purely hypothesized, as was also the two-dimensional statistics, for there is no evidence at all that a two-dimensional power spectrum should be the product of two one-dimensional ones.

To conclude this study, we can say that the previous analysis yields simple and useful results as to the prediction of oil spreading over a rough surface of ice; but, since the modelling of the power density spectra has been developed from a limited quantity of data, a strong experimental ground is required to completely justify this proposed model.

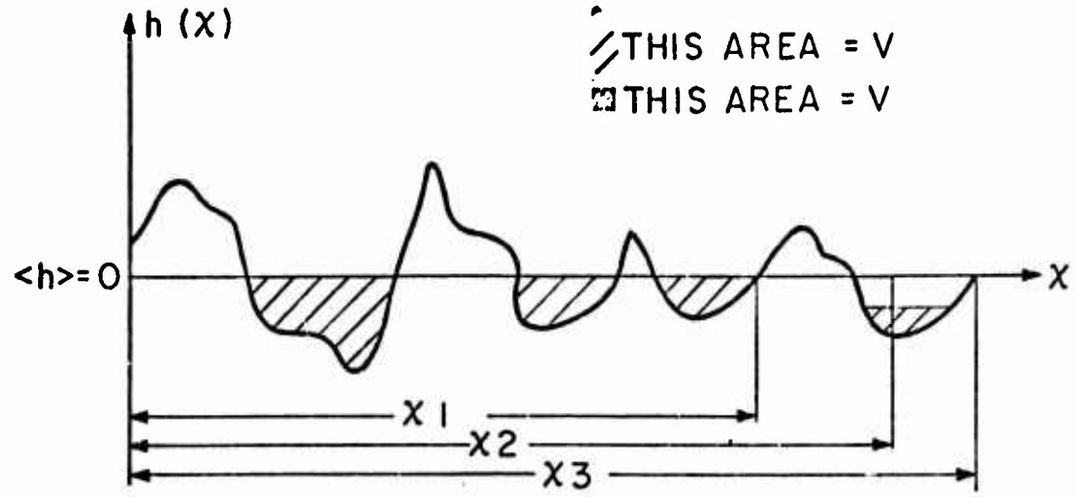

FIG. 1 GENERAL ASPECT OF ONE REALIZATION OF THE PROFILE

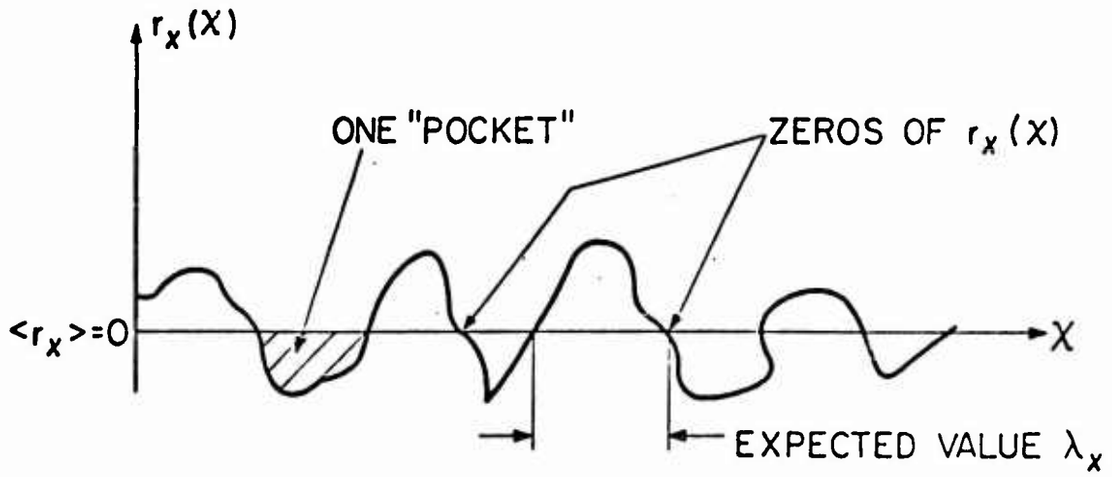

FIG. 2 AVERAGE LONGITUDINAL DIMENSION OF A POCKET

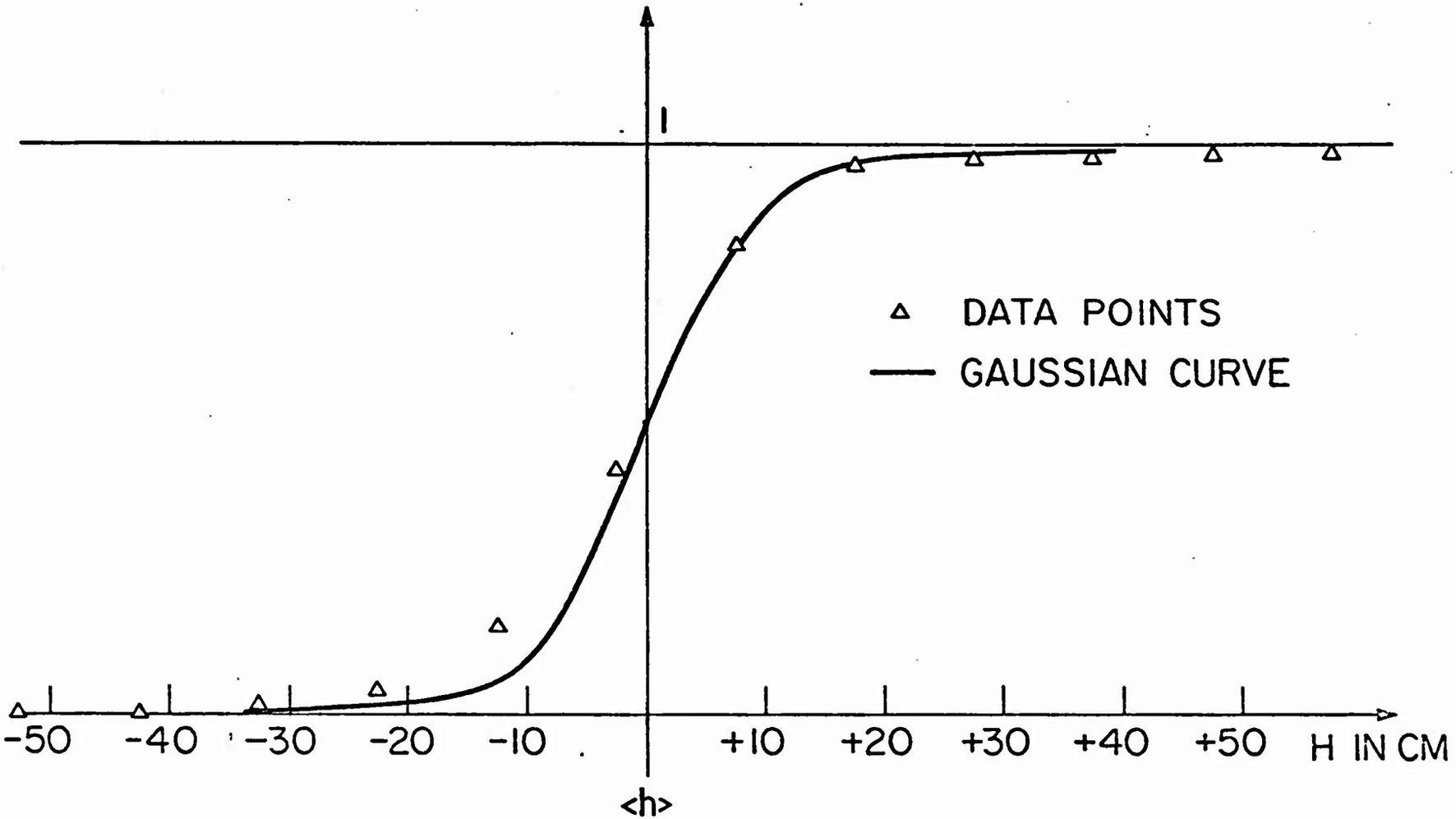

FIG. 3 VERIFICATION FOR h NORMALLY DISTRIBUTED

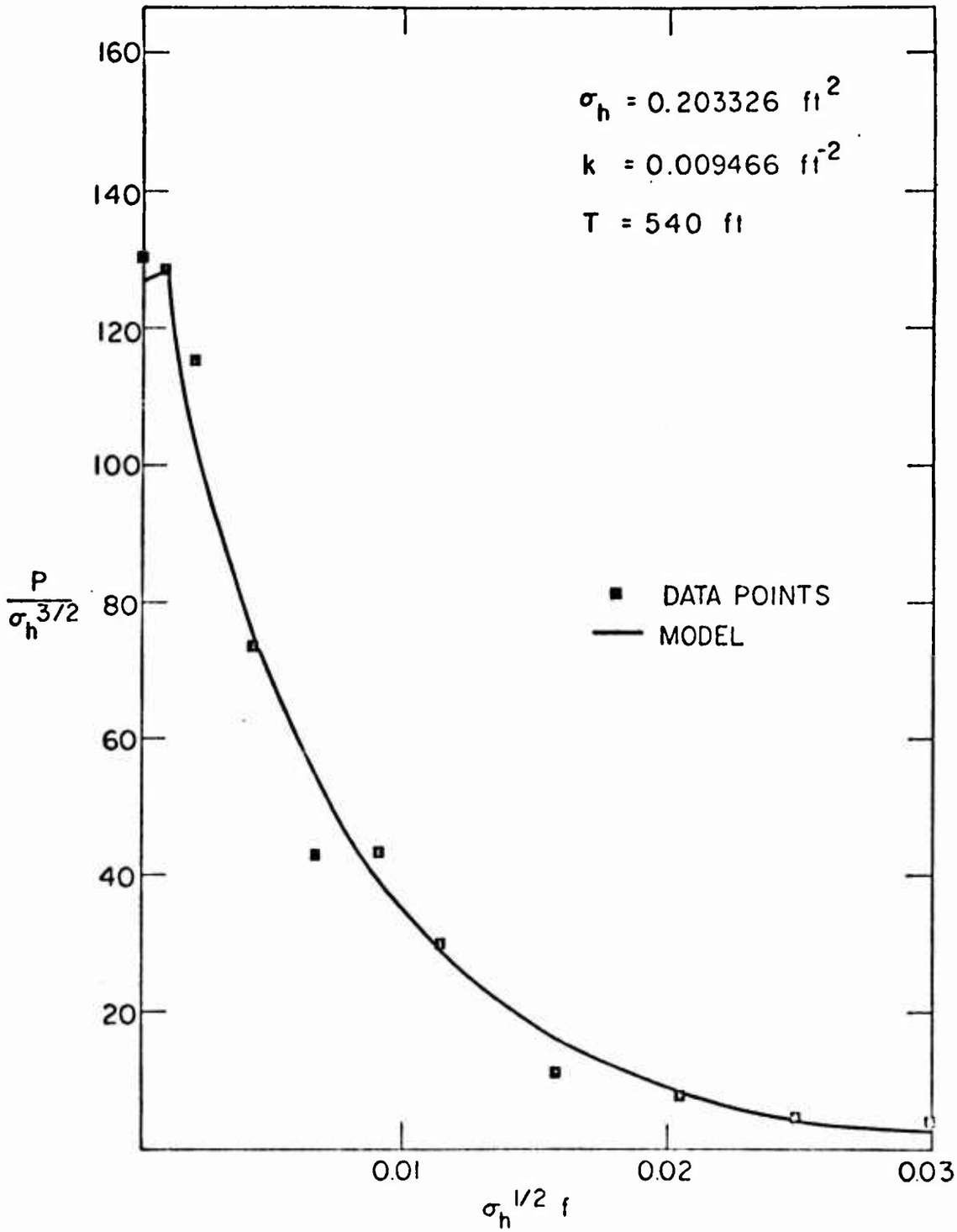

FIG. 4 EXAMPLE OF ONE-DIMENSIONAL POWER SPECTRUM

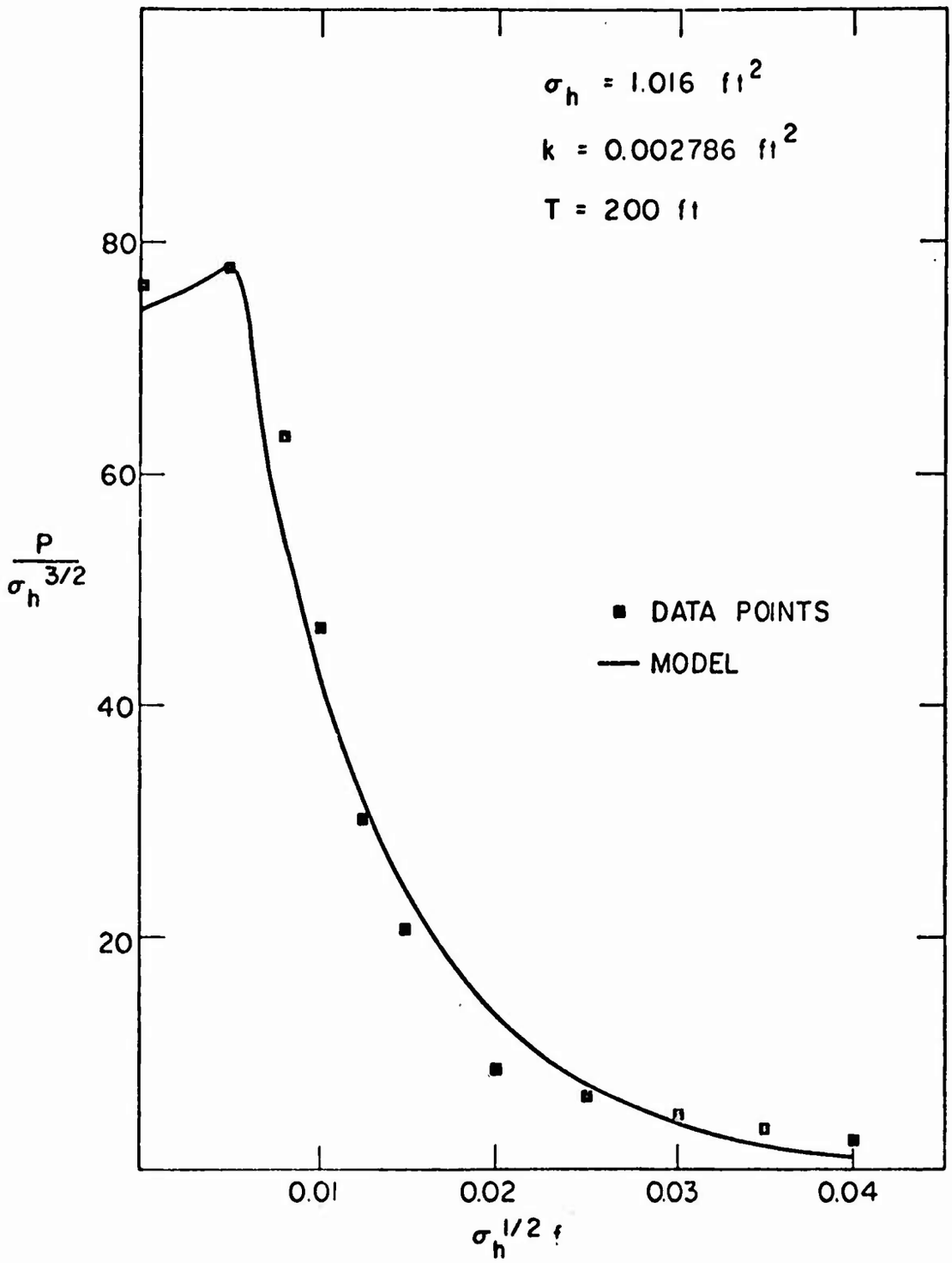

FIG. 5 EXAMPLE OF ONE-DIMENSIONAL POWER SPECTRUM

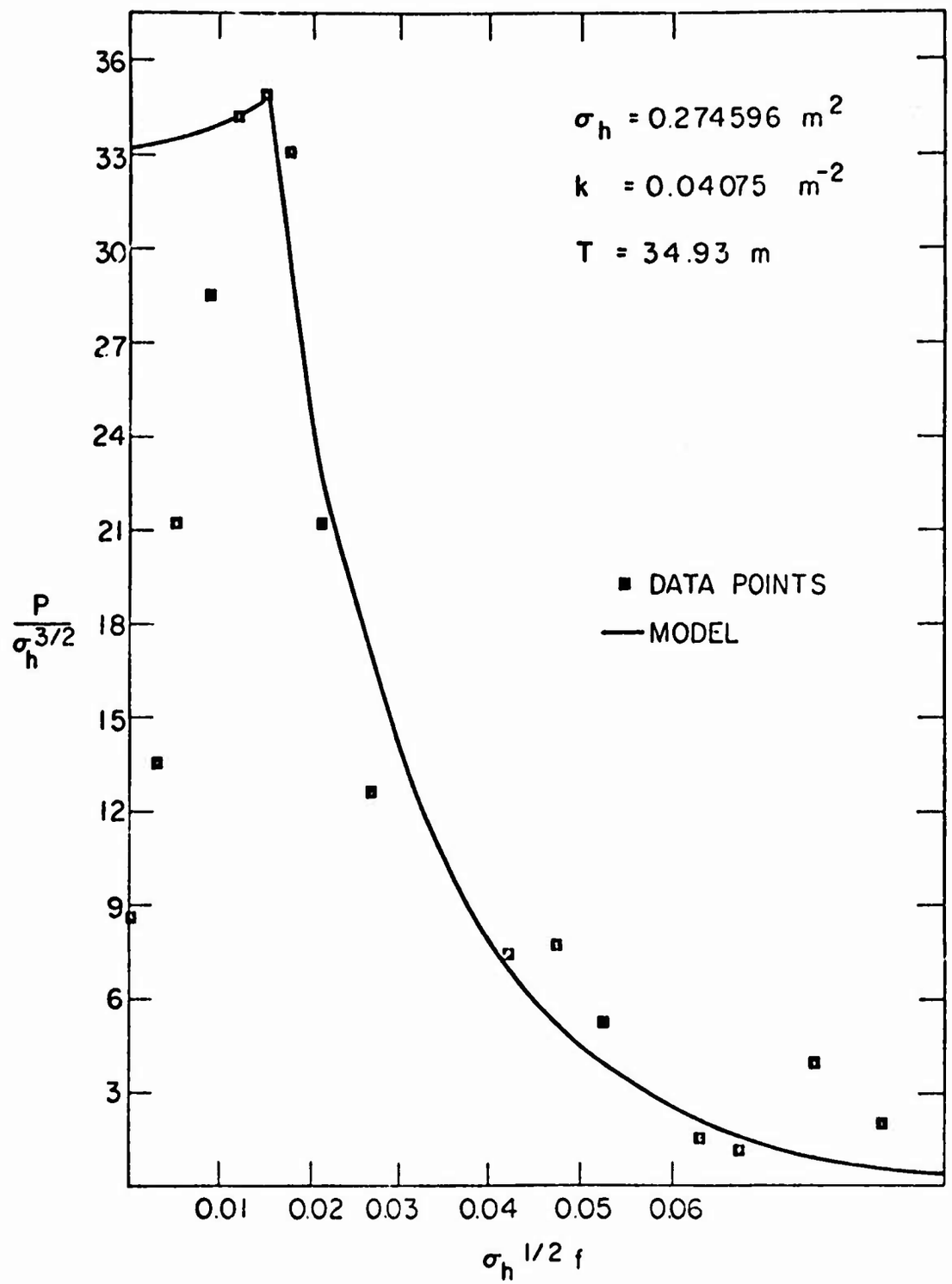

FIG. 6 EXAMPLE OF ONE-DIMENSIONAL POWER SPECTRUM

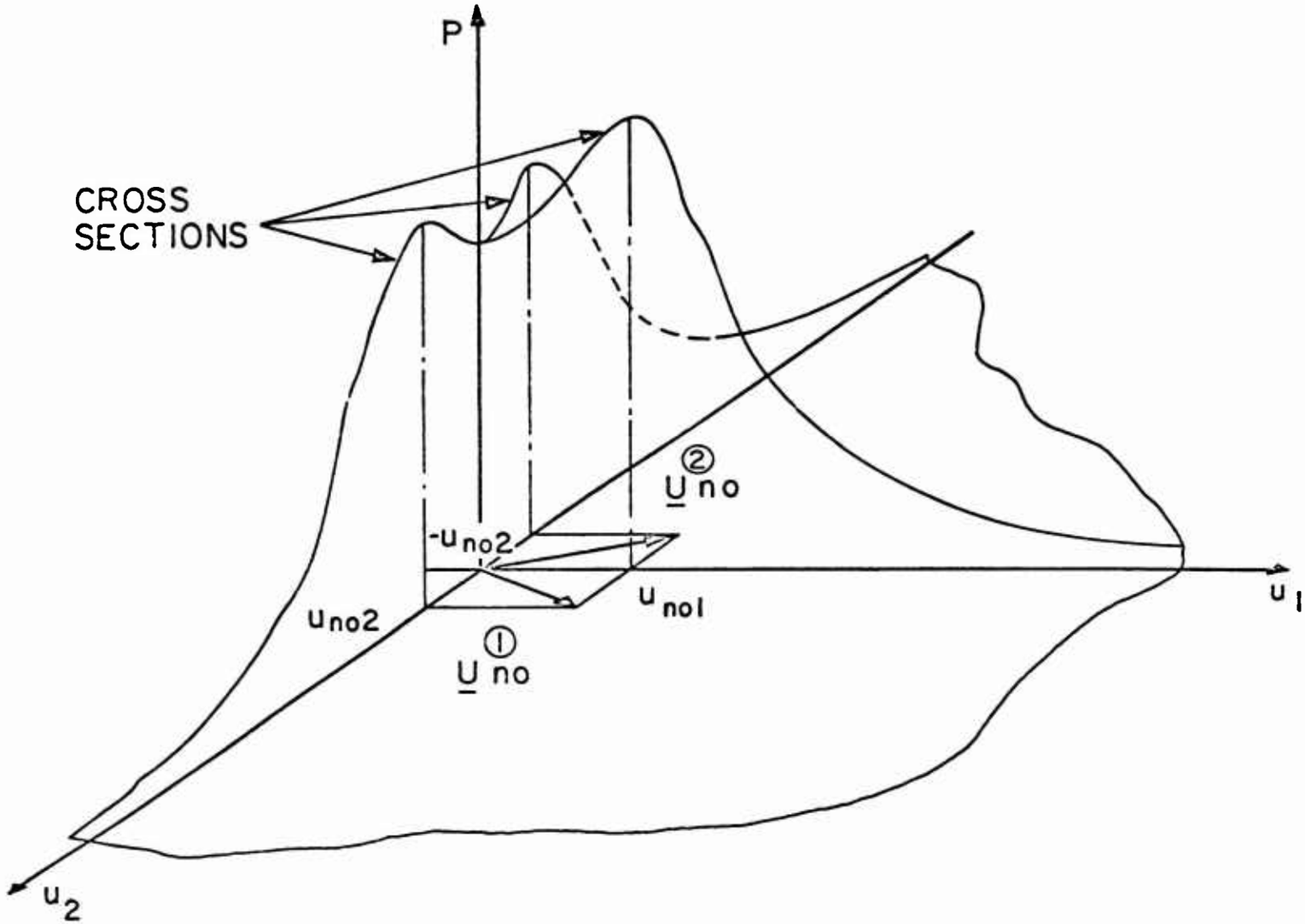

FIG. 7 EXAMPLE OF TWO-DIMENSIONAL POWER SPECTRUM

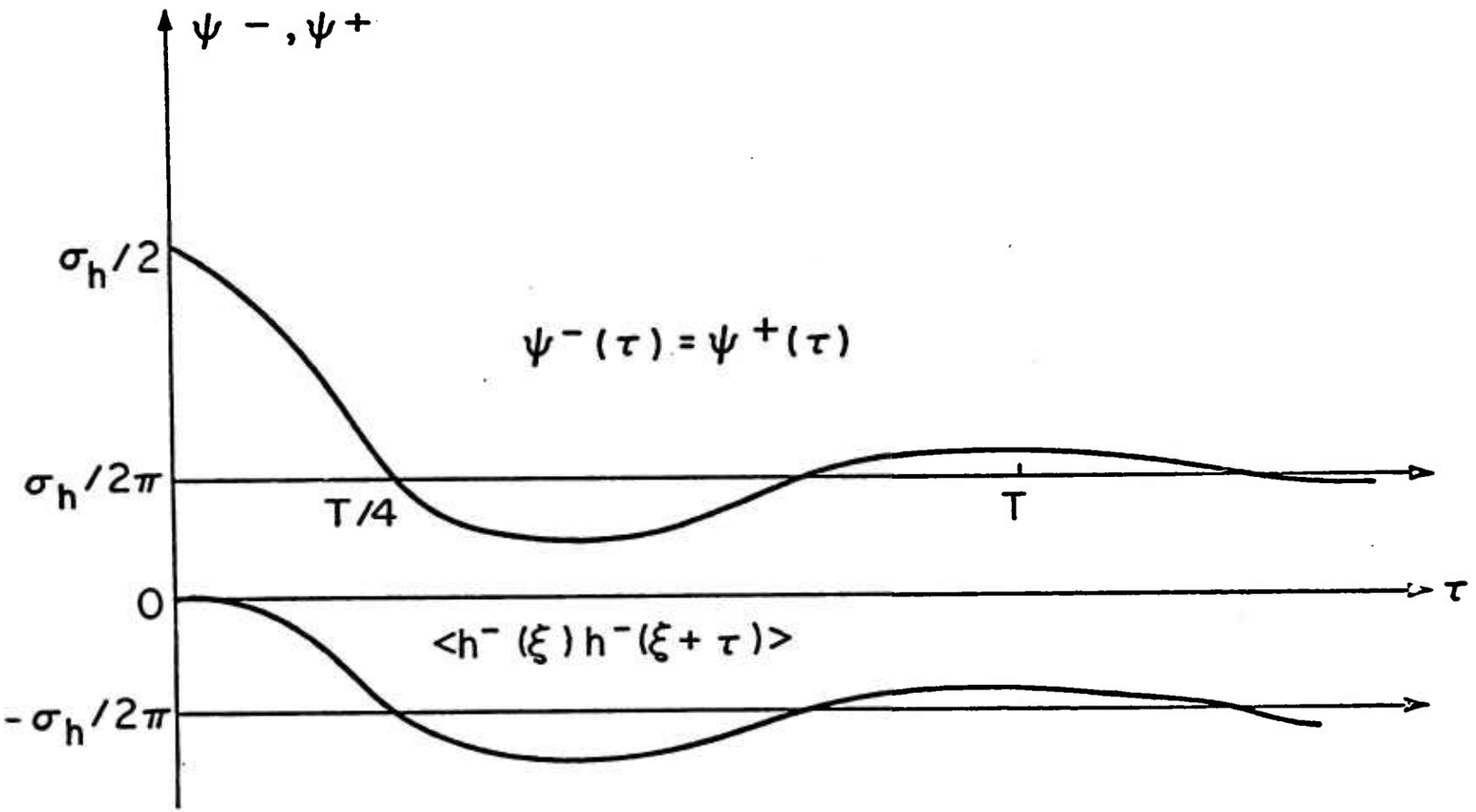

FIG. 8 ASPECT OF THE AUTO-CORRELATION FUNCTION OF h^- AND h^+

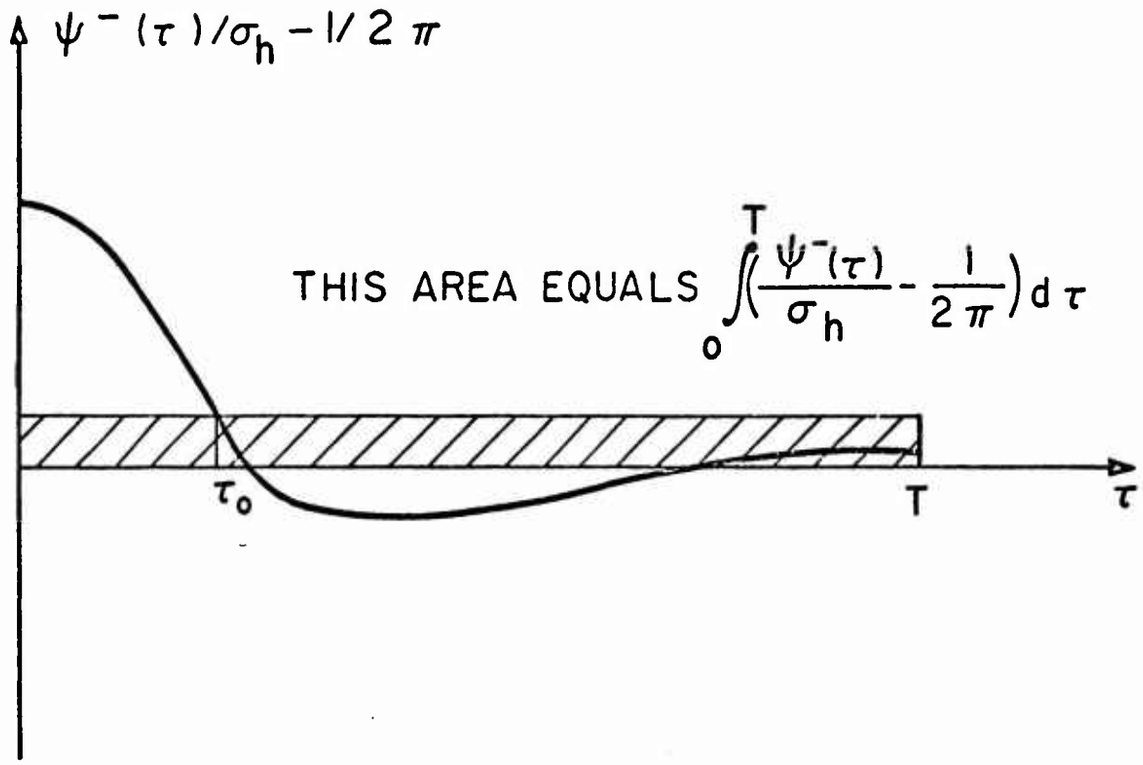

FIG. 9 POSITION OF τ_0 WITH RESPECT TO T
(SECTION IV - 3 OF THE TEXT)

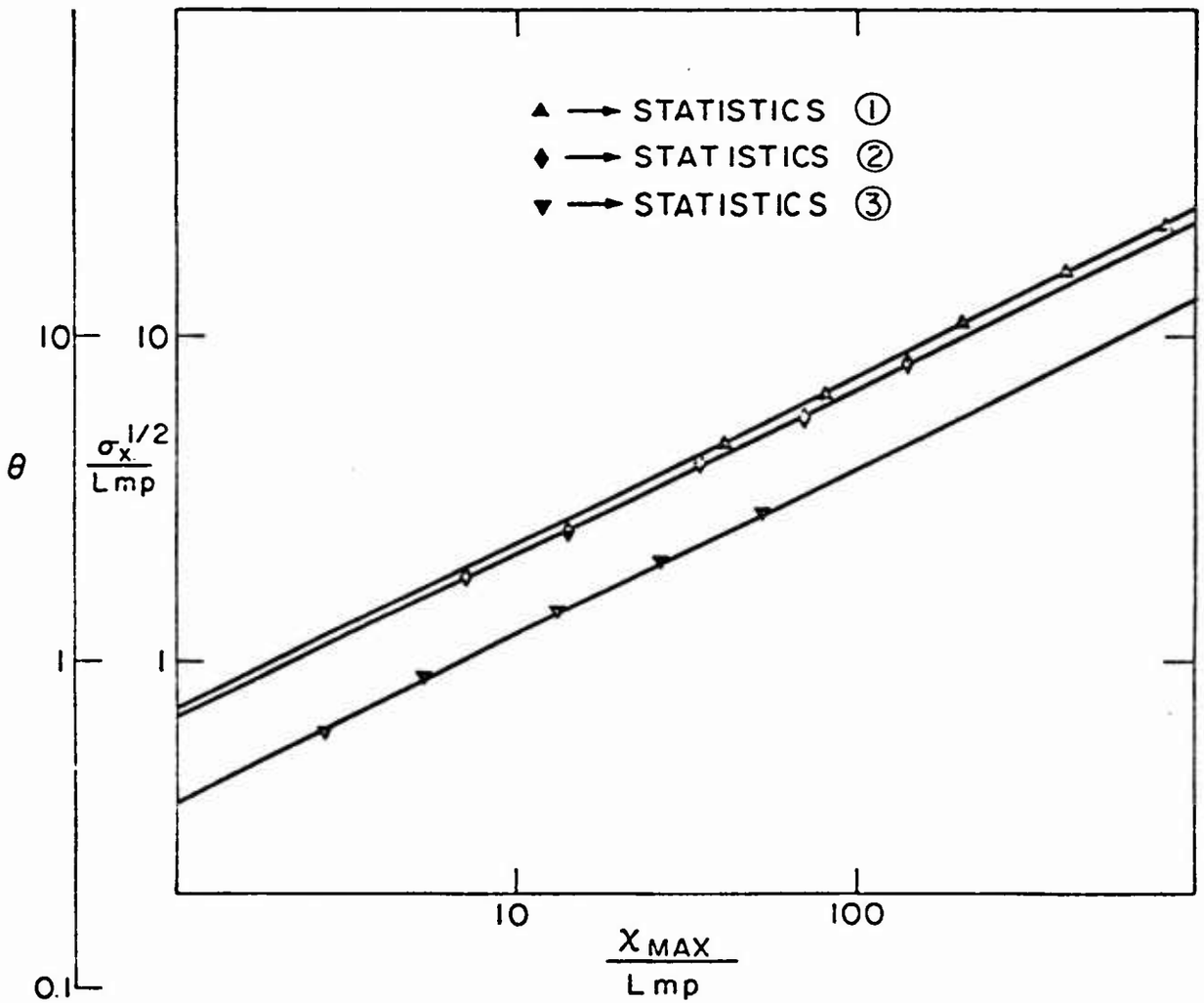

FIG. 10 RELATIONSHIP BETWEEN $\langle X_{MAX} \rangle$ AND $\sigma_X^{1/2}$. ONE-DIMENSIONAL CASE

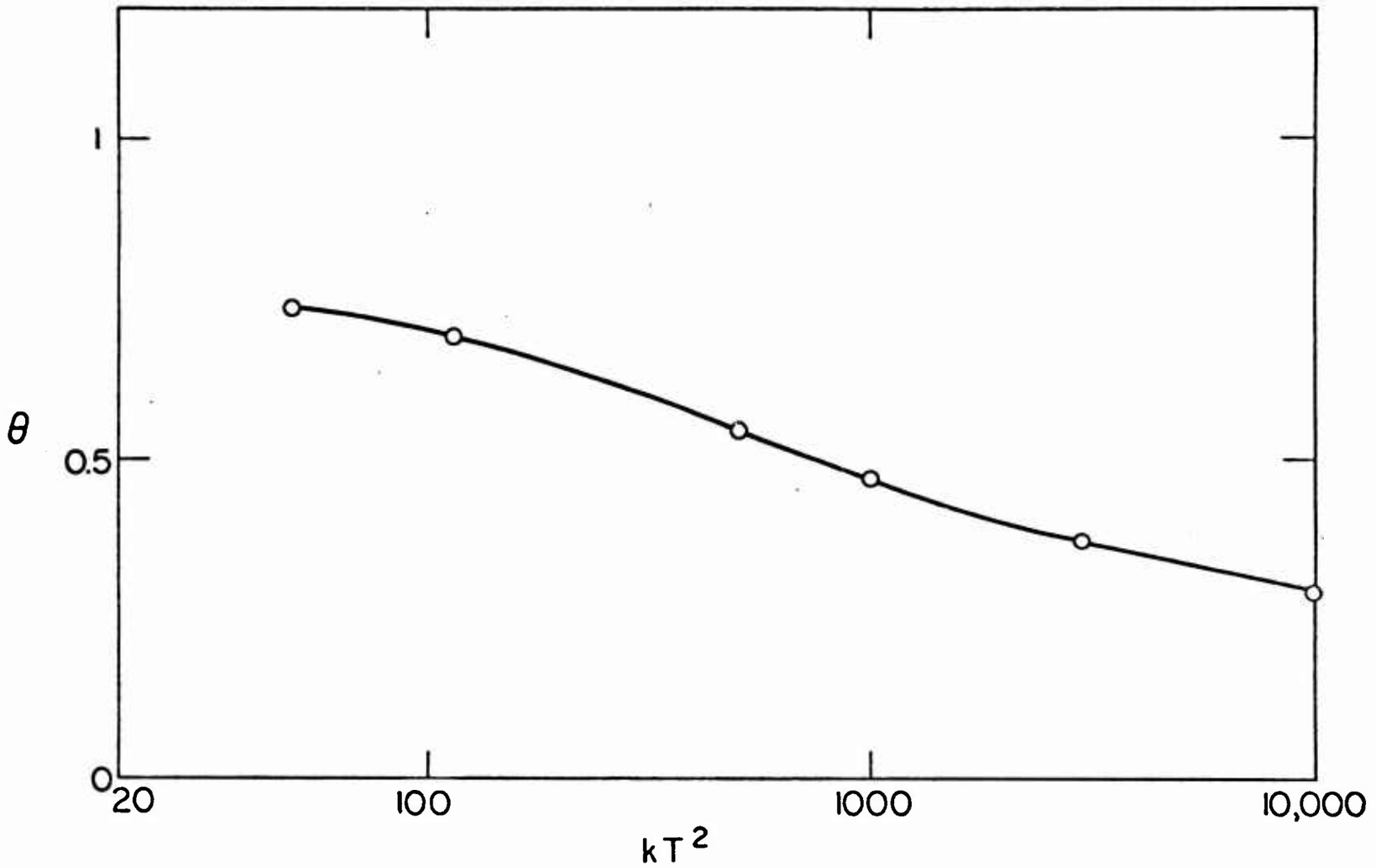

FIG. 11 SLOPE θ VERSUS NON-DIMENSIONAL GROUP kT^2. ONE DIMENSIONAL CASE

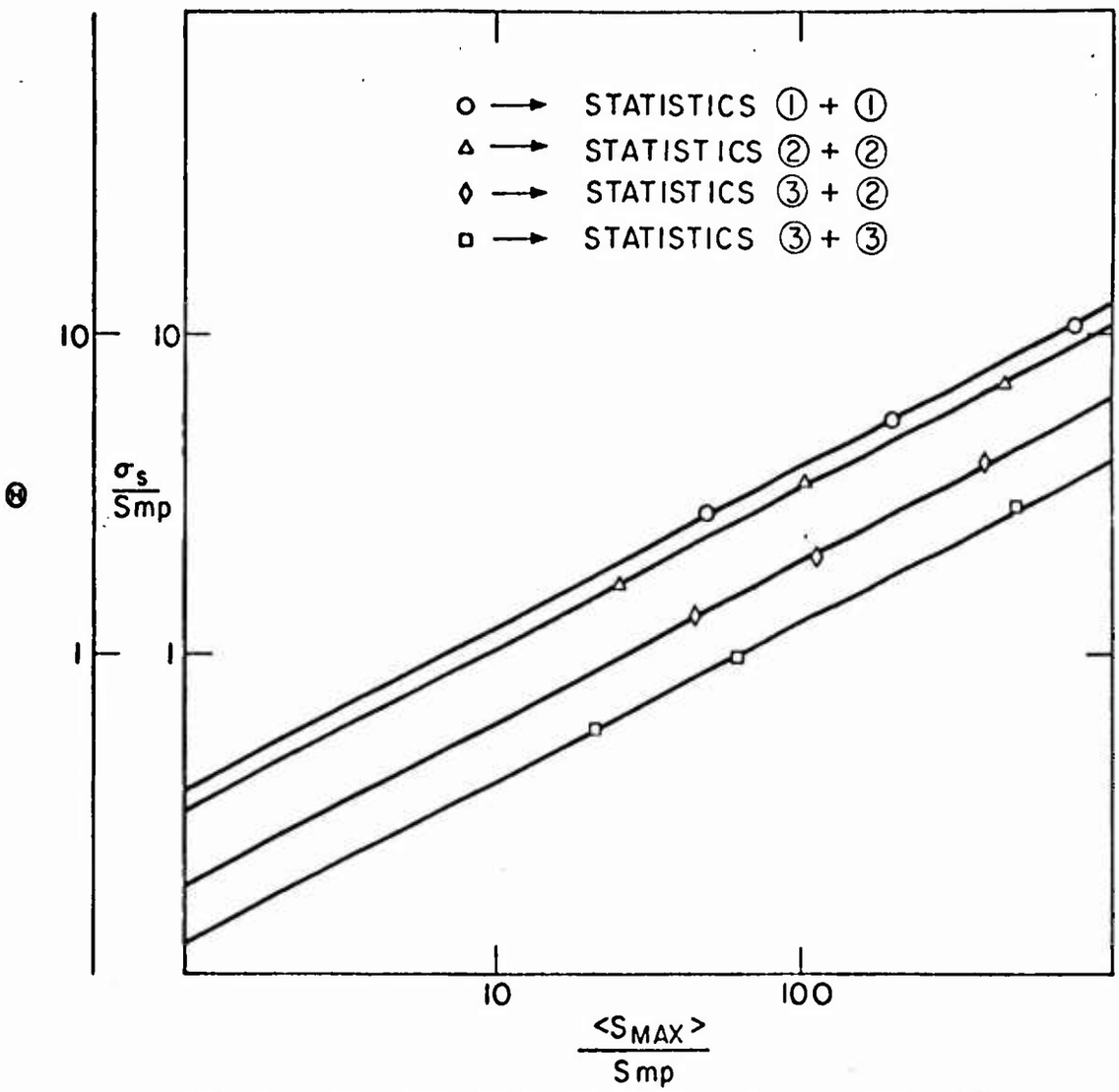

FIG. 12 RELATIONSHIP BETWEEN $\langle S_{MAX} \rangle$ AND $\sigma_S^{1/2}$ TWO-DIMENSIONAL CASE

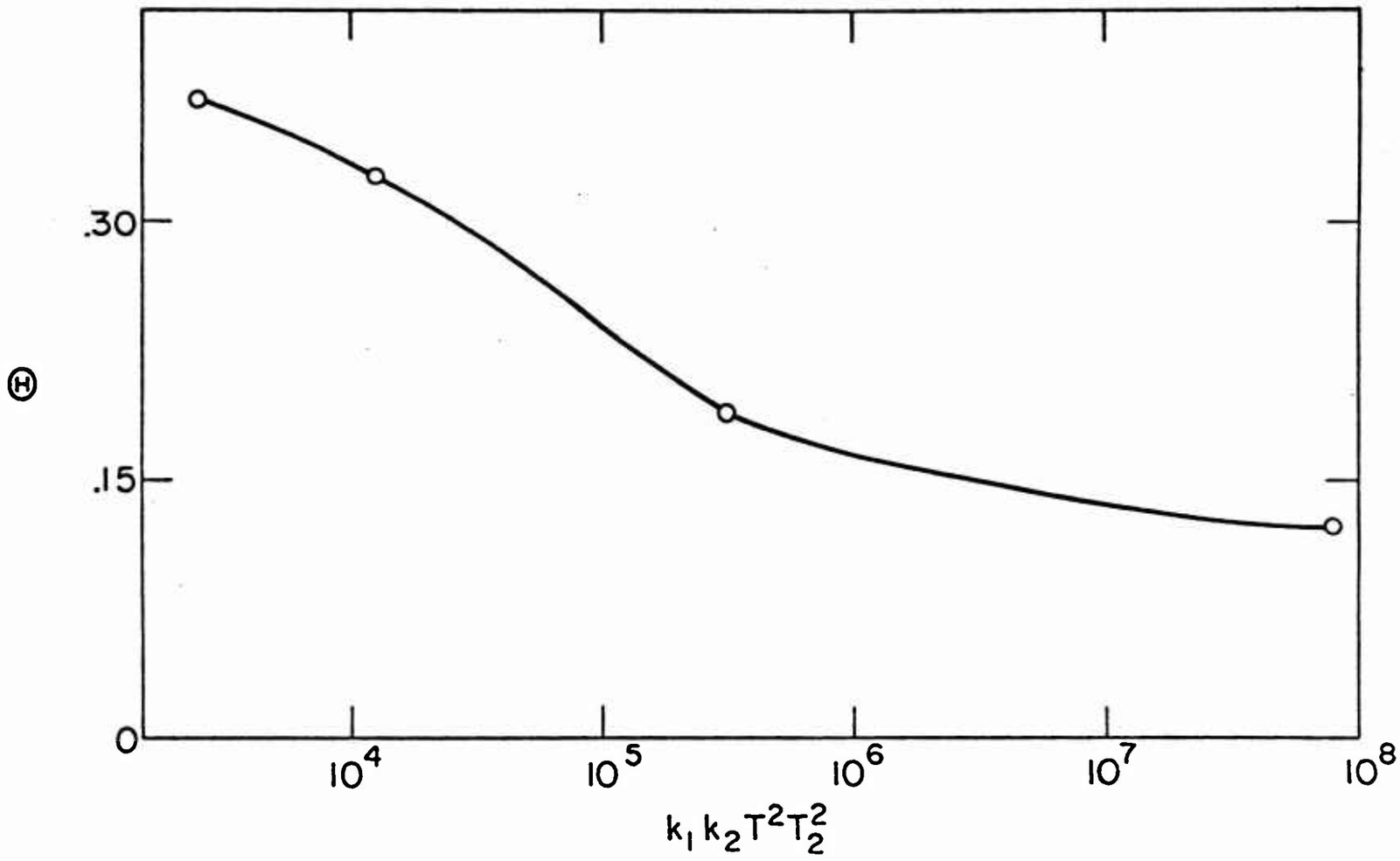

FIG. 13 SLOPE Ⓗ VERSUS NON-DIMENSIONAL GROUP $k_1 k_2 T_1^2 T_2^2$. TWO-DIMENSIONAL CASE

SUB-APPENDIX C-1

In this appendix, we will determine the "dissymmetry factor" defined as the ratio

$$\mu = \frac{\lambda x}{\lambda y} \tag{1}$$

where λx and λy are the average dimensions of a pocket in the x and y directions respectively.

Let us consider an actual laser profilometer trace parallel to the x direction. Let $r_x(x)$ denote the elevation of ice above the mean level $< h(x) > = 0$. Considering an ensemble average over all the traces parallel to x, we can write:

$$< r_x^2(x) > = \sigma_h \tag{2}$$

And:

$$< r_x(x + \xi)\, r_x(x) > = \Psi(\xi, 0) \tag{3}$$

Using our third hypothesis concerned with the way pockets are filled by oil, we can see that λx corresponds to the average distance separating two zeros of the function $r_x(x)$ (see Fig. 2). $r_x(x)$ is normally distributed from our second hypothesis and, since $\frac{dr_x}{dx}$ is linearly related to $r_x(x)$, it also holds a Gaussian distri-

bution. Hence, the vector

$$\begin{Vmatrix} r_x(x) \\ \dfrac{dr_x}{dx}(x) \end{Vmatrix}$$

is normally distributed.

Therefore, if $p(\alpha,\theta,x)$ represents the probability that:

$$\alpha \leqslant r_x(x) \leqslant \alpha + d\alpha$$

$$\theta \leqslant \frac{dr_x}{dx}(x) \leqslant \theta + d\theta \tag{4}$$

we have:†

$$p(\alpha,\theta,x) = \frac{1}{2\pi} |M|^{-1} \exp\left(-\frac{1}{2} \left\| \alpha\ \theta \right\| M^{-1} \begin{Vmatrix} \alpha \\ \theta \end{Vmatrix}\right) \tag{5}$$

where:

$$M = \begin{Vmatrix} \Psi(0,0) & 0 \\ 0 & -\dfrac{\partial^2 \Psi}{\partial \xi^2}(0,0) \end{Vmatrix} \tag{6}$$

†see Ref. 1.

Relation (5) can easily be reduced to:

$$p(\alpha,\theta;x) = \frac{(-\Psi_o\ \Psi''_{\xi o})^{-1/2}}{2\pi} \exp\left(-\frac{\alpha^2}{2\Psi_o} + \frac{\theta^2}{2\Psi''_{\xi o}}\right) \qquad (7)$$

in which we have set for convenience:

$$\Psi''_{\xi o} = \frac{\partial^2 \Psi}{\partial \xi^2}(0,0)$$

$$\Psi_o = \Psi(0,0) \qquad (8)$$

Now, let us find the probability that $r_x(x)$ has a zero between x and x + dx; in the interval, all the cross-sections of the possible realizations of the ice surface are regarded as straight lines.

At first, we will derive the probability for $r_x(x)$ to have a zero with positive slope. For this to happen, α and θ have to be

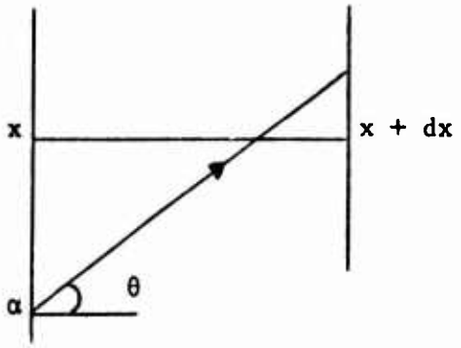

related by the inequality (clearly shown on the sketch beside):

$$-\theta dx < \alpha < 0$$

Then, the probability for $r_x(x)$ to have a zero between x and x + dx with a positive θ is:

$$\int_0^\infty d\theta \int_{-\infty}^0 p(\alpha,\theta,x)\,d\alpha$$

And, the probability density for this happening is:

$$\left[\frac{d}{d(\Delta x)} \int_0^\infty d\theta \int_{-\theta\Delta x}^0 p(\alpha,\theta,x)\,d\alpha\right]_{\Delta x = 0}$$

which reduces to:

$$\left[-\int_0^\infty (-\theta)\; p(-\theta\Delta x,\theta,x)\; d\theta\right]_{\Delta x = 0}$$

or:

$$\int_0^\infty \theta\; p(0,\theta,x)\; d\theta \qquad (10)$$

By the same token, the probability density for $r_x(x)$ to have a zero between x and x + dx with a negative slope is:

$$- \int_{-\infty}^{0} \theta \, p(0,\theta,x) \, d\theta \tag{11}$$

Adding relations (10) and (11), we obtain $\pi(x)$, probability density for $r_x(x)$ to have a zero between x and x + dx:

$$\pi(x) = \int_{-\infty}^{+\infty} |\theta| \, p(0,\theta,x) \, d\theta \tag{12}$$

Using relation (5) and integrating, it comes out:

$$\pi(x) = \frac{1}{\pi} \left(- \frac{\psi''_{\xi o}}{\psi_o} \right)^{1/2} \tag{13}$$

The integral of $\pi(x)$ over a unit length gives the number of expected zeros per unit of a x-direction since the integral from $-\infty$ to $+\infty$ obviously gives the total number of zeros.

Therefore, λx, the average distance between two zeros of $r_x(x)$,

can be approximated by:

$$\lambda x = \frac{1}{\pi(x)} = \pi \left(- \frac{\psi_o}{\psi''_{\xi o}} \right)^{1/2} \qquad (14)$$

All that has been done for profilometer traces parallel to the x-direction could be done for traces parallel to the y-direction simply by introducing the function $r_y(y)$, analogous to $r_x(x)$. Going through the same kind of calculations as the previous ones, we would end up with:

$$\lambda y = \pi \left(- \frac{\psi_o}{\psi''_{\eta o}} \right)^{1/2} \qquad (15)$$

It follows that μ defined in relation (1) is given by:

$$\mu = \frac{\lambda x}{\lambda x} = \left(\frac{\partial^2 \psi}{\partial \eta^2} (0,0) \Big/ \frac{\partial^2 \psi}{\partial \xi^2} (0,0) \right)^{1/2} \qquad (16)$$

SUB-APPENDIX C-2

The goal of this appendix is to calculate σ_v defined as:

$$\sigma_v = \left\langle \left[v(\langle x_{max} \rangle, \langle y_{max} \rangle) - \langle v(\langle x_{max} \rangle, \langle y_{max} \rangle) \rangle \right]^2 \right\rangle \quad (1)$$

where:

$$v(x,y) = - \int_{-x/2}^{x/2} \int_{-y/2}^{y/2} \bar{h}(u,v)\, du\, dv \quad (2)$$

Expanding the square in Eq. (1), we obtain:

$$\sigma_v = \langle v^2(\langle x_{max} \rangle, \langle y_{max} \rangle) \rangle - \langle 2v(\langle x_{max} \rangle, \langle y_{max} \rangle) \rangle$$

$$\langle v(\langle x_{max} \rangle, \langle y_{max} \rangle) \rangle + \langle v(\langle x_{max} \rangle, \langle y_{max} \rangle) \rangle^2 \quad (3)$$

or:

$$\sigma_v = \langle v^2(\langle x_{max} \rangle, \langle y_{max} \rangle) \rangle - \langle v(\langle x_{max} \rangle, \langle y_{max} \rangle) \rangle^2 \quad (4)$$

Making use of Eq. (2), we have:

$$\langle v^2(x_{max}, y_{max})\rangle = \Big\langle \int_{-\frac{\langle x_{max}\rangle}{2}}^{\frac{\langle x_{max}\rangle}{2}} \int_{-\frac{\langle y_{max}\rangle}{2}}^{\frac{\langle y_{max}\rangle}{2}} h^-(x_1,y_1)h^-(x_2,y_2)\,dx_1\,dx_2\,dy_1\,dy_2 \Big\rangle \quad (5)$$

Since ensemble averages commute with linear operations, we can write:

$$\langle v^2(\langle x_{max}\rangle, \langle y_{max}\rangle)\rangle = \int_{-\frac{\langle x_{max}\rangle}{2}}^{\frac{\langle x_{max}\rangle}{2}} \int_{-\frac{\langle y_{max}\rangle}{2}}^{\frac{\langle y_{max}\rangle}{2}} \langle h^-(x_1,y_1)h^-(x_2,y_2)\rangle\, d_{x1}\,dx_2\,dy_1\,dy_2$$

Or, introducing the auto-correlation function $\Psi^-(\xi,\eta)$:

$$\Psi^-(\xi,\eta) = \langle h^-(x+\xi, y+\eta)h^-(x,y)\rangle$$

it comes out that:

$$\langle v^2(\langle x_{max}\rangle, \langle y_{max}\rangle)\rangle = \int_{-\frac{\langle x_{max}\rangle}{2}}^{\frac{\langle x_{max}\rangle}{2}} \int_{-\frac{\langle y_{max}\rangle}{2}}^{\frac{\langle y_{max}\rangle}{2}} \psi^{-}(|x_2 - x_1|, |y_2 - y_1|)\, dx_1\, dx_2\, dy_1\, dy_2 \tag{6}$$

Introducing the new variables:

$$\xi = |x_2 - x_1|$$

$$\eta = |y_2 - y_1| \tag{7}$$

we obtain:

$$\langle v^2(\langle x_{max}\rangle, \langle y_{max}\rangle) = 16 \int_0^{\langle x_{max}\rangle/\sqrt{2}} \int_0^{\langle y_{max}\rangle/\sqrt{2}} \left[\frac{\langle x_{max}\rangle}{\sqrt{2}} - \xi\right]\left[\frac{\langle y_{max}\rangle}{\sqrt{2}} - \eta\right] \psi^{-}(\xi,\eta)\, d\xi\, d\eta \tag{8}$$

From relation (2), it is clear that:

$$\langle \upsilon(\langle x_{max} \rangle, \langle y_{max} \rangle) \rangle^2 = \langle S_{max} \rangle^2 \langle \bar{h}(\xi,\eta) \rangle^2 = V^2 \qquad (9)$$

We also notice that:

$$\langle S_{max} \rangle^2 \langle \bar{h}(\xi,\eta) \rangle^2 = 16 \int_0^{\langle x_{max} \rangle/\sqrt{2}} \int_0^{\langle y_{max} \rangle/\sqrt{2}} \left[\frac{\langle x_{max} \rangle}{\sqrt{2}} - \xi \right] \left[\frac{\langle y_{max} \rangle}{\sqrt{2}} - \eta \right] \frac{\sigma_h}{2} \, d\xi \, d\eta$$

Therefore, from Eqs. (4), (8) and (9), we end up with:

$$\sigma_\upsilon = 16 \int_0^{\langle x_{max} \rangle/\sqrt{2}} \int_0^{\langle y_{max} \rangle/\sqrt{2}} \left[\frac{\langle x_{max} \rangle}{2} - \xi \right] \left[\frac{\langle y_{max} \rangle}{2} - \eta \right] \left[\bar{\Psi}(\xi,\eta) - \frac{\sigma_h}{2\pi} \right] d\xi d\eta \qquad (10)$$

SUB-APPENDIX C-3

In this appendix, $\psi^{-}(\tau)$ in terms of $\psi(\tau)$ will be derived.

$$\psi^{-}(\tau) = \langle h^{-}(x)h^{-}(x+\tau)\rangle$$

$$\psi(\tau) = \langle h(x)h(x+\tau)\rangle \qquad (1)$$

where $h^{-}(x)$ is defined in relation (5)

At first, we introduce the following notations:

$$h(x) = a \qquad h^{-}(x) = a^{-}$$

$$h(x+\tau) = b \qquad h^{-}(x+\tau) = b^{-} \qquad (2)$$

Let $D(a,b,\tau)$ be the first joint probability density of the couple (a,b). $D(a,b,\tau)\,da\,db$ represents here the percentage of times that $h(x)$ will lie between a and $a + da$ while $h(x+\tau)$ lies between b and $b + db$.

Then, from our second hypothesis, $D(a,b,\tau)$ is Gaussian with mean value 0, and can thus be written:

$$D(a,b,\tau) = \frac{1}{2\pi}\,|M|^{-1}\exp\left(-\frac{1}{2}\,{}^{t}\|r\|\,M^{-1}\,\|r\|\right) \qquad (3)$$

where $$^{t}\|r\| = \|a \quad b\| \tag{4}$$

and M is the second moments matrix:

$$M = \begin{Vmatrix} \langle a^2 \rangle & \langle ab \rangle \\ \langle ab \rangle & \langle b^2 \rangle \end{Vmatrix} \tag{5}$$

From the definition of $\psi(\tau)$, it is obvious that:

$$\langle b^2 \rangle = \langle a^2 \rangle = \psi(0) \tag{6}$$

and

$$\langle ab \rangle = \psi(\tau) \tag{7}$$

in other words, M depends only on τ.

The mean value of a stochastic quantity Q is uniquely related to the couple of stochastic variables (a,b) is perfectly defined as soon as we know the joint frequency distribution of the latter, i.e.,

$D(a,b,\tau)$.

It is:

$$\langle Q \rangle = \int_{-\infty}^{+\infty}\int Q(a,b)\, D(a,b,\tau)\, dadb \qquad (8)$$

Or, when identifying Q with the product $a^{-}b^{-}$

$$Q = a^{-}b^{-} = \begin{cases} ab & \text{when} \quad a \text{ and } b < 0 \\ 0 & \text{when} \quad a \text{ or } b \geqslant 0 \end{cases} \qquad (9)$$

and, substituting for $D(a,b,\tau)$:

$$a^{-}b^{-} = \psi^{-}(\tau) = \frac{1}{2\pi(\psi_o^{\,2} - \psi^2)^{1/2}}$$

$$\int_{0}^{\infty}\int ab \exp\left(-\frac{(a^2 + b^2)\,\psi_o - 2ab\psi}{2(\psi_o^{\,2} - \psi^2)}\right) dadb \qquad (10)$$

in which we have set for convenience:

$$\psi = \psi(\tau)$$

$$\psi(0) = \psi_o \tag{11}$$

Introducing the new variables x and y such that:

$$a = x - y$$

$$b = x + y \tag{12}$$

Equation (10) becomes, noticing that the Jacobian of the transformation is 2:

$$\psi^-(\tau) = \frac{2}{\pi(\psi_o^2 - \psi^2)^{1/2}} \int_0^\infty dx \int_0^x (x^2 - y^2) \exp\left(- \frac{x^2}{\psi_o + \psi} - \frac{y^2}{\psi_o - \psi}\right) dy \tag{13}$$

And, making use of the error function defined as:

$$\text{erf}\,(x) = \frac{2}{\sqrt{\pi}} \int_0^x e^{-t^2}\, dt \tag{14}$$

we end up with:

$$\psi^-(\tau) = \left[\frac{(\psi_o - \psi)^3}{\pi(\psi_o + \psi)}\right]^{1/2} \left\{ \int_0^\infty (u^2 - \tfrac{1}{2})\, \text{erf}\,(u) \right.$$

$$\left. \exp\left(-u^2 \frac{\psi_o - \psi}{\psi_o + \psi}\right) du + \frac{\psi_o + \psi}{4\sqrt{\pi}\,\psi_o} \right\} \tag{15}$$

We notice that for the two-dimensional auto-correlation function $\Psi^-(\xi,\eta)$, the result is exactly similar to Eq. (15).

$$\Psi^-(\xi,\eta) = \langle h^-(x,y) h^-(x+\xi, y+\eta) \rangle$$

$$\Psi(\xi,\eta) = \langle h(x,y) h(x+\xi, y+\eta) \rangle \tag{16}$$

With the notation:

$$\Psi_o = \Psi(0,0)$$

$$\Psi = \Psi(\xi,\eta) \tag{17}$$

we have:

$$\bar{\Psi}(\xi,\eta) = \left[\frac{(\Psi_o - \Psi)^3}{\pi(\Psi_o + \Psi)}\right]^{1/2} \left\{ \int_0^\infty (u^2 - \tfrac{1}{2}) \operatorname{erf}(u) \exp\left(-u^2 \frac{\Psi_o - \Psi}{\Psi_o + \Psi}\right) du + \frac{\Psi_o + \Psi}{4\sqrt{\pi}\,\Psi_o} \right\} \tag{18}$$

SUB-APPENDIX C-4

The purpose of this appendix is to examine the behavior of $\psi^{-}(\tau)$.

From relation (15) of Sub-Appendix C-3, we have:

$$\psi^{-}(\tau) = \left[\frac{(\psi_o - \psi)^3}{\pi(\psi_o + \psi)}\right]^{1/2} \left\{ \int_0^\infty (u^2 - \tfrac{1}{2}) \operatorname{erf}(u) \exp\left(-u^2 \frac{\psi_o - \psi}{\psi_o + \psi}\right) du + \frac{\psi_o + \psi}{4\sqrt{\pi}\,\psi_o} \right\} \tag{1}$$

We can split the integral into two parts:

$$I = \int_0^\infty (u^2 - \tfrac{1}{2}) \operatorname{erf}(u) \exp\left(-u^2 \frac{\psi_o - \psi}{\psi_o + \psi}\right) du = I_1 + I_2 \tag{2}$$

where:

$$\left.\begin{aligned} I_1 &= \int_0^n (u^2 - \tfrac{1}{2}) \operatorname{erf}(u) \exp\left(-u^2 \frac{\psi_o - \psi}{\psi_o + \psi}\right) du \\ I_2 &= k_n \int_0^\infty (u^2 - \tfrac{1}{2}) \exp\left(-u^2 \frac{\psi_o - \psi}{\psi_o + \psi}\right) du \end{aligned}\right\} \tag{3}$$

with:

$$k_n = \frac{\int_n^\infty (u^2 - \frac{1}{2}) \operatorname{erf}(u) \exp\left(-u^2 \frac{\psi_o - \psi}{\psi_o + \psi}\right) du}{\int_n^\infty (u^2 - \frac{1}{2}) \exp\left(-u^2 \frac{\psi_o - \psi}{\psi_o + \psi}\right) du} \qquad (4)$$

k_n is perfectly defined since the two above integrals are convergent.

Since erf(z) as defined in Section 3 approaches unity when z tends to infinity, k_n tends to 1 when n approaches infinity.

$$I_2 = k_n (J + K)$$

where:

$$J = \int_n^\infty u^2 \exp\left(-u^2 \frac{\psi_o - \psi}{\psi_o + \psi}\right) du$$

$$K = \int_n^\infty \frac{1}{2} \exp\left(-u^2 \frac{\psi_o - \psi}{\psi_o + \psi}\right) du$$

After some algebra, it follows that:

$$I_2 = k_n \left\{ \frac{3}{2} \cdot \frac{\psi_o + \psi}{\psi_o - \psi} \exp\left(- n^2 \frac{\psi_o - \psi}{\psi_o + \psi} \right) + \frac{2\psi}{\psi_o - \psi} \sqrt{\frac{\pi(\psi_o + \psi)}{16(\psi_o - \psi)}} \operatorname{erfc}\left(n \sqrt{\frac{\psi_o - \psi}{\psi_o + \psi}} \right) \right\} \quad (5)$$

here, erfc(z) is the complementary function of erf(z)

1. $\tau \to 0$

When $\tau = 0$, $\psi = \psi_o$ and therefore relation (5) of Sub-Appendix C-1 becomes:

$$I_2 = k_n \left\{ \frac{3}{2} \cdot \frac{\psi_o + \psi}{\psi_o - \psi} \exp\left(- n^2 \frac{\psi_o - \psi}{\psi_o + \psi} \right) + \frac{2\psi}{\psi_o - \psi} \sqrt{\frac{\pi}{16} \cdot \frac{\psi_o + \psi}{\psi_o - \psi}} \right\}_{\psi = \psi_o} \quad (6)$$

having n increase to infinity, it follows from (1), (2), (3) and (6) of Sub-Appendix C-1 that the only remaining non zero term is:

$$\psi^-(0) = \left\{ \left[\frac{(\psi_o - \psi)^3}{\pi(\psi_o + \psi)} \right]^{1/2} \left[\frac{2\psi}{\psi_o - \psi} \sqrt{\frac{\pi}{16}} \left(\frac{\psi_o + \psi}{\psi_o - \psi} \right)^{1/2} \right] \right\}_{\psi = \psi_o}$$

$$\bar{\psi}(0) = \frac{\psi_o}{2} = \frac{1}{2}\psi(0) \tag{7}$$

2. $\tau \to \infty$

We have to go back here to relation (10) of Sub-Appendix C-3, namely:

$$\bar{\psi}(\tau) = \frac{1}{2\pi(\psi_o^2 - \psi^2)^{1/2}} \int_0^\infty\int_0^\infty ab \exp\left\{ - \frac{(a^2 + b^2)\psi_o - 2ab\psi}{2(\psi_o^2 - \psi^2)} \right\} dadb$$

$\tau \to \infty$ is equivalent to have $\psi \to 0$ since, at infinity, $\psi(\tau)$ is zero.

Hence, integrating the above relation for $\psi = 0$, one easily obtains:

$$\bar{\psi}(\infty) = \frac{\psi_o}{2\pi} = \frac{\sigma_h}{2\pi} \tag{8}$$

which is not surprising since, for an infinite τ, $\bar{h}(x)$ and

$h^-(x + \tau)$ are no more correlated and therefore:

$$\langle h^-(x)h^-(x+\tau)\rangle = \langle h^-(x)\rangle \langle h^-(x+\tau)\rangle$$

$$= \langle h^-(x)\rangle^2 = \frac{\psi_o}{2\pi}$$

The aspect of a typical $\psi^-(\tau)$ is sketched on Fig. 8.

3. application

For numerical computation of $\psi^-(\tau)$ from $\psi(\tau)$, it is interesting to notice that:

n = 3 in relation (3) of Sub-Appendix C-1 is highly sufficient since:

$$\text{erf}(3) = 0.99990 \simeq 1$$

implying $k_3 = 1$.

$$\psi^-(\tau) \simeq \left[\frac{(\psi_o - \psi)^3}{\pi(\psi_o + \psi)}\right]^{1/2} \left\{ \int_0^3 (u^2 - 1/2)\, \text{erf}\,(u) \exp\left(-u^2 \frac{\psi_o - \psi}{\psi_o + \psi}\right) du + \frac{\psi_o + \psi}{4\sqrt{\pi}\,\psi_o} + \frac{3(\psi_o + \psi)}{2(\psi_o - \psi)} \exp\left(-9\,\frac{\psi_o - \psi}{\psi_o + \psi}\right) + \frac{\psi_o}{2(\psi_o - \psi)} \sqrt{\frac{\pi(\psi_o + \psi)}{\psi_o - \psi}}\, \text{erfc}\left(3\sqrt{\frac{\psi_o - \psi}{\psi_o + \psi}}\right) \right\} \quad (9)$$

SUB-APPENDIX C-5

The purpose of this appendix is to give some details on the derivations relative to the mathematical analysis of the one-dimensional case. Thus, the first statistical moment $\langle x_{max} \rangle$ of the pool extent and its variance σ_x will be determined in terms of σ_h, the variance of the roughness height and $\psi(\tau)$ the auto-correlation of the latter.

We introduce the notations $h^+(x)$ and $h^-(x)$ such that

$$H(x) = h^+(x) + h^-(x) \tag{1}$$

and

$$\begin{aligned} h^+(x) &= h(x) \quad \text{when} \quad h > 0 \\ h^+(x) &= 0 \quad \text{when} \quad h \leqslant 0 \\ h^-(x) &= h(x) \quad \text{when} \quad h < 0 \\ h^-(x) &= 0 \quad \text{when} \quad h \geqslant 0 \end{aligned} \tag{2}$$

We define $\upsilon(x)$, amount of oil per unit width that would fill the pockets between abscissae 0 and x:

$$\upsilon(x) = - \int_0^x h^-(\xi)\, d\xi \tag{3}$$

The extent of the pool, x_{max}, for a given realization of the ice profile is such that:

$$V = \int_0^{x_{max}} \bar{h}(\xi)\, d\xi \tag{4}$$

If $\langle x_{max} \rangle$ denotes the ensemble average of x_{max}, we can always write Eq. (4) as:

$$-V = \int_0^{\langle x_{max} \rangle} \bar{h}(\xi)\, d\xi + (x_{max} - \langle x_{max} \rangle)\, \bar{h}(\xi) \tag{5}$$

since $\bar{h}$ is a continuous function of x; ξ corresponds here to a point of the profile where:

$$\langle x_{max} \rangle \leq \xi \leq x_{max} \tag{6}$$

As was done for the two-dimensional case and with the same limitations, we assume that:

$$\bar{h}(\xi) = \langle \bar{h}(\xi) \rangle \tag{7}$$

Equation (5) is then written:

$$-V = \int_0^{\langle x_{max} \rangle} h^-(\xi)\, d\xi + (x_{max} - \langle x_{max} \rangle)\, \langle h^-(\xi) \rangle \qquad (8)$$

Taking the ensemble average of Eq. (8) and noticing that this kind of average commutes with linear operations:

$$-V = \langle h^-(\xi) \rangle \langle x_{max} \rangle \qquad (9)$$

Then:

$$\langle x_{max} \rangle = -\frac{V}{\langle h^-(\xi) \rangle} \qquad (10)$$

To derive the variance σ_x of x_{max}, defined as:

$$\sigma_x = \langle (x_{max} - \langle x_{max} \rangle)^2 \rangle \qquad (11)$$

we come back to Eq. (8) and write it as:

$$\left\langle \left[\int_0^{\langle x_{max} \rangle} h^-(\xi)\, d\xi + V \right]^2 \right\rangle = \langle (x_{max} - \langle x_{max} \rangle)^2 \rangle \; \langle h^-(\xi) \rangle^2 \qquad (12)$$

Or:

$$\sigma_{\upsilon} = \sigma_{x} \langle \bar{h}(\xi) \rangle^{2} \tag{13}$$

where σ_{υ} is the variance of the volume υ ($\langle x_{max} \rangle$):

$$\sigma_{\upsilon} = \left\langle \left[\upsilon(\langle x_{max} \rangle) - \langle \upsilon(\langle x_{max} \rangle) \rangle \right]^{2} \right\rangle \tag{14}$$

Also, expanding Eq. (14):

$$\sigma_{\upsilon} = \langle \upsilon^{2}(\langle x_{max} \rangle) \rangle - \langle x_{max} \rangle^{2} \langle \bar{h}(\xi) \rangle^{2} \tag{15}$$

From Eq. (3), it is clear that

$$\langle \upsilon^{2}(\langle x_{max} \rangle) = \left\langle \int_{0}^{\langle x_{max} \rangle} \int \bar{h}(\xi) \bar{h}(\eta) \, d\xi \, d\eta \right\rangle$$

$$= \int_{0}^{\langle x_{max} \rangle} \int \langle \bar{h}(\xi) \bar{h}(\eta) \rangle \, d\xi \, d\eta$$

$$= \int_{0}^{\langle x_{max} \rangle} \int \bar{\psi}(|\xi - \eta|) \, d\xi \, d\eta \tag{16}$$

where $\psi^{-}(\tau)$ is the auto-correlation for h^{-}.

Making the following change of variables:

$$\tau = |\xi - \eta|$$

$$\theta = |\xi + \eta| \tag{17}$$

We end up with:

$$\langle v^2(\langle x_{max}\rangle)\rangle = 4 \int_0^{\langle x_{max}\rangle/\sqrt{2}} \left[\frac{\langle x_{max}\rangle}{\sqrt{2}} - \tau\right] \psi^{-}(\tau)\, d\tau \tag{18}$$

Noticing that:

$$\langle x_{max}\rangle^2 \langle h^{-}(\xi)\rangle^2 = 4 \int_0^{\langle x_{max}\rangle/\sqrt{2}} \left[\frac{\langle x_{max}\rangle}{\sqrt{2}} - \tau\right] \frac{\sigma_h}{2\pi}\, d\tau \tag{19}$$

and using Eqs. (13) and (15), we obtain:

$$\sigma_x = 4 \int_0^{\langle x_{max}\rangle/\sqrt{2}} \left[\frac{\langle x_{max}\rangle}{\sqrt{2}} - \tau\right] \left[\psi^{-}(\tau) - \frac{\sigma_h}{2\pi}\right] d\tau \tag{20}$$

$\psi^{-}(\tau)$ in terms of $\psi(\tau)$ is determined in Sub-Appendix C-3 (Eq. (15)) while the value of $\dot{h}^{-}$ has already been determined in terms of σ_h in Eq. (22) of Appendix C.

REFERENCES

1. S. O. Rice, "Mathematical analysis of random noise", p.133 in Selected papers on noise and stochastic processes, edited by Nelson Wax., Dover Publications, New York, 1954.

2. J. L. Lumley and H. A. Panofsky, "The structure of atmospheric turbulence", Interscience, New York, 1964.

3. CRREL - Corps of Engineers, Hanover, New Hampshire, "Sev Arctic Environment data package", 1970.

4. Norbert Wiener, "Generalized harmonic analysis - Tauberian theorems", MIT Press, 1964.

5. Dr. Hibler, CRREL, Hanover, New Hampshire, personal communication.

LIST OF FIGURES

Fig. 8. Aspect of the auto-correlation function of h^- and h^+.

Fig. 9. Position of τ_o with respect to T (Section IV - 3 of the text).

Fig. 10. Relationship between $<x_{Max}>$ and $\sigma_x^{1/2}$. One-dimensional case.

Fig. 11. Slope Θ versus non-dimensional group kT^2. One-dimensional case.

Fig. 12. Relationship between $<S_{Max}>$ and $\sigma_s^{1/2}$. Two-dimensional case.

Fig. 13. Slope Θ versus non-dimensional group $k_1 k_2 T_1^2 T_2^2$. Two-dimensional case.

*U.S. GOVERNMENT PRINTING OFFICE:1975 629-369/673 1-3